Highly Crosslinked Natural Rubber-Cellulose Nanocrystals Composites for Sustainable Material Applications

by

Ewomazino Constance Ojogbo

A thesis

presented to the University of Waterloo

in fulfillment of the

thesis requirement for the degree of

Doctor of Philosophy

in

Chemical Engineering

Waterloo, Ontario, Canada, 2024

Examining Committee Membership

The following served on the examining committee for this thesis. The decision of the examination committee is by majority vote.

External Examiner:	Michael Thompson Professor, Chemical Engineering Department McMaster University
Supervisors:	Tizazu Mekonnen Associate Professor, Chemical Engineering Department, University of Waterloo Costas Tzoganakis Professor, Chemical Engineering Department, University of Waterloo
Internal Examiners:	Alex Penlidis Professor, Chemical Engineering Department, University of Waterloo Aiping Yu Professor, Chemical Engineering Department, University of Waterloo
Internal-External Examiner:	Jean Duhamel Professor, Chemistry Department, University of Waterloo

Author's Declaration

I hereby declare that I am the sole author of this thesis. This is a true copy of the thesis, including any required final revisions, as accepted by my examiners. I understand that my thesis may be made electronically available to the public.

Abstract

In a bid to develop environmentally friendly rubber materials, the use of renewable and sustainable additives and reinforcing fillers that could provide suitable mechanical property enhancement is of great interest. In this thesis, cellulose nanocrystals (CNCs) are employed as reinforcing fillers due to their availability, sustainability, high aspect ratio, and excellent mechanical properties. In the first part of this study, various processing and fabrication methods of natural rubber (NR) – CNCs nanocomposite formulations were investigated to obtain optimal dispersion of CNCs and hence physical properties. Rheology, morphology, and various physico-mechanical property testing were also employed to understand the effects of the processing method on the NR-CNC vulcanizates. While co-coagulation and extrusion provided improved reinforcement of the nanocomposites attributed to the optimal dispersion of CNCs, batch mixing processed samples exhibited poor dispersion even at low CNCs loadings as observed from transmission electron microscopy and inferior composite properties.

The second and third part of this thesis involved chemical modification of the CNCs to enhance hydrophobicity and increase dispersion. Firstly, CNC was grafted on epoxidized natural rubber (ENR) in a base thermo-catalyzed reactive extrusion process. Successful grafting was confirmed using Fourier transform infrared spectroscopy (FTIR), X-ray photoelectron spectroscopy (XPS), and toluene swelling experiments. The new covalently grafted ENR – CNC was then added as a masterbatch into a rubber formulation. The ENR acted as a carrier of CNCs in the rubber leading to efficient dispersion of the CNCs and subsequently improved the tensile strength and rheological properties of the composite. In a separate study, CNC was modified with 3-isocyanotopropyltriethoxysilane (IPTS) and employed as a reinforcing filler for natural rubber. Successful modification was verified using FTIR and nuclear magnetic resonance (NMR)

spectroscopy. As it is important to retain the crystalline structure of the CNC after modification, X-ray diffraction (XRD) studies showed that the crystal structure of the CNC was retained. The composition of the modified CNC with natural rubber improved the mechanical properties, reduced the cure time, and had no negative effect on the processability.

Overall, this study aimed to develop environmentally friendly and renewable nanocomposite systems based on rubber and CNCs in a bid to replace or complement the incumbent fillers in the rubber industry. Particularly, to generate knowledge on the chemical modification, processing, and applications of CNC in highly crosslinked rubber compounds, and investigate their suitability in material applications such as tires.

Acknowledgements

I want to thank my supervisors, Prof. Tizazu Mekonnen and Prof. Costas Tzonagakis, for training, guiding, mentoring, and supporting me throughout my program. During my program, I underwent multiple life changes, and my supervisors accommodated, encouraged, supported, and were patient with me. During one of my most challenging times, Prof. Mekonnen told me, "Zino, you are a brilliant woman with lots of potential." This statement changed my outlook and gave me the zeal to keep going. I will never forget your kindness towards me. Thank you.

Special thanks to Judy Caron. Judy was so helpful in providing guidance and resources to navigate graduate school. When I was hospitalized and emailed Judy, she helped me navigate funding because she didn't want me worrying about money while trying to get better. She also called a few times to check how I was doing. Like she used to say, "I am here, so you don't have to worry; let me do the worrying for you while you do what you have to do." Thank you so much, Judy.

I want to thank Joy Spandler of Air Boss of America, Kitchener, Bert Habicher Ralph Dickhout, Ankita Saikia of Tyromer, and Charles del Castel for their technical support and assistance with some experiments. I would also like to thank the members of Prof. Mekonnen's research group, especially Dylan Jubinville, who was always happy to help with things around the lab. I sincerely thank Prof. Valerie Ward for showing me that balancing family life and academia is possible. She was there to listen when I had challenges and offered support and encouragement.

This work would not have been possible without the support of my family and friends. My partner, Paul, for supporting me and picking up the slack when need be; my children, Somto and Isabella, for understanding that Mummy had to work and being my motivation to be the best

version of myself every day; my siblings, for supporting me, and being a positive influence in my life, and my Mom, Comfort Isawode, for her support and prayers. Finally, I wish to thank Ajirioghene, a friend turned sister who helped me navigate challenging times; Christine, who has been a loyal friend through the years; and Lizzy, who's the best friend anyone could have.

Finally, I would like to thank the Natural Sciences and Engineering Research Council of Canada (NSERC) and Waterloo Institute of Nanotechnology (WIN) for providing me with a scholarship, Natural Resources Canada (NRCan) for funding my research, and Airboss of America for technical support and donating rubber slab used for this research.

Dedication

To my Dad, the Late Engr. Samuel Enwenede. I wish you were here to see me complete this program and become the earn my doctorate degree. Thank you for teaching me the importance of education and encouraging me to work hard. The values you taught me have brought me this far, and I will forever be grateful for your love. I hope I am making you proud.

Table of Contents

List of Figures

List of Tables

List of Abbreviations

-OH	Hydroxyl	g/cm3	grams per cubic meter
%	Percent	g/min	gram per minute
AGU	Anhydro glucose unit	GA	State of Georgia
ANOVA	Analysis of variance	GPa	Gigapascal
ASTM	American society for testing and materials	h	hour
BC	Bacterial cellulose	Hz	Hertz
BR	polybutadiene	IPTS	3-isocyanotopropyltriethoxysilane
CB	Carbon black	IR	Infrared
cm	Centimeter	kN	Kilonewton
CNC	Cellulose nanocrystals	kV	Kilovolts
CNF	Cellulose nanofiber	LVE	Linear viscoelastic region
CNF	Cellulose nanofiber	M100	Modulus at 100
CTAB	Hexadecyl-trimethylammonium bromide	M300	Modulus at 300
DDMSiCl	n-dodecyldimethylchlorosilane	MCC	Microcrystalline cellulose
DI	Deionized water	mCNC	Modified cellulose nanocrystal
DMF	dimethylformamide	MH	Maximum Torque
DMSO	Dimethylsulphoxide	MI	Initial Mooney
DOE	Design of experiment	ml	Milliliter
DS	Degree of substitution	ML	Minimum Torque
EA	Elemental analysis	mm	millimeter
EDX	Energy dispersive X-ray spectroscopy	MPa	Megapascal
ENR	Epoxidized natural rubber	MPS	Methacryloxy propyltrimethoxy silane
eV	Electron volts	MV	Mooney viscosity
FTIR	Fourier transform infrared spectroscopy	N/A	Not applicable
g	Grams	NaOH	Sodium hydroxide
G’	Storage modulus	nm	nanometer
G”	Loss modulus	NMR	nuclear magnetic resonance
G*	Complex modulus	NR	Natural rubber
g/cc	gram per cubic centimetre	O	Oxygen
g/cm	gram per centimetre	OH	Hydroxyl
ON	Ontario	TEM	Transmission electron microscopy
Phr	Parts per hundred rubber	THF	Tetrahydrafuran

Psi	Pounds per square inch	TS2	Scorch time
QC	Quebec	USA	United States of America
RHA	Rice husk ash	Vr	Volume fraction of rubber
RPA	Rubber processing analyzer	Vro	Volume fraction of rubber in solvent swollen gum
rpm	revolution per minute	wt %	weight percent
s	second	Wt.	weight
SBR	styrene-butadiene rubber	XPS	X-ray photoelectron spectroscopy
SEM	Scanning electron microscopy	XRD	X-ray diffraction
SI	Swelling index	Zn	Zinc
Sn(Oct)2	Tin (II) ethylhethanoate	ZnO	Zinc oxide
TBBS	N-tert-2-benzothiazyl sulfonamide	β	Beta
T_C90	Optimum cure time	Ø	Volume fraction of filler
		µL	microlitre

List of Schemes

Chapter 1. Introduction and Objectives

1.1 Problem Statement

The practical use of natural rubber (NR), styrene-butadiene rubber (SBR), polybutadiene (BR), etc in their native form is limited because of their inferior strength, poor abrasion resistance, and undesirable responses to weather conditions. Rubber vulcanization, a chemical process which creates crosslinks between the long rubber chains, transforms the rubber from a material with low modulus and tensile strength into a tougher material with improved tensile strength[1]. In addition to vulcanization, most practical applications of rubbers involve the incorporation of fillers, mainly to enhance their physical and chemical properties and to reduce compound cost[2]. For instance, rubber applications requiring high strength and stiffness such as tires, conveyor belts, and footwear need to be filled with carbon black and other mineral fillers[2]. The presence of the fillers improves the abrasion resistance, tear, tensile properties, hardness, resistance to chemical attack, and overall durability[3].

While fillers improve the properties of rubber, the overall reinforcement of the rubber composite depends on the filler properties such as the shape, size, and interaction between the rubber matrix and the fillers[3–7]. The common fillers used in rubber are carbon black, silica, and clay. In recent times, interests have shifted from these common fillers to renewable due to environmental impact and sustainability. While this thesis will touch briefly on the common fillers, it lays emphasis on renewable fillers, specifically cellulose nanocrystals.

Carbon black is extensively studied and widely used as a reinforcing filler in tires and several other rubber products and as a color pigment in paints, plastics, and inks [8]. It is reported that an estimated 70% consumption of carbon black is as a filler in tires for strength and wear resistance [9]. Carbon black, which is obtained from the incomplete combustion of petroleum products utilizes

high energy during production and contributes to the increase in greenhouse gases and climate change. Moreover, according to the international agency for research on cancer, inhalation of carbon black is associated with health problems such as respiratory and cardiovascular diseases, cancer (Group 2B), and birth defects [10,11]. Also, the density of rubber (1.79 g/cm^3)[12] results in increased weight of the composite, which defeats one of the remarkable properties of rubber being a lightweight material. For these reasons, developing and utilizing bio-based and sustainable nano-reinforcements, to mitigate the impact on health and environment by replacing carbon black is of great interest.

Cellulose nanocrystal (CNC), due to its renewability, biodegradability, low density, nontoxicity, and high strength [13,14] is a possible substitute or complementary additives for carbon black in rubber applications. Also, CNC is rich in surface hydroxyl groups, which are amenable to several chemical modifications, enabling the tailoring of CNC to a wide range of applications. It is hypothesized that using CNC as an alternate filler in rubber will mitigate the high energy consumption, increased greenhouse gases, and environmental impact associated with carbon black production. Although CNC presents several advantages, preparation of a composite of pristine CNC and rubber is challenged with poor CNC dispersion, agglomeration, and poor interfacial adhesion resulting from the incompatibility between the non-polar rubber matrix and the polar CNC filler[15–17]. To improve CNC dispersion in non-polar matrices, various approaches have been investigated, including surface modification of CNCs [18–20]. While CNC modification is widely studied, studies on the utilization of CNCs for highly filled rubber composites is rather scarce. Therefore, this study aims to investigate and optimize the dispersion of CNC in highly filled rubber composites to improve the properties of the resulting rubber biocomposites.

1.2 Study goals and objectives

A literature review has revealed that studies of CNC filled rubber vulcanizates is rather limited. This is especially true when the intended application requires high strength, such as tire applications. Therefore, this study is aimed at developing processing technologies and modification chemistries that enable efficient dispersion of CNCs in rubber for optimal rubber composite properties. In addition to the sustainability and environmentally friendly attributes of CNCs, it is hypothesized that it can interact with rubber polymer at a molecular level due to its nano-size, which could substantially improve the mechanical properties of rubber. This project involves the following subprojects :

(I) To investigate the optimal processing method for rubber CNC composites by compounding of rubber and CNCs at varied concentrations using different processing techniques, such as co-coagulation, batch mixing, and extrusion, and characterizing the rubber composites thereafter. The parameters of the fabrication techniques will be optimized to obtain the method that provides the most efficient dispersion of the CNC in the rubber matrix.

(II) To graft CNC onto specialty rubber, epoxidized natural rubber (ENR), and generate a CNC – ENR masterbatch based rubber composites and study the processing and properties. This study aims to prepare a masterbatch of ENR-filled CNC composite to be utilized as a filler for natural rubber to improve the dispersion of CNC in the rubber.

(III) To evaluate the effect of silane modification of the surface of CNC and its dispersion in highly filled rubber composite. This study aimed to improve the dispersion, mechanical properties, and reduce the Payne effect in the composite while retaining the properties of the CNC.

1.3 Outline of Thesis Chapters

This doctoral thesis consists of 6 chapters which contributes to the overall objective of this thesis work.

Chapter 1: This chapter introduces the work. It presents the research problem, objectives, and direction of the work. The chapters following this provide support for the research objectives outlined in this chapter.

Chapter 2: This chapter reviews the literature and discusses the common fillers of rubbers with emphasis on CNC as a filler for highly filled rubber composites, parameters affecting the reinforcement of fillers and characterization of the nanocomposites. Finally, it discusses the potential applications for nanocomposites based on CNCs and natural rubber.

Chapter 3: This chapter summarizes findings on the effect of fabrication methods on the dispersion of CNC in rubber. In this chapter, different loadings of CNC (2.5- 10 wt%) were dispersed in rubber using batch mixing, extrusion, and co-coagulation methods and the properties of the composites were analyzed and compared. The properties of the composites were analyzed using transmission electron microscopy, mechanical property testing, toluene swelling studies and rheological property studies.

Chapter 4: In this chapter, the CNC formation of covalent grafts with epoxidized natural rubber (ENR) and the formation of secondary hydrogen bonds in a base-catalyzed reactive extrusion process was studied at varying temperatures. The grafting reaction was confirmed using Fourier transform infrared spectroscopy, X-ray photoelectron spectroscopy, and toluene swelling experiments. The properties of the ENR-CNC composite were analyzed using mechanical property and rheological property experiments.

Chapter 5: This chapter explored the use of cellulose nanocrystals (CNC) modified with 3-isocyanotopropyltriethoxysilane (IPTS) as a reinforcing agent of natural rubber. A single-step heterogeneous reaction was employed to modify the surface hydroxyl (OH) groups of the CNC using IPTS. Successful surface modification was evaluated using Fourier transform infrared spectroscopy (FTIR), elemental analysis, and nuclear magnetic resonance. As it was important to retain the crystalline structure of the CNCs after modification, X-ray diffractometry (XRD) verified the preservation of the crystal structure of CNC, while contact angle measurements and wettability studies verified the altered polarity of the modified CNCs. Subsequently, nanocomposites of natural rubber (NR) were developed by incorporating the modified CNCs (mCNC) at varying concentrations (2.5%, 5%, 10%, and 20%). The composite was vulcanized, and the mechanical and rheological properties were evaluated. The modified CNC-reinforced rubber composites exhibited reduced cure time, ease of processibility, and improved mechanical properties.

Chapter 6: This is the concluding chapter of this thesis. It provides a concise conclusion of all studies carried out as well as direction for future work to expand on this research effort.

Chapter 2. Literature review

2.1 Nanocomposite systems

The development of high-performance bio-nanocomposites has attracted considerable attention in recent years due to the interest in developing polymeric materials that are simultaneously sustainable and multifunctional. Bio-nanocomposites are nanocomposite systems where one of the constituents is bio-sourced and renewable[21,22]. A nanocomposite is a heterogeneous mixture containing two or more components with differentiated physicochemical properties. Fundamentally, a nanocomposite consists of a homogenous polymeric matrix reinforced by typically a high modulus, high strength, mineral or organic nano sized filler of characteristic size, shape, and surface properties[23].

Nanocomposites based on rubber are attractive due to their flexibility and wide range of applications from automobiles to personal goods. To use rubber for industrial applications, the individual rubber chains are made to form a three-dimensional network structure by crosslinking reaction in the process of vulcanization. To vulcanize rubber, additives, such as crosslinking agent, activators, chain extenders, accelerators, etc. are incorporated in the rubber formulation followed by a thermo-mechanical process. Although vulcanized rubber can be used for certain applications such as rubber gaskets and seals, the addition of reinforcing fillers can provide superior physical and mechanical properties and extend its application. In most cases, the properties of the filler, such as structure, aspect ratio, particle size, particle shape, in conjunction with the interfacial interaction with the rubber determines the property of the nanocomposite. **Figure 2.1** shows the classification of reinforcing fillers used for rubber applications.

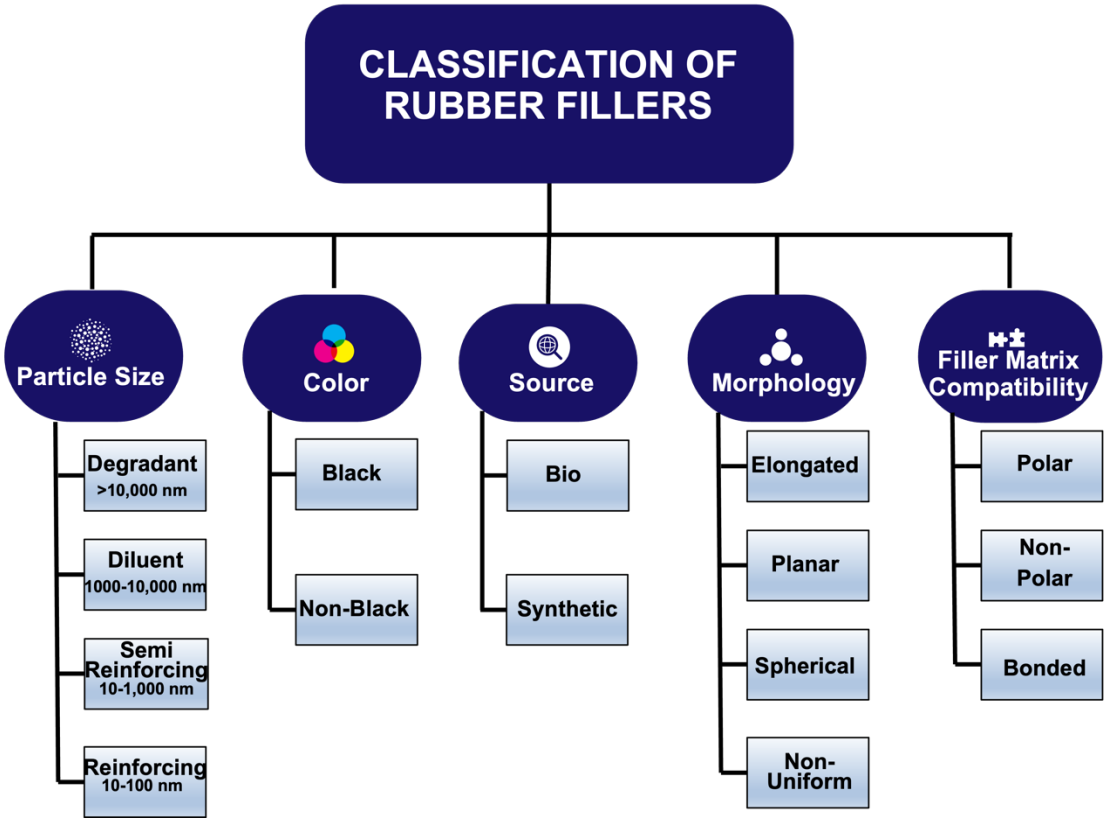

Figure 2.1. Classification of fillers based on properties (Adapted from with permission from Low et al.[24]).

2.2 Common fillers for natural rubber

2.2.1 Carbon Black

Carbon black (CB) is extensively studied and widely used as a reinforcing filler in tires and several other rubber products and as a color pigment in paints, plastics, and inks [8]. It is reported that of the 15 million metric tons global production of carbon black per year, 93% are used for rubber applications (73% and 20% for tire and non-tire applications, respectively), and 7% for other non-rubber applications[25]. Generally, carbon black is a spherical aggregate of carbon atoms which consist of 98% carbon and is obtained from the incomplete combustion of petroleum

products. Typically, diameters of carbon black aggregates range from 10 nm to 500 nm and this variation in size is influenced by the processing conditions[26]. Based on these processing conditions, carbon black can be classified into thermal black, furnace black and channel black[27].

The elemental aggregates of carbon in CB fuse together to form agglomerates which are broken down during rubber compounding. As it is widely known, the filler particle size is an important factor influencing the reinforcement of rubber by the filler. CB with particle size exceeding 1000 nm do not provide reinforcement but rather increase the viscosity and volume of the material. It is well known that CB provides reinforcement in rubber and several mechanisms of reinforcements have been postulated, including the particle size, interface slippage, and reaction sites on surface. Generally, more active sites on the filler surface are better as it increases the affinity for the filler to bond with the rubber and as presented in **Figure 2.2**, carbon black is rich in surface functional groups which permits inter- and intra- molecular interactions with rubber. According to research conducted by Nagornaya *et al..,* this mechanism was proven by the removal of the reactive sites on the CB prior to compounding with rubber and a reduction in the abrasion resistance and modulus were observed[28].

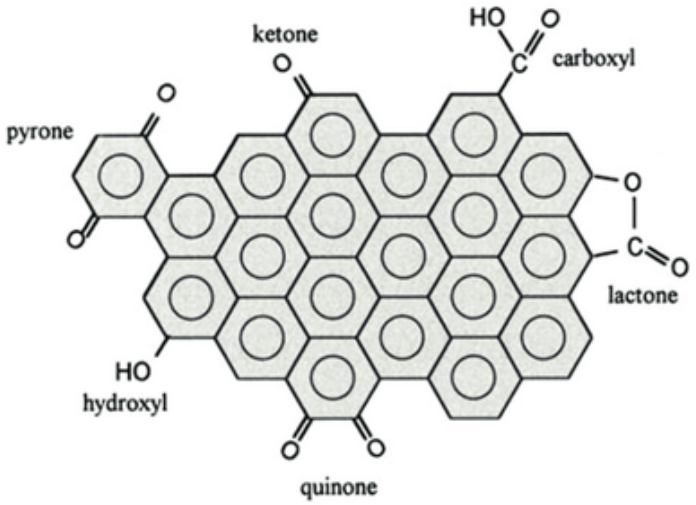

Figure 2.2. Functional groups on the surface of carbon black (Adapted with permission from from Hassan *et al.*[29])

When used as a reinforcing filler, the aggregation of CB in rubber leads to the Payne effect in the rubber composite exhibited as a dependence of storage and loss modulus on the amplitude of applied strain. The Payne effect, absent in unfilled rubbers, depends on the nature of filler-filler interaction and the filler content. The mechanism of Payne effects has been described by several researchers including formation/breakdown of filler aggregates and/or network[30–33], filler-polymer breakdown/formation[34,35], nanoparticle chain desorption[34,35], unraveling of adsorbed chains, glassy polymer shell softening of particle surfaces[36]. The significant Payne effects in CB filled tires are reported to be responsible for the rolling resistance in tire applications. Although, new grades of carbon black, such as super-active carbon black and inversion blacks give promising results for the improvement of rolling resistance[37], other methods such as the use of hybrid filler systems and alternate fillers, such as silica, another common filler in the rubber industry have been extensively studied.

2.2.2 Silica

Silica, the most abundant mineral on earth is a popular non-black reinforcing filler employed in industrial applications because of abrasion resistance, tear strength, and low rolling resistance in tires[38]. Silica is thermally stable, has low toxicity, and is hydrophilic with surface hydroxyl groups[39]. While the surface hydroxyl groups allow silica to be modified and tailored for specific applications, it also causes incompatibility with hydrophobic polymer matrices and filler-filler interactions which impacts the mechanical performance of the rubber composites. To mitigate the compatibility challenge and improve dispersion, different methods including the use of functionalized rubbers, surface treatment, addition of coupling agents such as silane[40], silica-rubber masterbatch fabrication[41], and surface modification methods have been employed[42–44].

Silane is the most employed coupling agent for silica because under optimal processing conditions, silane chemically bonds with silica and then with rubber during vulcanization making silanes act as both coupling agents and compatibilizers for rubbers. Kaewsakul *et al.*[40] presented the reaction mechanism of different types of silanes and rubber in **Figure 2.3** showing how silanes simultaneously hydrophobicize the CNC and compatibilize with rubber.

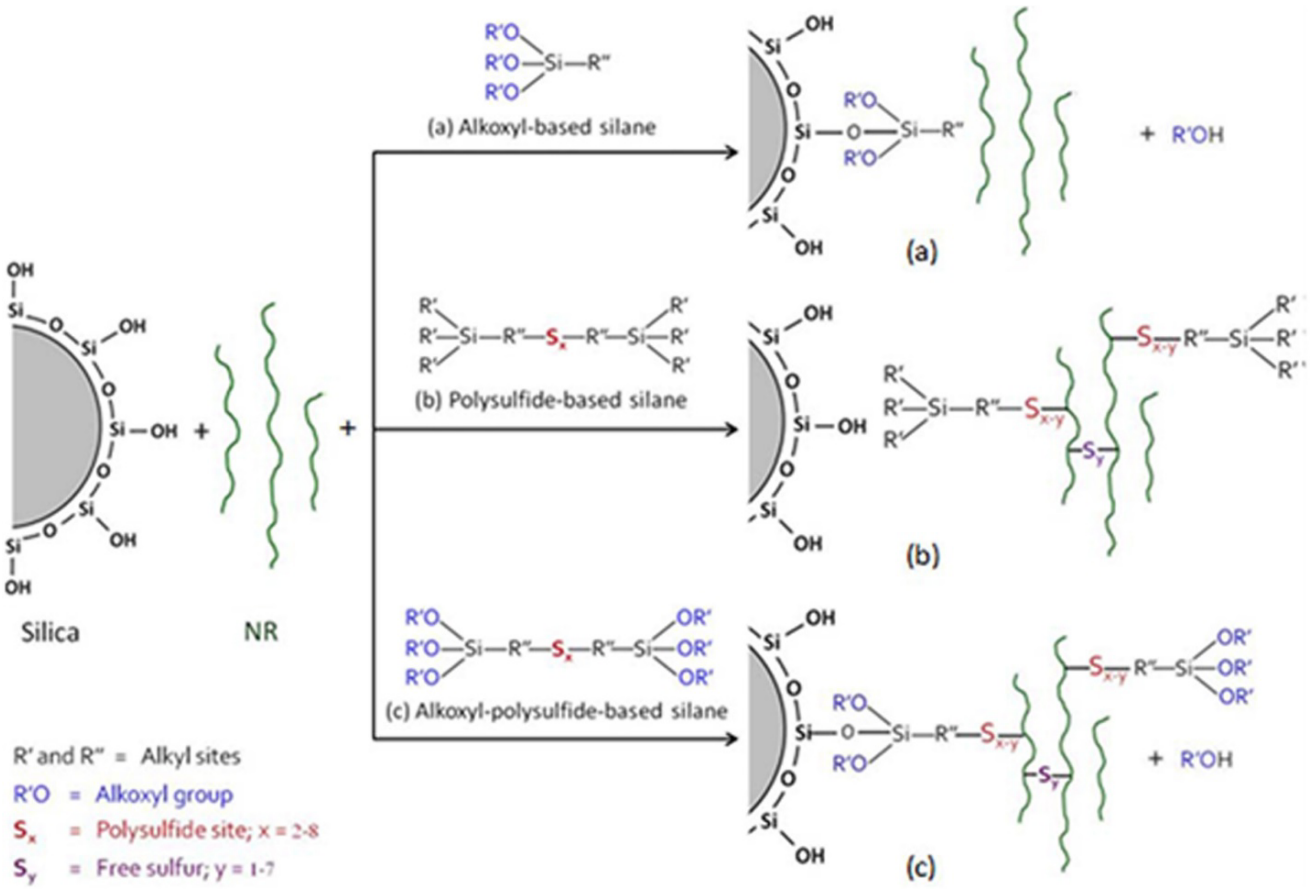

Figure 2.3. Reaction mechanism of silica with silane with different functional groups employed for silica-filled NR composites (Adapted with permission from Roy *et al*.[45]).

Although silica is widely studied and employed for rubber applications, problematic processing behavior during modification and the high energy consumption involved with the production of silica limits its use[46–48]. As a result, researchers continue to explore alternative fillers for rubber.

2.2.3 Bio-sourced fillers

As discussed in the previous sections, carbon black (CB) and silica are extensively studied and commercially utilized in many rubber products[27,49–52]. Furthermore, other inorganic fillers have also been investigated as rubber reinforcing agents such as nanoclay[53], carbon nanotube[54],

graphene[55], calcium carbonate[56], etc. However, the complicated preparation process along with the associated high cost has limited their industrial use. Most recently, there has been an increased shift from the dependance on fossil fuel feedstock to sustainable materials and this has led to an interest in bio-sourced fillers due to the environmental benefits. Renewable fillers, such as starch[57], chitostan[58], lignin[59], soy protein[60], natural fiber[52], rice husk[61], and eggshells[62] have been reported in the literature. The functional groups on these bio-sourced fillers render them hydrophilic and subsequently incompatible when compounded with rubber leading to poor dispersion and interfacial adhesion. Researchers have used coupling agents such as silane and surface modifiers to improve these problems. Ishak and Bakar[63] compared the epoxidized natural rubber reinforcement of rice husks and commercial carbon black and silica vulcanizates with and without silane coupling agents for all the studied fillers. Their results showed a comparable tensile strength result without the coupling agent and on addition of silane, rice husks showed 4% less strength than CB and silica.

Additionally, cellulosic fillers which will be discussed extensively in the following sections have been sparsely studied and showed promise for highly filled rubber composites. When considering the promise of these renewable fillers, the strength, cost, and abundance are factors that should be considered. While these bio-sourced fillers show promise as a reinforcement for rubber, most of the studies were carried out in rubber films and research on highly crosslinked bio-sourced filled rubber vulcanizates are rather scarce. Nonetheless, the reinforcing effect of these bio-sourced materials do not compare to that of CB due to their difference in dispersibility, structure and interfacial interaction with the rubber, particle size and shape, etc. Cellulose nanocrystals have been studied as a potential filler due to their many benefits including, high aspect

ratio, nano-size and its potential to interact at molecular level, strength, sequestration of carbon, and environmental friendliness.

2.2.3.1 Cellulosic fillers

The use of cellulosic fillers is of high interest due to their many benefits, including safety, carbon sequestration benefits, and environmental friendliness. Cellulose is the most abundant material on earth as it can be extracted from a wide variety of biomass. It is a high molecular weight polysaccharide made up of repeating units of 10,000 to 15,000 β-(1,4)-bound-Dglucopyranosyl[64,65] units which are linked together to form crystalline structures of cellulose or elementary fibrils. Cellulose is rich in hydroxyl functional groups that provide properties, such as chirality, hydrophilicity, and chemical modification. These properties vary based on the source or origin of cellulose and the degree of polymerization. Cellulose in nature consists of crystalline and amorphous phases, depending on the isolation technique and source. Amorphous phases have a lower density compared to crystalline ones and are more prone to react with other molecules. On the other hand, crystalline domains are generally more resistant to mechanical, chemical, biological, and enzymatic treatments[64].

Cellulosic fillers can be utilized in the form of cellulose, microcrystalline cellulose (MCC), and nanocellulose. As cellulose consists of both amorphous and crystalline regions, microcrystalline cellulose (MCC) is the crystalline cellulose obtained after the acid hydrolysis of cellulose fibers to remove the amorphous regions. It typically measures approximately 10-50 microns and 100-1000 microns in diameter and length, respectively. As the particle size is an important parameter for filler reinforcement, recently nano-sized cellulose, which is cellulose based materials with at least one nanoscale dimension has been studied as result of their high specific area and mechanical strength. Nanocellulose, the product of the chemical and mechanical

modification of cellulose, can be classified into bacterial cellulose (BC), cellulose nanofiber (CNF), and cellulose nanocrystals (CNC). Bacterial cellulose, synthesized by fermentation methods using bacteria, with diameter between 20-100 nm micrometer length, is employed in medical applications because it is resistant to mechanical wear while being soft and elastic[66]. Cellulose nanofibers, obtained via a mechanical process with diameters between 5 to 30 nm and length in microns and comprise of amorphous and crystalline regions[67]. Finally, cellulose nanocrystals, a highly crystalline biomaterial is obtained from acid hydrolysis of cellulose to extract the amorphous regions. Dissolving the amorphous part produces tiny rod-like particles of CNC with diameter ranging from 5-10 nm and lengths in hundreds of nanometers[67,68]. The crystallinity and size of CNCs impart high strength and high specific surface area, making it suitable as a reinforcing filler. As CNC can reinforce rubber due to its desirable qualities, the rest of this study focuses on CNC as a reinforcing filler for natural rubber.

2.2.3.2 Cellulose nanocrystals (CNC) filled rubber vulcanizates

CNC has been studied as a potential filler for rubber due to its high specific surface area (ca 400 g/cm)[69], high strength and modulus (100-150 GPa)[69,70], high aspect ratio, low density (1.556 g/cc),[71] biocompatibility, bioavailability, and biodegradability which make CNCs promising nanofillers for rubber[72]. In addition, the abundant surface hydroxyl groups (hydrophilic) of CNCs facilitate various chemical surface modifications.[58] Cellulose nanocrystals can be obtained from plants and animal sources (e.g., bacteria and aquatic tunicate), though most of the CNCs available in the market are produced from wood cellulose[64]. Compared to other fillers, the incorporation of CNC in a rubber matrix enhances the mechanical properties of the nanocomposites at relatively low loading levels than conventional composite fillers due to its size, high crystallinity, and aspect ratio[73]. Additionally, this behavior can be attributed to molecular

level interactions, and strong intermolecular forces, such as covalent bonds, van der Waals forces, mechanical interlocking, and molecular entanglements between the CNCs and the rubber matrix[74].

The key parameters for preparing high-performance rubber composites are the improvement of the filler dispersion and the filler rubber interaction[75]. The compatibility between the rubber and the filler is a key determinant of the dispersion of the filler in the rubber matrix. Due to the high density of surface hydroxyl groups and high surface energy of CNC (highly hydrophilic), the particles tend to aggregate and agglomerate, making the dispersion of CNC in the hydrophobic rubber matrix problematic. The resulting composite is typically non-homogenous with uneven large particle size filler dispersion and poor rubber-CNC interactions (**Figure 2.4**). As a result, the CNC aggregates act as a stress concentrator, resulting in cracks from the agglomerates under tension. Furthermore, the poor compatibility between the hydrophilic CNC filler and hydrophobic rubber matrix results in poor interfacial bonding, thereby causing porous structure and creating weak points in the nanocomposite[1]. Other parameters such as the crosslinking density, the type of crosslinks, and the type of rubber also affect the properties of the rubber composite[76].

To improve the dispersion and achieve a positive reinforcing effect, the following CNC treatment strategies have been reported: physical modification, compatibilizing treatment, surface modification, the use of coupling agents, filler hybridization, and effective mixing methods to improve dispersion[59].

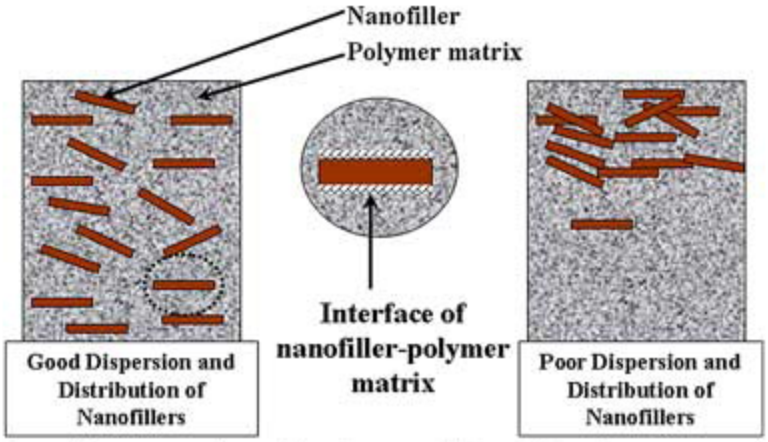

Figure 2.4. Schematic representation of poorly dispersed CNC in rubber showing aggregates of CNC and poor interfacial bonding with matrix (Adapted with permission from Subrata Mondal[45]

2.3 Parameters affecting the reinforcing effect of fillers

The properties of nanocomposites depend largely on the characteristics of the fillers. The parameters that determine the reinforcing effect of the filler includes the filler geometry (particle size, particle shape, particle surface area) and the filler surface activity.

2.3.1 Particle and aggregate size and shape

The size, distribution, and shape of fillers in the matrix are considered important physical properties of the reinforcing effect of fillers. Particularly, the particle size or specific surface area, along with the loading levels impacts the effective contact area of the filler and matrix. It is well known that materials with high strength can reinforce rubber on the condition that it is in a finely divided state and can be dispersed in the polymer matrix. Carbon black for instance has grade dependent reinforcement properties determined by their particle size. The grades with particle diameter above 300 nm show little reinforcement, 100-200 nm grades are termed semi-reinforcing,

grades with sizes of about 40 nm provide high abrasion, and the super-abrasion grades have particle diameters below 35 nm[77]. The particle size can also be affected by the degree of dispersion (aggregates) of the filler in the matrix. For instance, a poorly dispersed nanosized filler forms micro-sized aggregates in the polymer matrix which could act as gritty particles causing cracks under tension.

The morphology of CNC, which varies slightly upon the cellulose source and the nanocellulose preparation conditions, is typically rod-shape (**Figure 2.5**) with length ranging from 50-1000 nm and width from 3 to 50 nm[78]. Thus, the aspect ratio, defined as the ratio of length to width of CNC, is high (10-100). The nanoscopic morphological features of CNCs affect the macroscopic properties of the nanocomposite like rheology, cure properties, and mechanical reinforcement. For instance, the formation of the CNC-polymer network depends on the percolation threshold that relies on the shape, aspect ratio, and filler-filler interactions[79]. Simply put, the higher the aspect ratio, the lower the loading of filler required to reach percolation (the continuous network of filler along a path). Therefore, a lower loading of CNC is required to attain percolation compared to carbon black or silica which are spherical. A percolated filler network provides better reinforcement and minimizes tear propagation of the composite[72,80]

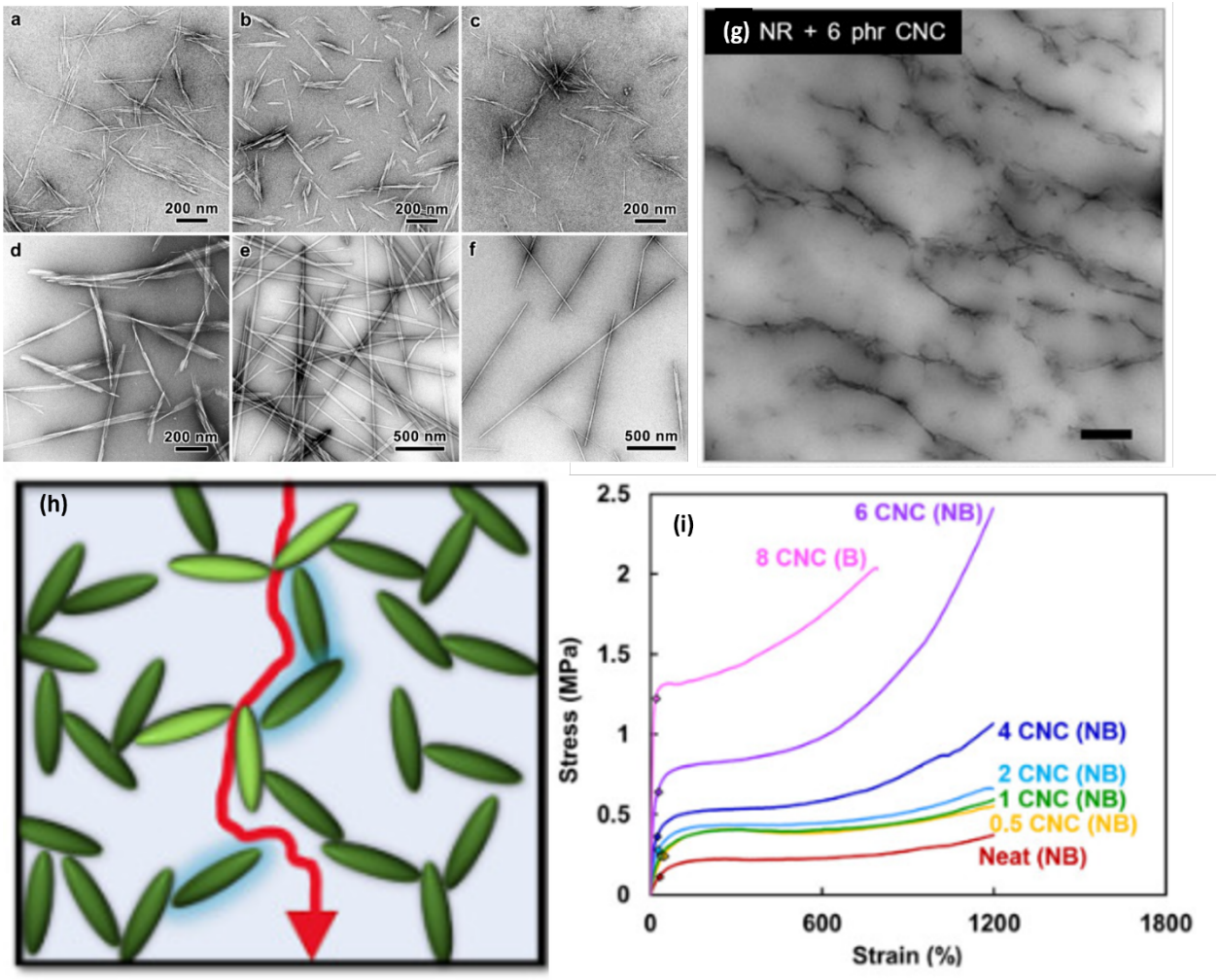

Figure 2.5. TEM images of CNCs from various origins: (a) wood, (b) cotton, (c) bamboo, (d) Gluconacetobacter cylinus, e) Glaucocystis, f) Halocynthia papillosa[81](Adapted with permission from Kaushik *et al.* [81]); fully percolated CNC network (g), slower tear propagation resulting from percolated CNC network (h) tensile curve showing increase in tensile strength with increased CNC loading (i) of CNC filled natural rubber composite (Adapted with permission from Jardin *et al.*[82])

2.3.2 Filler-Matrix Adhesion

2.3.2.1 Surface activity of CNC

Phase compatibility is an important determinant of the dispersion and interfacial adhesion between the matrix and the filler. Depending on the nature of the fillers, compatibilizers, or surface treatment can be employed to mitigate the polarity difference. For instance, silane coupling agent has been reported to be effective due to its dual functional groups that allow one functional group to form a covalent bond with the filler and the other with rubber[83–85]. Silane modification can be carried out on cellulosic materials due to the abundance of surface hydroxyl groups available for grafting reactions.

2.3.2.2 Silane modification of CNC for rubber composites

Silanes are extensively used as coupling agents in composites due to their large-scale commercial availability. Several researchers have used silane as a coupling agent to improve dispersion in a non-polar matrix. Kargarzadeh *et al.*[86] treated CNC with N-(β-aminoethyl)-γ-aminopropyl-treimethoxysilane and prepared a composite of unsaturated polyester resin toughened with natural rubber. They reported well-dispersed CNC in the matrix and improved tensile strength, modulus, and viscoelastic behavior of the nanocomposite. Similarly, Yu *et al.*[87]. modified CNC using 3-isocyanatepropyltriethoxysilane (IPTS) for the reinforcement of rubber. Compared to the neat CNC, the silylated CNC showed improved dispersion and reinforcing effect owing to improved dispersion and interfacial adhesion.

The general mechanism of the silylation reaction with CNC is presented in **Figure 2.6** below. In the first step of the reaction, an aqueous solution containing the silane is first hydrolyzed with a weak acid and the alkoxy group on the silane is replaced by the hydroxyl groups to form

silanol. The silanol then self-condenses to form Si-O-Si bonds by the removal of water, and finally, the intermediate silanol groups react with the OH groups on CNC.

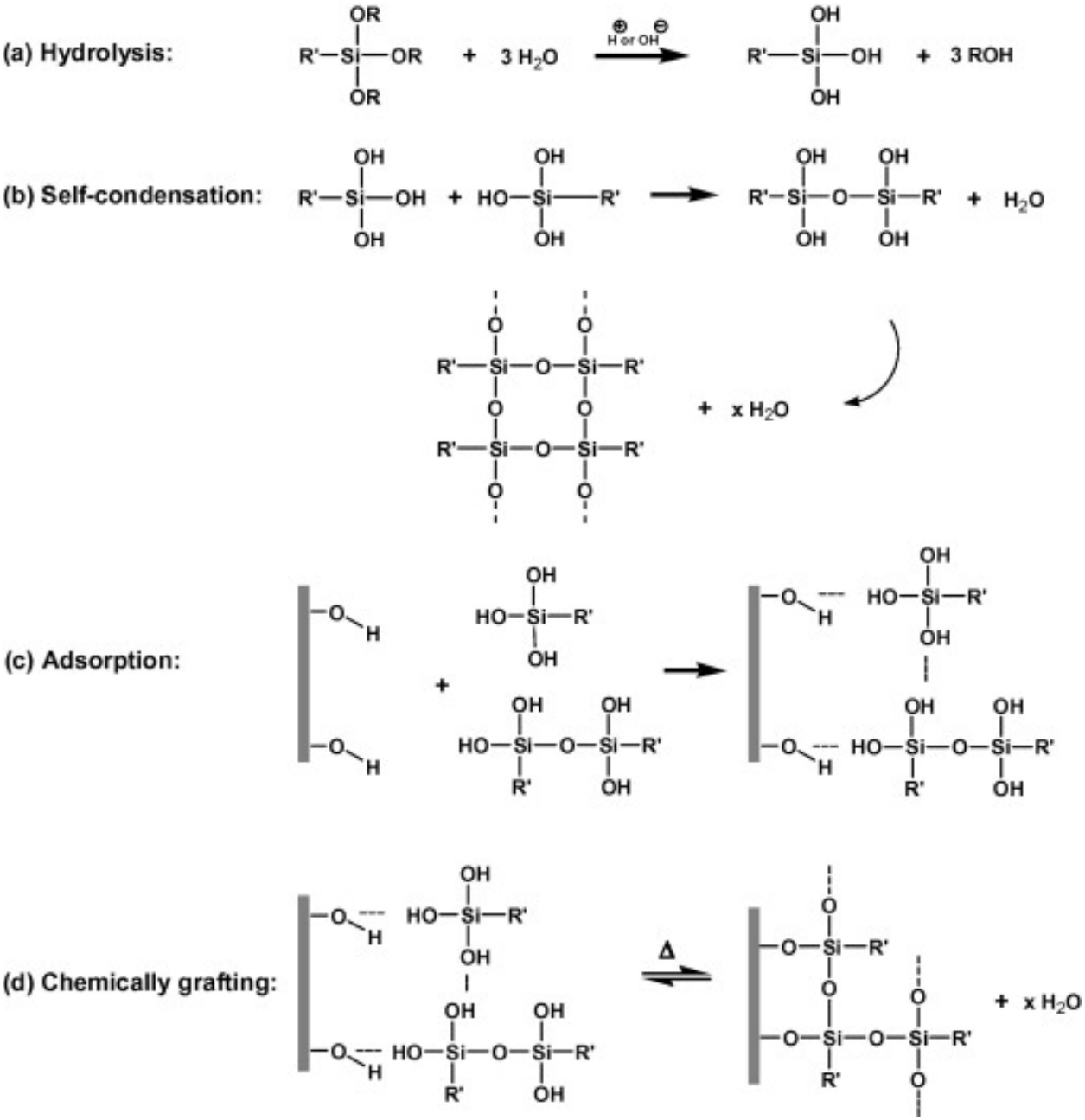

Figure 2.6. Reaction mechanism of silane coupling agent and CNC (Adapted with permission from Xie *et al.* [88])

2.3.2.3 Other modification of CNC for rubber composites

Shafik[89] modified CNC using a cationic surfactant hexadecyl-trimethylammonium bromide (CTAB) and prepared a bio-composite of varied loadings of the modified CNC and natural rubber using a two-roll mill. Results revealed a decrease in curing time of the modified CNC composite compared to the pristine CNC composite, indicating that CNC modification accelerates the curing process and an increase in tensile strength of the modified CNC filled rubber composite up to 5 phr loading level and a decrease beyond that. In another study, Imiete *et al.*.[90] partially desulfated CNCs and prepared a composite with rubber using silanes as compatibilizing agents. Comparing the results from the modified CNC composites and pristine CNC composites, they reported increased mechanical properties, reduced loss in storage modulus at low strains, and reduced tan delta indicative of reduced Payne effect and rolling resistance. Although CNC modification is widely studied in the literature, studies of CNC modification and fabrication for highly filled natural rubber composites is rather scarce.

2.3.3 The effect of fabrication method on rubber-CNC composites

The method of fabrication of the nanocomposite affects the dispersion and properties of the composite material. The physical properties of the nanocomposite depend on the dispersion of the filler in the matrix. Therefore, the fabrication technique employed must ensure optimal dispersion of the nanoparticles in the matrix and provide sufficient shear stress to break down the aggregates. Various methods have been employed to produce rubber-CNC nanocomposites. The common ones are latex mixing, two-roll mill, batch mixing, and extrusion.

2.3.3.1 Latex mixing

Latex mixing also known as co-coagulation is a common fabrication method for rubber-CNC composites[91–93]. The method involves the addition of the CNC dispersed in a suitable medium into the rubber latex. The rubber composite mixture is then coagulated using a suitable acid to prepare a masterbatch for further processing[93] or made into films by casting/evaporation method[91,92]. The unit operations for the masterbatch preparation as presented in **Figure 2.7** involves the dispersion of the CNC in an aqueous medium, homogenization of dispersed CNC in rubber latex, coagulation of the mixture by the addition of acid, and drying to obtain CNC incorporated rubber. Alex *et al.*[94] compared the mechanical properties of rubber filled rubber vulcanizates fabricated by latex compounding and two-roll mill to elucidate the mixing efficiency using this method. Results showed improved mechanical properties of composites prepared by latex compounding attributed to the improved dispersion of the nanofiller in the liquid phase. Similarly, Ojogbo *et al.*.[95] compared different processing methods of CNC-NR composites including batch mixing, co-coagulation, and extrusion to elucidate the optimal processing method to achieve desirable physical properties. They reported optimal dispersion using the co-coagulation processing method as revealed by transmission electron microscopy and improved mechanical properties compared to the other processing methods resulting from the superior dispersion.

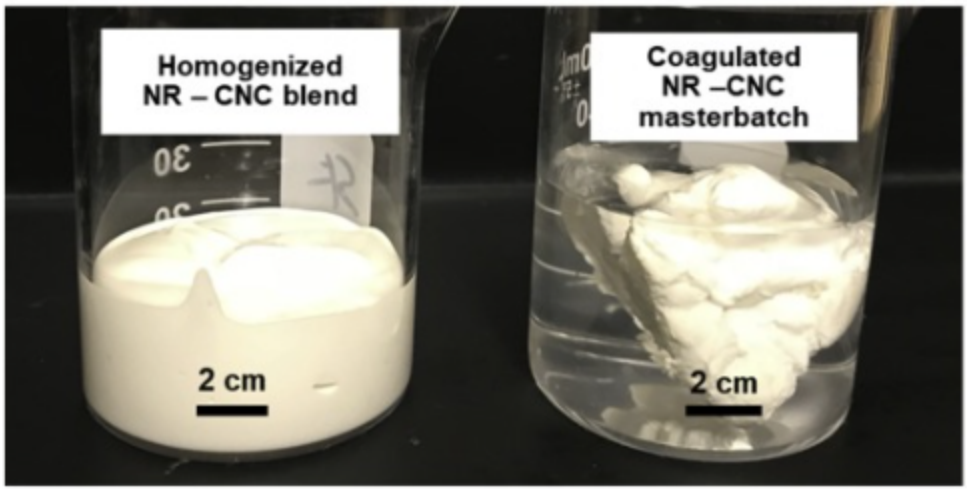

Figure 2.7. Homogenized NR-CNC blend and Coagulated NR-CNC masterbatch (Adapted with permission from Mekonnen *et al.*[96])

2.3.3.2 Two roll-mill

The two-roll mill method is widely used for mixing and masticating rubber, rubber blends, and rubber composites. This method of mixing is carried out using two counter-rotating hollow metal cylindrical rotors as presented in **Figure 2.8.** The rotors possess slightly different speeds called the friction ratio, which enables the rubber to experience a pressure that increases the displacement energy and breaks the rubber molecule bonding[53,97]. This shearing action and breakage allows the compounding ingredients to be uniformly mixed with the rubber. Parameters such as the nip gap, speed, friction ratio, mixing direction, and sequence of addition of ingredients can affect the filler dispersion[98]. The two-roll mill can also be employed for sheet masticating and compounding using other fabrication methods. Visakh *et al.*[99] prepared CNC-rubber nanocomposites by roll milling and showed that a masterbatch based on latex followed by roll milling produced CNC-rubber nanocomposites with improved mechanical properties compared to using either of the processing methods. The mill compounding has two major advantages: high shear dispersion provided by the nip, which breaks down agglomerates and surface exposure that

minimizes heat buildup from torque, thereby retaining stiffness. The disadvantages on the other hand include the number of mixing cycles, exposure to dust and dirt during mixing, the challenge in controlling batch to batch uniformity, and strong dependence on operator skill.

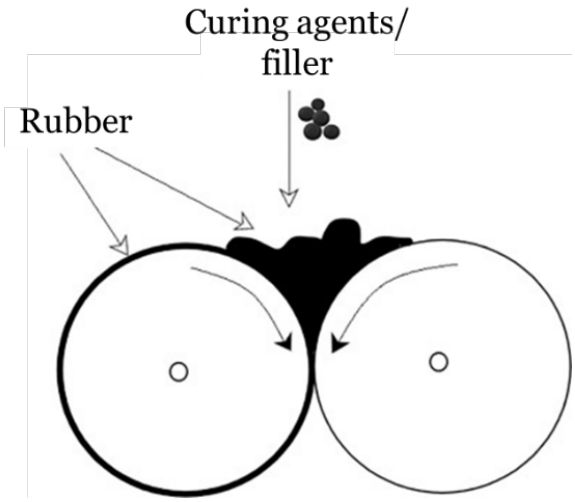

Figure 2.8. Rubber mastication showing the addition of curing agents and/fillers using the two-roll (Adapted with permission from Fan *et al.* [27])

Other methods of fabrication by dry blending include internal batch mixing and extrusion. These methods involve the addition of dried CNC into the processing unit during mixing. The batch mixer has two non-interlocking rotors operating at slightly different speeds that aid in the mixing of the CNC in the rubber. The mixing is done between the rotors and the walls of the batch mixer and between the rotors themselves. Due to the non-interlocking nature of the rotors, the mixing is more distributive than dispersive at the nanoscale. The extruder, on the other hand, contains two intermeshing screws that aid the shearing of the CNC in the matrix[100].

2.4 Nanocomposite Property Characterization

2.4.1 Vulcanization/ Cure Characteristics

Natural rubber is made up of long chains of cis 1,4- polyisoprene, which move independently to each other. In an uncured state, NR is sticky, elastic, has poor weathering conditions, swells in solvent at elevated temperatures, and shows poor fatigue resistance. Therefore, to make rubber a useful and durable material, uncured rubber is cured in a vulcanization process to modify the polymer by forming crosslinks between the individual chains to improve elasticity, resilience, and mechanical properties[101]. Vulcanization is a chemical process in which the individual rubber chains are cross-linked to form a strong three-dimensional network by the insertion of polysulphide bonds[102] as seen in **Figure 2.9** below. Compounding ingredients such as vulcanizing agents, activators, antioxidants, accelerators, extenders, and fillers are incorporated during vulcanization.

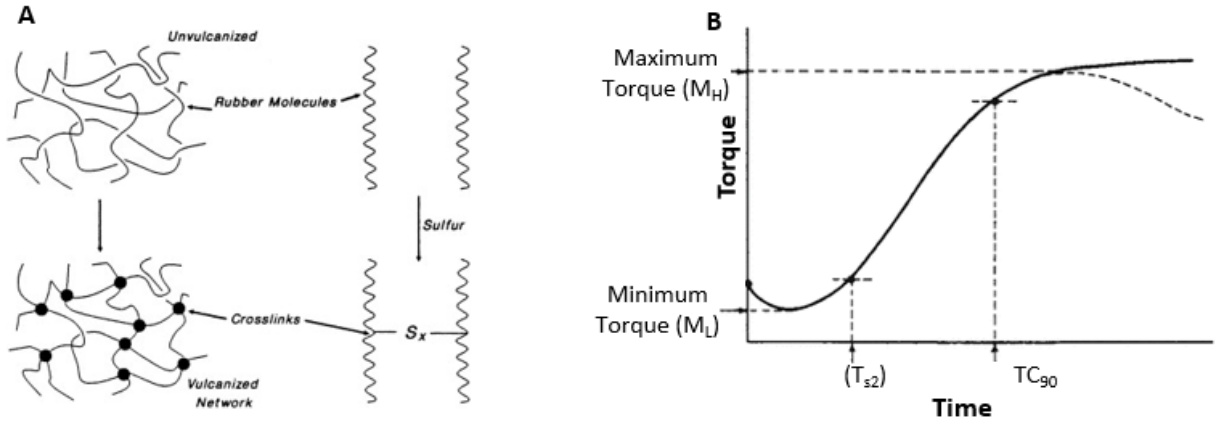

Figure 2.9. (A) Network formation of rubber chains via the vulcanization process (Adapted with permission from A.Y Coran[103]) and (B) rheometic data showing the different stages of vulcanization (Adapted with permission from Jacques W.M. Noordermeer [104])

The cure properties test that provides information regarding the vulcanization of rubber is carried out using a die rheometer and the rheometric data obtained (**Figure 2.9B**) are defined as minimum torque (M_L) which is the lowest viscosity of the rubber compound at the start of the vulcanization, maximum torque (M_H) which is the highest viscosity reached by the rubber compound during vulcanization, scorch time (T_{S2}) which is the elapsed time at a given temperature before the rubber vulcanization begins, and optimum cure time (TC_{90}) which is defined as the time taken for the torque to reach 90% of its maximum value. Generally, the introduction of fillers increases the viscosity and chain restriction of rubber composites because of filler reinforcement and hence, increases the maximum torque. This torque value increases with filler loading. Several researchers have reported the decrease in scorch time with the increase in filler loading due to the restriction of chain mobility and the deformation of the matrix caused by the mechanical filler restraints[105,106].

2.4.2 Mechanical Properties

As reinforcing fillers are incorporated to improve the strength of the composites, the mechanical property is a very important parameter in analyzing composites. The mechanical properties of filled nanocomposites show an increasing trend with filler loading at optimal filler concentration provided that the dispersion and interfacial bonding are good. The modulus, and hardness, which provides information on the rigidity of the composite, increases with filler loading. Bendahou *et al.*[107] studied the tensile properties of cellulose nanowhiskers as reinforcing fillers in rubber. The study showed that the mechanical properties could be substantially improved depending on the amount of filler, dispersion in the matrix, and the formation of percolating network formed by hydrogen bonding above the percolating threshold[107]. The elongation at break on the other hand decreases with filler loading. This was because the filler deforms much less than

the matrix, therefore the filler withstands a higher deformation and improves the overall deformation response of the composite.

2.4.3 Swelling Behavior

The degree of swelling of composites is an important parameter to evaluate the filler-rubber interactions and to analyze the performance of nanocomposites upon contact with solvents. It has been reported that one characteristic of filled vulcanizates compared to unfilled vulcanizates is the reduction of swelling in solvents[108]. Although vulcanized rubber composites cannot be solubilized completely by any solvents, they swell. When the filler bonds effectively to the rubber matrix, it restricts the swelling of the composite. During swelling, small mobile molecules diffuse into the chain segments of the rubber. In the beginning, the surface of the rubber has a high liquid concentration while the concentration of the bulk is zero. As the diffusion proceeds, uniform swelling is achieved throughout the rubber chains and equilibrium swelling is reached. The swelling behavior can be correlated to the crosslink density by the Flory Rehner equation and for a given solvent, the higher the crosslink density, the lower the swelling. In a study by Da Costa *et al.*[108] to investigate the utilization of rice husk ash (RHA) as an alternative filler for natural rubber, they reported a deviation from linearity of the swelling-crosslink density correlation. This was attributed to the weak adhesion forces between the RHA and rubber and void formation, the spacing between particle and vulcanizates filling up with solvent.

2.4.4 Viscoelastic Behavior

The interactions in the rubber nanocomposites can be elucidated by studying the viscoelastic properties, using a rubber processing analyzer, and the so-called Payne effect (reduction of storage modulus with applied strain/deformation). Payne[30,109] reported the following contributions to the

reinforcement of filled elastomer: I) the crosslink density, II) the hydrodynamic effect of the filler, III) the rubber-filler interactions, and IV) the filler-filler interactions. While the first three are independent of deformation, the last one is quantified by a loss in storage modulus (G') with applied strain/deformation. When deformation is applied, the weak filler network is broken down releasing the trapped rubber between the filler particles and increasing mobility of the elastomer, followed by a loss in G".

Carbon black is known for forming a filler-filler physical network in the rubber matrix (**Figure 2.10A**) and at low strains, this network is disrupted (**Figure 2.10B).** When the strain is removed, the network reforms. This disruption and formation of network generates heat and leads to high rolling resistance in tires. The tire industry has developed highly filled silica tires with lower Payne effect and low rolling resistance with improved traction, low fuel consumption, and similar wear life compared to CB filled tires[110].

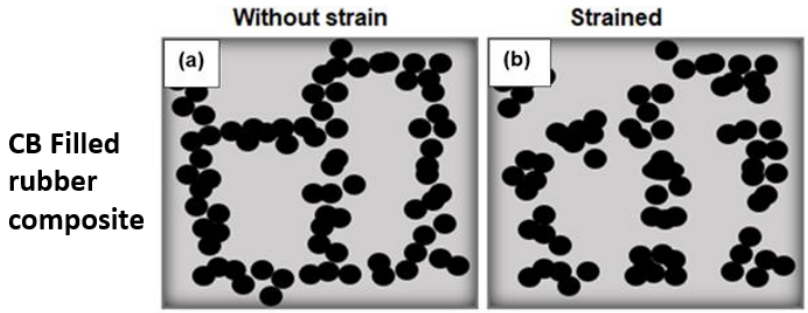

Figure 2.10. Network formation without strain (A) and network disruption with strain (B) of carbon black in rubber matrix.

2.5 Potential applications for rubber CNC composites

Due to the unique combination of properties of CNC and natural rubber, composites based on NR-CNC holds promise. The incorporation of CNC in natural rubber enhances the physico-mechanical properties that can be used for various applications. Furthermore, depending on the

desired properties of the nanocomposite, CNC can be tailored to provide unique properties. While it is important to note that research in this field is ongoing, and the applications of NR-CNC composites continue to expand as more studies explore their properties and potential uses, this section presents some applications.

One important application is sustainable tires. Sustainable tires are obtained from renewable feedstock and exhibit low rolling resistance[111]. Low rolling resistance is important for sustainable tire applications because of reduced fuel consumption and low carbon emissions. In a study by Dominic *et al.*.[111] to explore the hybridization of carbon black and CNC from rice husk, their dynamic mechanical analysis revealed a high value of loss tangent at 0 ^{o}C and lower value at 60 ^{o}C compared to the composites filled with carbon black alone. This indicates better wet grip and lower rolling resistance in tires respectively which translates to lower fuel consumption and carbon emissions from vehicles.

Another application for NR-CNC composites is in masterbatch preparation to be utilized as fillers for other hydrophobic rubbers to enhance the CNC dispersion. Mekonnen *et al.*[96] investigated the co-coagulation of natural rubber latex in aqueous solutions. The aim of the study was to provide masterbatches of CNC-natural rubber composites. The utilized natural rubber latex with a suspension of dispersed CNCs and evaluated the filler loading and most efficient coagulant that provides optimal dispersion of CNC in the coagulated rubber. Their results showed excellent dispersion using formic acid as coagulant and investigation of the properties of the vulcanized rubber composites revealed improved tensile strength and modulus. Based on these properties, the masterbatch of well dispersed CNC in rubber can be employed as a filler in other rubbers to enhance the dispersion in the rubber matrix.

Chapter 3. Effect of extrusion, batch-mixing, and co-coagulation on the dispersion of CNCs in Natural rubber - CNC nanocomposites[1]

3.1 Introduction

The practical use of natural rubber (NR), styrene-butadiene rubber (SBR), polybutadiene (BR), and other rubber in their native form is limited because of their low strength and undesirable responses to environmental conditions. Rubber vulcanization, a chemical process that creates crosslinks between the long rubber chains, transforms the rubber from a material with low modulus and tensile strength into a tougher material with improved tensile properties [1,112]. In addition to vulcanization, many practical applications of rubber involve incorporating fillers, primarily to enhance their physical and chemical properties and to reduce costs. For instance, rubber applications requiring high strength and stiffness, such as tires, conveyor belts, and footwear, need to be filled with carbon black and other mineral fillers. The presence of the fillers improves the abrasion resistance, tear, tensile properties, hardness, resistance to chemical attack, and overall durability. Carbon black has been extensively studied and is widely used as a filler in tires and several other rubber products and as a color pigment in paints, plastics, and inks [8]. It is reported that an estimated 70% consumption of carbon black is employed as a filler in tires for strength and wear resistance [9]. Carbon black, which is obtained from the incomplete combustion of petroleum products, utilizes high energy during production and contributes to greenhouse gas emissions and climate change. Moreover, according to the international agency for research on cancer, inhalation

[1] A version of this chapter has published in a peer-reviewed journal. Ojogbo E, Tzoganakis C, Mekonnen TH. Effect of extrusion, batch-mixing, and co-coagulation on the dispersion of CNCs in natural rubber - CNC nanocomposites. *Compos Part A Appl Sci Manuf*. 2021;149:106580. doi:10.1016/J.COMPOSITESA.2021.106580

of carbon black is associated with health problems such as respiratory and cardiovascular diseases, cancer (Group 2B), and congenital disabilities [10,11]. Also, the density of this filler results in increased weight of the rubber composite, which defeats one of the remarkable properties of rubber, being a lightweight material. For these reasons, developing and utilizing bio-based and sustainable nano-reinforcements as a replacement or complement of carbon black to mitigate its health and environmental impact is of great interest.

Cellulose nanocrystals (CNCs), due to their renewability, biodegradability, low-density, nontoxicity, and high strength [13,14,113], are potential substitutes or complementary additives to carbon black in rubber applications. Also, CNCs are rich in surface hydroxyl moieties, which are amenable to several chemical modifications, enabling the tailoring of CNCs to a wide range of applications. It is hypothesized that using CNCs as a substitute or complementary reinforcing filler in rubber will mitigate the high energy consumption, increase in greenhouse gases, and environmental impact associated with carbon black production. Although CNCs present several advantages, their poor dispersion in elastomers resulting from the lack of interfacial adhesion between polar CNCs and non-polar elastomers in conjuncture with deficient processing methods that do not break CNC aggregates and agglomerates limits the touted potential of CNCs as efficient reinforcing fillers.

The physical properties of nanocomposites are influenced by stress transfer from the matrix to the filler and the stress concentration in the composites. Therefore, the fabrication technique employed must provide sufficient shear stress to break down aggregates and ensure optimal dispersion of the nanoparticles in the matrix[114]. Various methods such as co-coagulation, mastication with roll mills, batch mixing, and extrusion have been employed to fabricate rubber composites. However, most reported works on CNC-rubber composites studied lightly crosslinked

rubber and prepared samples by solution casting[91,92,115–118]. Limited research results are reported in the literature concerning NR-CNC vulcanizates, with high crosslinking density formulation considerations[119,120].

Two-roll mill is widely used in the rubber industry for masticating rubber and breaking down agglomerates. However, it has the disadvantage of uncontrolled batch uniformity and a high number of mixing cycles resulting from pan sweeping to recover any dropouts[121]. Co-coagulation that entails latex mixing with fillers or additives is among the most popular rubber composite fabrication methods, which displays improved mechanical properties of filled rubber vulcanizates[94]. Processing in an internal batch mixer and an extruder involves dry blending of CNCs with rubber in the processing unit at an elevated temperature. By employing these processing methods at varied mixing conditions, the dispersion of the CNCs can either be distributive, dispersive, or a combination of both.

Due to the limited studies on NR-CNC vulcanizates in the literature[99], this work seeks to advance the knowledge of dispersing CNCs in highly crosslinked rubber composite formulations. Additionally, to the best of our knowledge, a comparison of the effect of the fabrication method on the dispersion of CNCs or other nanofillers in rubbers has not been studied. Thus, results and approaches employed in this study can be adopted in other filler systems as well. NR was chosen as the model rubber system because of its sustainability attribute similar to CNCs. Moreover, NR has an excellent balance of physical properties such as high elasticity, excellent tear resistance, and overall toughness compared to other synthetic rubbers. The dispersion of CNCs in the rubber matrix was investigated by employing batch mixing, co-coagulation, and extrusion to achieve an optimal method for the dispersion of CNCs in the rubber matrix. The rheological and physical

properties of the resulting rubber vulcanizate composites were investigated and correlated with the processing and fabrication methods.

3.2 **Materials and methods**

3.2.1 Materials

CNCs with nominal length, width, aspect ratio, and sulphur content of 150 nm, 7.5 nm, and 20 nm, 5000-9000 mg/kg, respectively, were supplied as spray-dried powder by CelluForce Inc (Quebec, Canada). NR latex (ammonia stabilized, 65 wt.% solids) was purchased from Chemionics Corp (OH, US). Formic acid, zinc oxide, stearic acid, N-tert-2-benzothiazyl sulfonamide (TBBS), and sulphur were purchased from Sigma-Aldrich. Polycoat 323HS anti-tack was purchased from Sasco Chemical group (GA, USA).

3.2.2 Methods

3.2.2.1 CNCs dispersion in NR latex

CNCs were dispersed in deionized water (5 wt.%) and sonicated for 30 min using a Fisher brand ultra sonicator. The size distribution of the sonicated CNCs in water was evaluated using a Zetasizer (Nano ZS90) by diluting it to 0.1 wt. %. Calculated amounts of the CNC - dispersion were slowly poured into a beaker that contained NR Latex (65 wt.%) to prepare samples that would contain 2.5%, 5%, 7.5%, and 10% of CNCs in the NR latex calculated on a dry weight basis. During the preparation of the NR latex and CNC dispersions, values were always adjusted to ensure that a 200 g batch of final dried product was produced. The NR-CNC dispersion mix was then stirred for 5 min using a glass stir rod and then blended using a handheld blender (Hamilton Beach 59766C) (medium setting) for 30 min. After blending, the CNC/NR latex mixture was

placed in a bath sonicator (Fisher Scientific, CPX2800 Ultrasonic, high setting) for 10 min to obtain a stable NR latex-CNC dispersion. These mixtures were consistently prepared for all coagulation studies. The thorough mixing of both the CNC/water and CNC/NR latex are expected to provide excellent encapsulation of the CNC particles by the NR latex.

3.2.2.2 Co-coagulation of NR-CNCs nanocomposites

The blended NR-CNC dispersions were co-coagulated using 25% v/v formic acid. For this, the NR-CNCs latex mixtures were slowly poured into a glass bowl containing the formic acid solution. After it appeared that coagulation had been fully induced, determined by the amount of liquid latex present and clarity of the ejected solution, the NR-CNC coagulated master-batch was separated and thoroughly washed with deionized (DI) water. The coagulated latex was then cut into approximately 2.5 cm cubes and thoroughly washed once again with DI water to remove residual formic acid. The masterbatch cubes were placed in an oven at 80 °C and allowed to dry to constant weight. NR samples containing no CNCs were prepared using the same method to prepare control samples for the subsequent processing and fabrication studies.

The coagulated NR-CNCs or NR latex solids were passed through a two-roll mill several times to form a thin sheet. The sheets were then cut, dipped in liquid nitrogen, and ground to pellets (approximately 0.1-inch) using a Wiley mill (model No. 2) industrial grinder into a bowl containing an anti-tack agent (Polycoat 323 HS) to prevent the pellets from sticking to each other and dried at room temperature before further processing. The NR control and the NR-CNCs masterbatches were pelletized before processing to ensure consistency with the extrusion and batch-mix processing methods.

3.2.2.3 NR-CNC nanocomposites fabrication

To process and prepare the samples for testing, the NR-CNC nanocomposite pellets containing different levels of CNCs were masticated in a two-roll mill into sheets. The curing agents were then incorporated in folded sheets portion by portion according to the recipe shown in **Table 3.1** and further processed with the two-roll mill five times. For comparison, NR control without CNC was processed similarly and kept for further characterization.

Table 3.1. Formulation composition for NR-CNC nanocomposite

Ingredients	**Sample Codes**				
	NR-0% CNC (Control)	NR-2.5% CNC	NR-5% CNC	NR-7.5% CNC	NR-10% CNC
NR	100	100	100	100	100
Sulphur	1.5	1.5	1.5	1.5	1.5
Stearic acid	1	1	1	1	1
TBBS	1.5	1.5	1.5	1.5	1.5
Zinc oxide	3	3	3	3	3
CNC	0	2.5	5	7.5	10

3.2.2.4 Fabrication by batch mixing

For samples fabricated by batch mixing, the rotors were set to a speed and temperature of 80 rpm and 50 ^{o}C, respectively. Approximately 200 g of coagulated NR was added into the batch mixer (Haake Rheocord 90) and masticated until constant torque (approximately 3 mins) was achieved. The curing agents were then added slowly and allowed to mix for approximately 3 mins, and finally, calculated concentrations of CNCs were added and mixed for another 4 mins. The total

mixing time was 10 mins. The concentrations of CNCs incorporated into the NR ranges from 2.5% to 10% (dry weight basis) as shown in **Table 3.1.** The NR-CNCs nanocomposites produced were then passed through the two-roll mill to make sheets for curing.

3.2.2.5 Fabrication by extrusion

Samples for the extrusion study were prepared by moistening the coagulated NR pellets with DI water, mixing with measured amount of CNCs (ranging from 2.5% to 10%). and drying to a constant weight for ease of feeding into the extruder. The extrusion was carried out in a twin-screw mini extruder (Prism USALAB 16 mini extruder) with five heating zones. The extruder screw speed was set at 200 rpm and the temperature was set at 50 ^{o}C in the screws and 80 ^{o}C in the die (actual temperature ranged between 50 to 85 ^{o}C in the screws and 100 ^{o}C in the die). To arrive at the screw speed and temperatures used in this study, an optimization study was carried out according to **Table 3.2** for the 10% CNCs with tensile properties as an output. For the extrusion, the CNC coated rubber pellets were fed into the extruder at an average feed rate of 8.5 g/min. The mixed nanocomposite was transferred to the two-roll mill where the compounding agents were added according to the recipe in **Table 3.3.** After adding all components, the nanocomposite was milled several times in the grain direction in preparation for vulcanization.

Table 3.2. Design of experiment for extrusion of rubber composite (10 wt. % CNCs)

Screw temperature	50 ^{o}C			100 ^{o}C			150 ^{o}C
RPM	200	250	300	200	250	300	300

3.2.2.6 Vulcanization process

The vulcanization of all premixed samples was carried out in an electrically heated hydraulic press (Pasadena Hydraulics Inc., model. P-215C, CA, USA) that has a 45 cm × 45 cm platen, at 165 ^{o}C and 1.2 MN using approximately 70 g of samples. The respective vulcanization time used was determined by the cure property test results shown in **Table 3.3**and varied with the amount of CNCs present in the composites. The composites were vulcanized to their respective optimum cure time (TC_{90}). The rubber vulcanizate sheets were removed from the hot press and transferred into DI water to quench the vulcanization process. The sheets were then conditioned for 24 h at room temperature before testing.

3.2.3 Characterization

3.2.3.1 Cure characteristics

The cure properties and Mooney viscosity of the composites were determined using a rubber process analyzer (Pioneer MDR 2000) as per ASTM D 2084 and ASTM D1646-19A, respectively. For the cure property test, about 5 g of the samples were placed in the lower die and the test was carried out at 165 ^{o}C. The torque as recorded by the torque transducer in the upper die was plotted as a function of time on the cure graph. The data recorded from the torque-time graph were the minimum torque (M_L), scorch time (T_{S2}), and optimum cure time (T_{90}) as presented in **Table 3.3.**

Table 3.3. Cure properties of NR-CNC vulcanizates.

	NR (Control)	NR-2.5% CNC	NR-5% CNC	NR-7.5% CNC	NR-10% CNC
M_L (lb-in)	0.63	0.49	0.46	0.42	0.50
Ts_2 (min)	3.23	3.31	3.09	3.00	2.97
Tc_{50} (min)	3.36	3.46	3.25	3.18	3.17
Tc_{90} (min)	3.86	3.96	3.73	3.66	3.60
M_H (lb-in)	5.85	6.09	6.45	6.71	7.60

3.2.3.2 Transmission electron microscopy

Transmission electron microscopy (TEM) (Philips, CM 10) study was performed to evaluate the dispersion of the CNCs in the rubber matrix. Cryotomed sections of samples at -80 ºC for NR and NR containing 2.5% CNC from all fabrication methods were analyzed. For this, the cryo-microtomed sections were placed on a copper grid and imaged on the TEM at 300 kV.

3.2.3.3 Tensile properties

The tensile behavior of the NR and NR-CNC dumbbell nanocomposite specimens were analyzed using an Instron universal tensile testing machine with a load cell of 2 kN as per ASTM D 412. Test specimens were cut from the vulcanized sheets along the mill grain direction. The

tensile strength, elongation, and modulus measurements were carried out at a crosshead speed of 500 mm/min. Five replicates were tested and analyzed for each formulation.

3.2.3.4 Hardness test

The hardness test was conducted according to ASTM D2240 using Shore A digital durometer. The specimens stacked to approximately 6 mm thickness were placed on a hard flat surface and the indentor for the instrument was pressed into the specimen. Readings were taken within 1 s after the indentor established firm contact with the specimen. Readings were taken at 3 points and the mean was calculated.

3.2.3.5 Toluene swelling studies

Rubber vulcanizate swelling in toluene was employed to estimate the changes in crosslink density. Samples weighing approximately 0.2 g were cut from each specimen and immersed in toluene at room temperature until equilibrium swelling was attained for all samples (72 h). The weight of each sample was recorded at intervals of 24 h by blotting the excess surface toluene with wipes and immediately weighing the sample. The volume fraction of the rubber, V_r, in the swollen network was calculated using equation 3.1 [122,123].

$$V_r = \frac{m_1/\rho_1}{\frac{m_1}{\rho_1}+\frac{m_2}{\rho_2}} \quad (3.1)$$

Where,

m_1= weight of dry rubber sample; ρ_1=density of the dry polymer sample

m_2= m_3-m_1; = weight of solvent in swollen sample; ρ_2= density of solvent

m_3= weight of the measured swollen sample

After V_r is determined, the crosslink density (ν) is estimated using the Flory-Rehner equation as shown in equation (3.2).

$$\nu = -\frac{1}{2V_s}\frac{ln(1-V_r)+V_r+\chi V_r^{\,2}}{V_r^{\,1/3}-\frac{V_r}{2}} \quad (3.2)$$

Where,

ν = Crosslink density in mol per unit volume (mol/cm^3)

V_r = Volume fraction of rubber in equilibrium swollen vulcanized rubber sample

V_s = Molar volume of used solvent at room temperature in cm^3/mol

χ = Flory-Huggins polymer-solvent interaction parameter (0.393 for toluene-NR)

The CNCs effect was calculated using the Kraus equation[124] presented in equation (3.3)

$$\frac{V_{ro}}{V_r} = 1 - \{m\frac{\emptyset}{1-\emptyset}\} \quad (3.3)$$

Where $m = 3c\{[1 - V_r^{1/3}] + V_r - 1\}$ (3.4)

V_{ro} = volume fraction of rubber in solvent swollen gum

V_r = Volume fraction of rubber in the filled vulcanizates

m = slope of the plot obtained V_{ro} / V_r versus $\frac{\emptyset}{1-\emptyset}$

c = the CNC-NR interaction parameter obtained from equation (3.4) by using different V_{ro} values and a particular m value

Ø = the volume fraction of CNC in the vulcanizate = $\frac{m_f}{\rho_f}\left[\frac{m_f}{\rho_f}+\frac{m_p}{\rho_p}\right]^{-1}$

m_f and m_p = mass of CNCs and rubber, respectively

ρ_f and ρ_p = density of CNCs (1.6 g/cc) and rubber (0.908 g/cc), respectively

According to Kraus, the higher the V_{ro} / V_r value, the lower the extent of interaction (non-adhering) between the filler and the matrix.

3.2.3.6 Frequency and strain sweep test

Dynamic oscillatory shear measurements of the unvulcanized rubber composites were performed using a rubber process analyzer (RPA) (Pioneer MDR 2000) to investigate the filler-filler interaction. For this test, 5 g of each sample was loaded into the RPA die and a frequency sweep test was carried out at 28 ^{o}C in the range of 5 to 50 Hz. The storage modulus (G'), and loss modulus (G") were then measured as a function of frequency.

A strain sweep test of the unvulcanized rubber composite was also carried out to further elucidate the filler-filler interaction. This test was conducted using a rubber process analyzer (RPA) (Pioneer MDR 2000) as per ASTM D 6204-99. For this test, 5 g of the sample was loaded into the RPA die and the strain sweep was conducted at 60 ^{o}C in the range of 0.3 to 100, from high to low strain at 1.67 Hz frequency. The storage modulus G', loss modulus G" and complex modulus G* with the change in strain amplitude were measured.

3.2.4 Statistical analysis

A one-way analysis of variance (ANOVA) was conducted to determine the significance between the means of the different filler loadings. The difference in means was statistically significant when $p < 0.05$.

3.3 Results and discussion

3.3.1 Fabrication method

A filler's ability to improve the properties of the nanocomposite system depends on fillers compatibility with the matrix and dispersibility in the matrix[92]. The rich hydroxyl groups on the surface of CNC renders it polar; thereby CNC tends to aggregate, resulting from the ease of intra- and intermolecular hydrogen bond formation. Additionally, these polar groups make the dispersion

of CNCs in the hydrophobic matrix difficult due to the polarity difference, thereby leading to a mix of individualized CNCs and aggregates in the nanocomposite. These aggregates are undesirable as they can act as stress concentrators, resulting in an overall poor nanocomposite performance. Thus, an effective processing and fabrication method that breaks down aggregates and agglomerates is crucial to enhance the dispersion and distribution of CNCs in the rubber matrices. To elucidate this dispersion, the fabrication of NR-CNC composites using co-coagulation, batch mixing, and extrusion are studied, and the effect of these methods on the physical properties is discussed.

The sonicated CNCs provided a stable dispersion in water with an average particle size of 90 nm as shown in **Scheme 3.1** insert, indicating that the CNC agglomerates are dispersed into primary CNC particles. Thus, the mixing of the CNC dispersion and the NR latex colloid could provide intimate mixing due to the mutual aqueous colloidal stability of the CNC and NR latex. The subsequent co-coagulation process could then entrap the well-mixed CNCs in the NR matrix resulting in the desired high dispersion of the CNCs in the NR-CNCs [93]. A batch mixer provides distributive rather than dispersive mixing due to the non-intermeshing nature of the screws, which could be limiting in breaking down the CNC aggregates and agglomerates into individualized particles. A twin-screw extruder on the other hand has intermeshing screws that provide high shearing of the composite as it travels through the different zones of the screws, providing dispersive and distributive mixing of CNCs in the rubber and break-down aggregates.

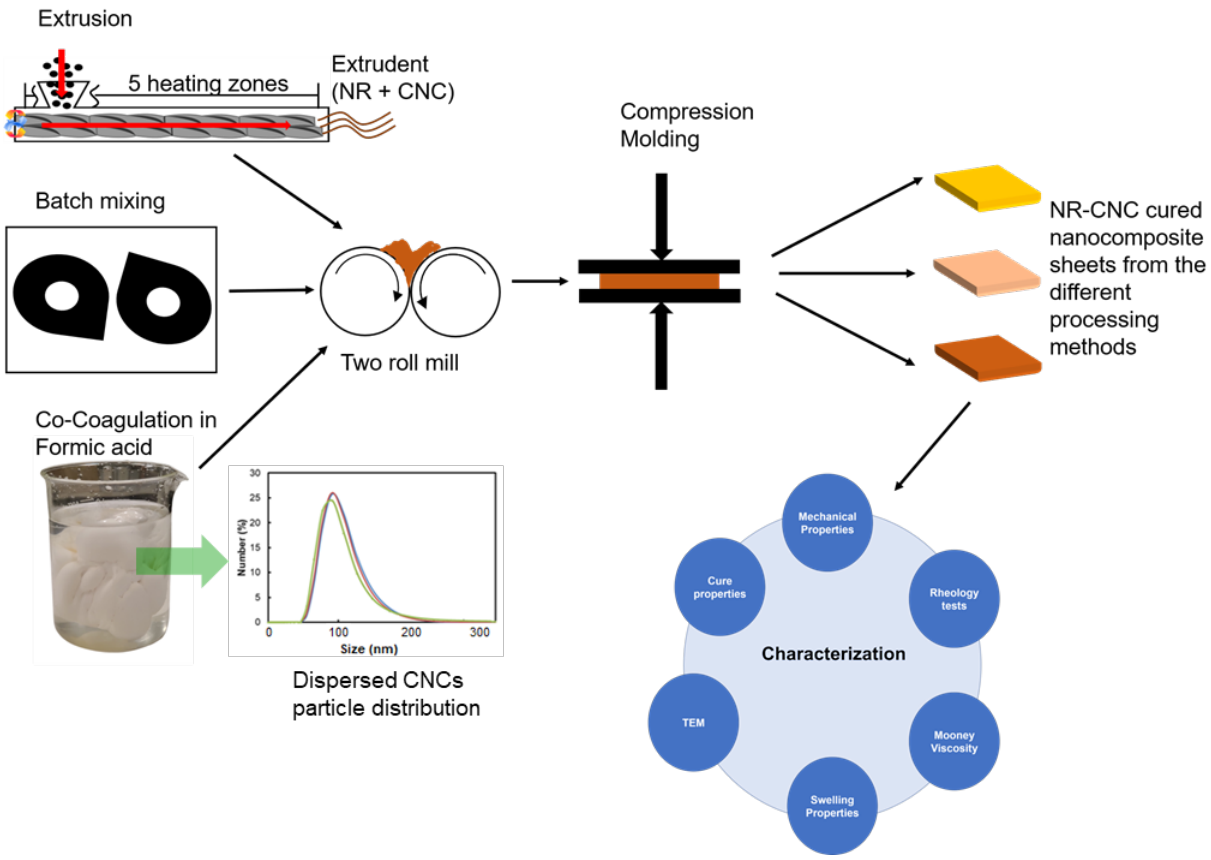

Scheme 3.1. Process description of NR-CNC nanocomposite compounding using the different processing methods.

3.3.2 Cure property

The optimum cure time (T_{c90}) and maximum torque (M_H) of the unfilled rubber vulcanizate and the filled NR-CNC composites prepared by extrusion (representative samples) are presented in **Figure 3.1**. As noted in the figure, the maximum torque has slightly increased with filler loading. This increase can be attributed to the addition of rigid CNC filler into the rubber matrix, which inhibits the mobility of the rubber chains. Furthermore, the nano-sized and large surface area of the CNCs restricted the mobility of the NR chains as a result of the entrapment of the rubber chains between the CNC fillers, thus increasing the M_H and resulting in more rigid nanocomposites[108]. The optimum cure time on the other hand showed no statistical difference ($p > 0.05$) with the use

of the CNCs. Furthermore, the optimal cure time did not vary with the use of the batch-mixing, co-coagulation, and extrusion processes. This was because the level of CNCs used in this study was too low to affect the NR curing behavior.

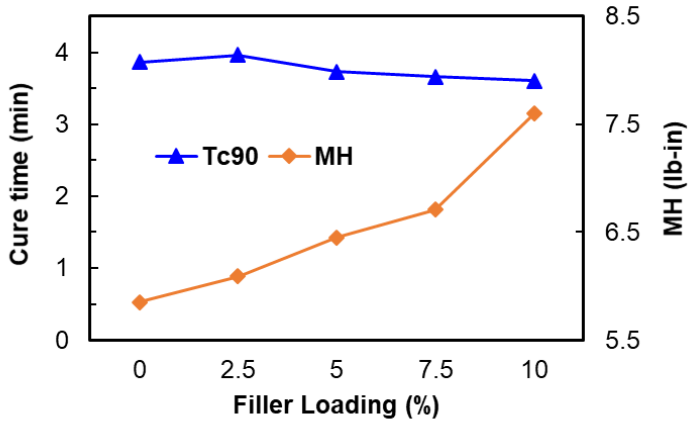

Figure 3.1. The effect of reinforcing filler loading on the optimum cure time (Tc90), and maximum torque (MH) of the different concentrations of NR-CNC nanocomposites at 165 °C.

3.3.3 Mooney viscosity

The Mooney viscosity characterizes the processability of rubbers and is influenced by the filler-filler and rubber-filler interactions, which has an overall effect on the final properties of the composite. **Figure 3.2** presents the Mooney viscosity of the unfilled rubber, and the composites filled with 2.5 and 10 % CNCs processed by all methods. For the samples prepared by co-coagulation, the Mooney viscosity increased with an increase in the filler loading, while for the other processing methods, there was a slight decrease in the Mooney viscosity with an increase in the filler loading. Typically, the addition of a rigid filler in rubber causes a restriction in the molecular chains mobility and reduces the flow of the rubber (hydrodynamic effect). However, the batch-mixed samples displayed a drop in viscosity with the addition of small fillers loading (2.5%), and further increase in filler loading from 2.5% to 10% had no effect on the Mooney viscosity. In

a similar study by Li *et al.*[125], a drop in Mooney viscosity was reported and attributed it to chain scission and reduction in molecular weight resulting from mixing. Therefore, the initial reduction in Mooney viscosity could be from chain scission resulting from the elevated temperature and shear of the batch-mixing and milling of the composite in conjuncture with the poor dispersion of the CNCs. The extruded nanocomposites on the other hand showed a reverse trend compared to the co-coagulated counterpart. This was rather unexpected. A plausible explanation for this observation could be shear and temperature-mediated degradation (chain scission) during processing. Bai *et al.*[126] in their partial replacement of silica with microcrystalline cellulose observed a similar trend for rubber composites aged for one-two weeks. They attributed their findings to a reduction in the migration rates of the fillers. For the co-coagulation processed nanocomposites, the increase in the Mooney viscosity appears to be in line with the improved dispersion of the CNCs in the rubber as compared to other processing methods, and hence a much higher surface area to volume ratio of CNCs in the rubber matrix. As a result of this, higher torque is required to overcome the movement restriction of the rubber composites as evidenced by the Mooney viscosity units.

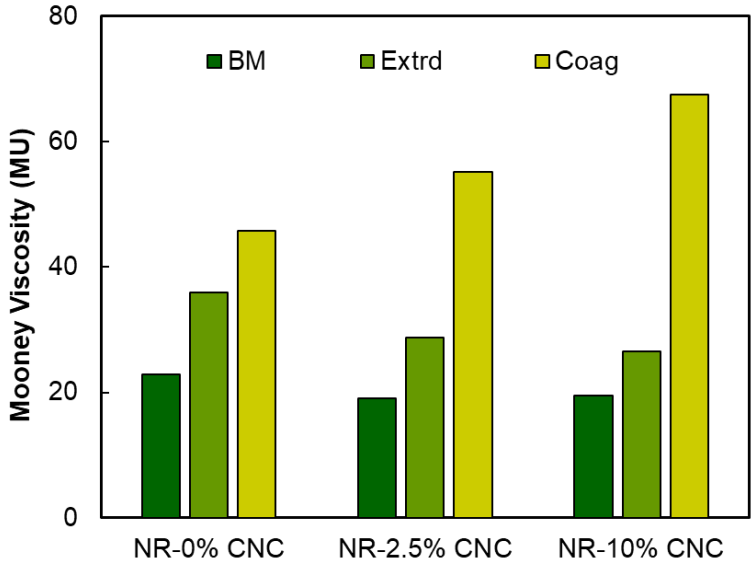

Figure 3.2. Mooney Viscosity of NR-CNC nanocomposites fabricated using the different processing methods.

3.3.4 Transmission electron microscopy (TEM)

TEM micrographs were used to evaluate the nanoscale morphology and dispersion of the CNCs in the NR matrix. TEM is a useful technique generally used to provide information about the homogeneity of nanocomposites, nanocrystal-matrix adhesion, existence of voids, dispersion level of the filler, and the shape size and orientation of the filler within the matrix[99]. **Figure 3.3** presents the TEM images of unfilled NR and NR loaded with 2.5% CNC fabricated by the three fabrication methods. The 2.5% CNC filled rubber was chosen because this composition provided composites with the highest tensile strength. The micrograph of unfilled NR (**Figure 3.3A**) showed the presence of microparticles, which can be attributed to the vulcanization additives. The NR-CNC sample images (**Figure 3.3B-D**) displayed individualized nanocrystals presented as rods and some aggregates of bound CNCs, in addition to the vulcanization additive microparticles. Compared to the unfilled NR (**Figure 3.3A**), the nanocomposites fabricated by extrusion and co-

coagulation (**Figure 3.3B &C**) reveal an overall uniformly dispersed CNCs with no visible aggregates. Although both micrographs in **Figure 3.3B** and **C** showed good dispersion, the co-coagulated samples micrograph (**Figure 3.3C**) exhibited a more homogenous matrix of CNCs highlighted by the continuous and connected rod-like structure of dispersed CNCs within the matrix. On the other hand, the micrograph of the batch-mixed nanocomposites (**Figure 3.3D**) was like NR with additional visible aggregates of CNCs. The visible aggregates displayed the inability of the batch mixer to provide sufficient shear for the dispersive mixing of the CNCs, hence the formation of a heterogeneous composite. Comparing the micrographs of the nanocomposites from all fabrication methods with the unfilled NR, it can be concluded that processing by co-coagulation was the most effective method in enhancing the dispersion of CNCs in the rubber matrix.

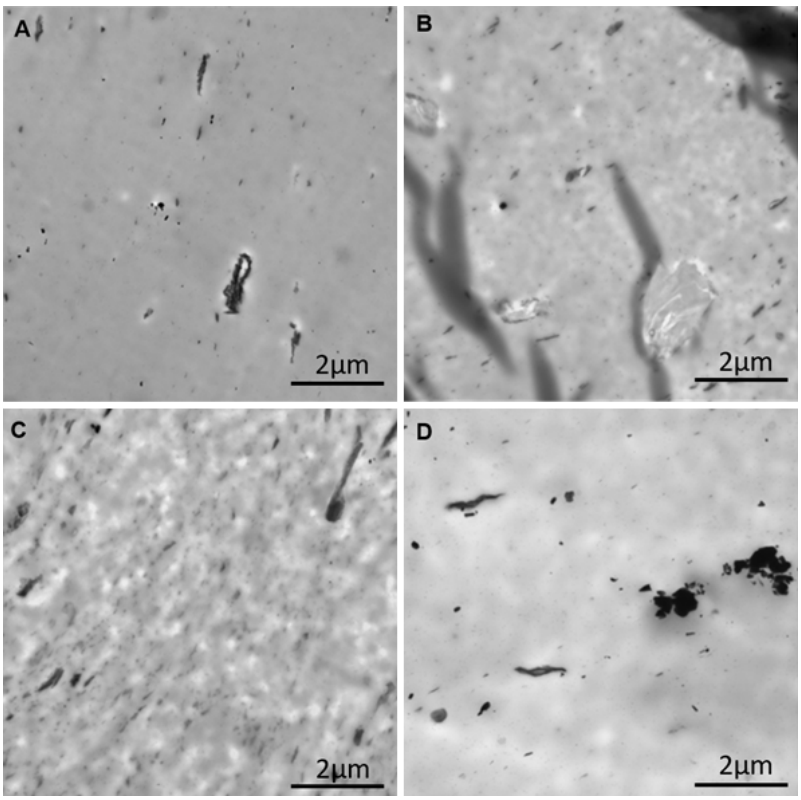

Figure 3.3. TEM image of unfilled (A) NR, (B), 2.5% NR-CNC nanocomposite fabricated by extrusion, (C) co-coagulation, and (D) batch mixing

3.3.5 Crosslinking

The crosslinking density of rubber is obtained from the degree of swelling in the solvent. For any given solvent, the lower the swelling, the higher the crosslink density of the rubber and vice versa. The relationship between swelling and crosslink density can be obtained using the Flory-Rehner equation[122] and is often used for calculating the crosslink densities of rubber. When a given rubber composite is combined with fillers, the fillers could be adhering or non-adhering depending on the compatibility with the matrix. For fillers that adhere to the matrix, swelling is restricted around the filler and away from the filler assuming fillers do not swell, and as a result the composite swells as it would in gum vulcanizates. Conversely, for non-adhering type fillers, due to the poor interfacial bonding with the matrix, a void form around each filler particle (filler effects) which fills with solvent, therefore, the swelling ratio should be calculated to correct for the filler effects[127–129]. According to the Kraus theory[130], when fillers poorly adhere to the rubber matrix, there will be an increase in the apparent volume fraction of the rubber in the swollen gel (V_r) compared to its true value (V_{ro}), such that for unfilled polymers, the ratio of V_{ro} to V_r equals unity. Furthermore, if the filler swells as much as the surrounding rubber matrix, then the ratio of V_{ro} / V_r remains unity even with increased filler loading. But since most fillers do not swell, and due to molecular chain restriction from the fillers, the ratio decreases as the filler loading increases[129]. However, according to Kraus, this ratio increases for non-adhering type fillers. For simplicity, $V_{ro}/V_r < 1$ for adhering fillers (crosslinks unaffected by fillers) and $V_{ro}/V_r > 1$ for non-adhering fillers are typically considered. This ratio shows the extent of the restriction of the solvent uptake by the rubber due to the rubber-filler interaction[131].

Figure 3.4 presents the Kraus equation plot for the swelling of the NR-CNC vulcanizates processed by the different methods. According to the Kraus equation, the plot of V_{ro}/V_r versus

Ø/(1- Ø) shows the restriction of swelling for a given volume of filler. It can be observed that the vulcanizates processed by extrusion and co-coagulation deviate from the proposed linear model and based on ANOVA analysis, these samples display no change in V_{ro}/V_o with increased filler loadings for all processing methods. CNCs being inherently hydrophilic bonds poorly with the rubber matrix; this means that as the rubber swells, there is a dewetting of the CNC in the composite, leading to the formation of voids around the CNC filler, and ultimately increase in solvent uptake from voids fill-up. This increase in V_{ro}/V_r evidences the CNCs- rubber interaction because the formation of fewer crosslinks per rubber chain increases the swelling in the solvent. Ismail *et al.*[132] in their study of the crosslink density of the hydrophilic rattan-powder-filled NR composites obtained similar results. The specimens prepared by batch mixing on the other hand displayed a somewhat linear model. In this case, there is evidence of the formation of aggregates of CNCs in the rubber matrix as seen from the TEM studies, hence, the poor dispersion could translate to a reduction in the chain restriction from the fillers which increases the possibility of higher crosslink formation in the rubber chains.

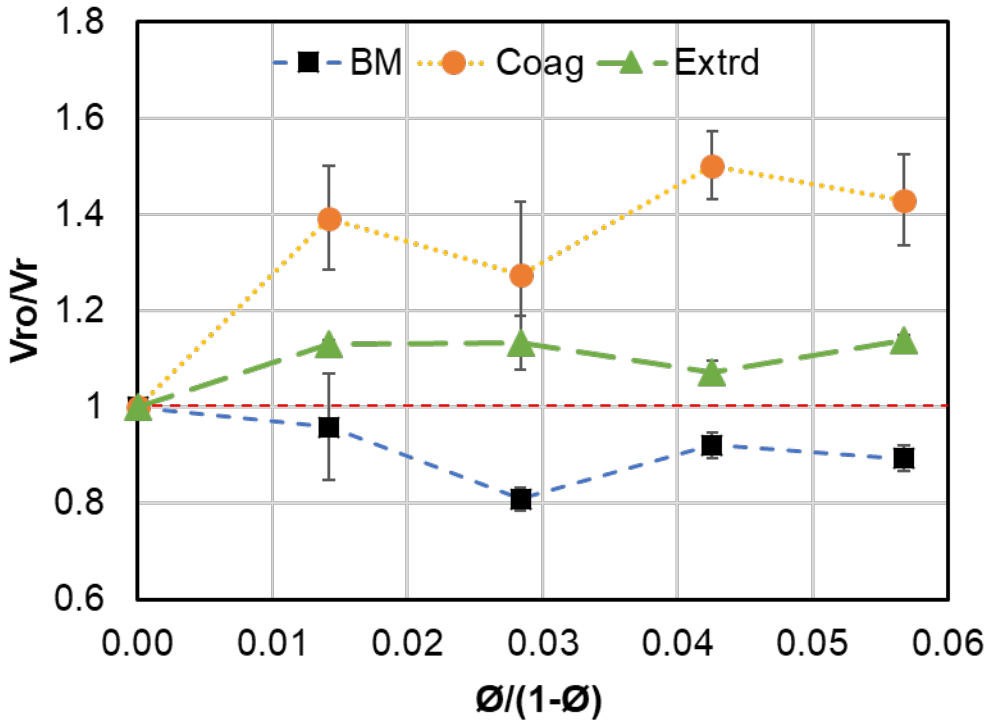

Figure 3.4. Kraus equation for swelling test

3.3.6 Mechanical properties

3.3.6.1 Tensile strength

The degree of dispersion and content of a filler in the matrix are important factors that can affect the mechanical behavior of nanocomposites. Tensile tests were performed at room temperature for the unfilled NR and all NR-CNC nanocomposites, and the stress-strain curves are presented in **Figure 3.5**. For all fabrication methods, there was an increase in the tensile strength of the nanocomposites at 2.5% CNC loading followed by a decrease thereafter, except for the batch mixed nanocomposites which showed either the same level or a decrease in tensile strength in all loading ranges.

The nanocomposites prepared by batch mixing presented in **Figure 3.5A** showed a reduction in the tensile strength with the addition of the CNC fillers. This behavior could be a

result of the poor dispersion of the CNCs in the rubber matrix provided by the batch mixer leading to the formation of CNC aggregates. As the concentration of CNCs increases to 5% and beyond, the degree of agglomeration increased, and the filler-matrix interaction became poorer with a possible increase in porous structure from poor interfacial bonding. Furthermore, these agglomerates of CNCs generate stress concentration in the NR leading to the observed poor tensile properties and premature failure. These results are consistent with the TEM micrograph where visible aggregates were seen even at the lowest concentration of CNCs. The increase in the tensile strength of the 7.5% CNCs loaded NR was rather unexpected and further investigation is required to explain the behavior.

The tensile strength of the nanocomposites fabricated by co-coagulation and extrusion (**Figure 3.5B & C**) increased with the addition of CNCs content compared to NR. Even though there was an overall improvement with the incorporation of CNCs at all loading levels, the 2.5% CNC-filled nanocomposites showed the highest strength with a 26% and a 21% increase compared to the control for the co-coagulated and extruded nanocomposites, respectively. The enhanced strength for co-coagulated composites compared to the other processing methods could be as a result of the absence of chain scission caused by heat processing that occurs in the extrusion and batch mixing processes. These results agree with the Mooney viscosity results where a decrease in viscosity with an increase in filler loading was observed for the heat-processed nanocomposites. Furthermore, for all processing methods, the tensile strength peaked at 2.5% CNCs loading and beyond that, it decreased with concentration. This behavior could be due to the formation of aggregates of CNCs at higher loadings, which acted as stress concentrators in the matrix, and hence resulted in poor tensile performance. The strain at break for the vulcanizates fabricated by extrusion as presented in **Figure 3.5C** decreased with increased filler loading. This happened

because the addition of fillers restricted chain mobility, thereby increasing the stiffness of the rubber, which led to a break at lower strain. For the batch mixed and coagulated vulcanizates, a similar trend was observed except that the 5% CNCs filled vulcanizates seemed to be out of place, which was rather unexpected.

The moduli at 100% elongation (M100) and 300% elongation (M300) are presented in **Figure 3.6**. All batch mixed and extruded vulcanizates showed no significant change in modulus with CNCs loading increase. This could be a result of poor mixing of the CNCs in the rubber. On the contrary, the coagulated vulcanizates showed an increase in M100 and M300 with increasing filler loading levels. This was associated with the increased stiffness with filler loading resulting from adding a rigid filler in the nanocomposite. It is noteworthy to state that the modulus of the co-coagulation-based samples was one order of magnitude higher than that of the batch-mixed and extrusion fabricated samples. This observation could be attributed to the even dispersion of CNC in the latex before coagulation and the high coagulation efficiency of CNC entrapment in the rubber matrix granted by this process.

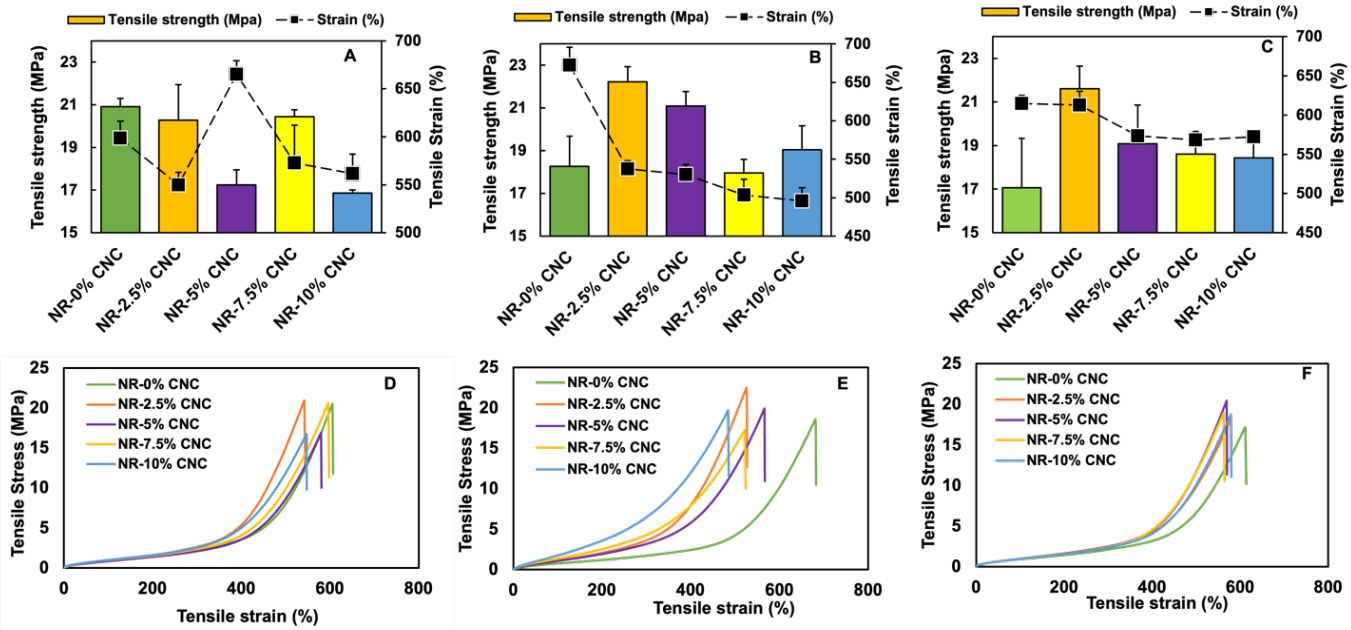

Figure 3.5. Tensile strength of NR-CNC nanocomposites fabricated by (A) batch mixing, (B) co-coagulation, and (C) extrusion, and typical tensile strength vs strain plot of NR-CNC nanocomposites fabricated by (D) batch mixing, (E), co-coagulation, and (F) extrusion

3.3.6.2 Hardness test

The results from the hardness tests are presented in **Figure 3.6**. Hardness is a measure of modulus and shows the net effect of the filler loadings and crosslinking[133]. Results presented in **Figure 3.6D** indicated an increase in hardness as the filler content increased. For all samples except the 2.5 and 10% CNCs fabricated by batch mixing, one-way ANOVA showed a significant increase ($p < 0.05$) in the hardness compared to the control. The hardness of the 10% filled composite fabricated by batch mixing was the lowest of all the tested specimens. This could be due to the poor dispersion and formation of aggregates of the CNCs at that loading. On the other hand, the hardness of the vulcanizates fabricated by co-coagulation and extrusion increased linearly with filler loading. By definition, hardness is a measure of a material's resistance to

localized surface deformation. Experimental results can be impacted by the non-planarity of the materials surface, surface defects or voids, and non-homogeneities near the surface from poor mixing[134]. The substantial increase in the hardness of the co-coagulation-based samples agrees with the modulus result, which was attributed to the superior filler dispersion provided by the co-coagulation process.

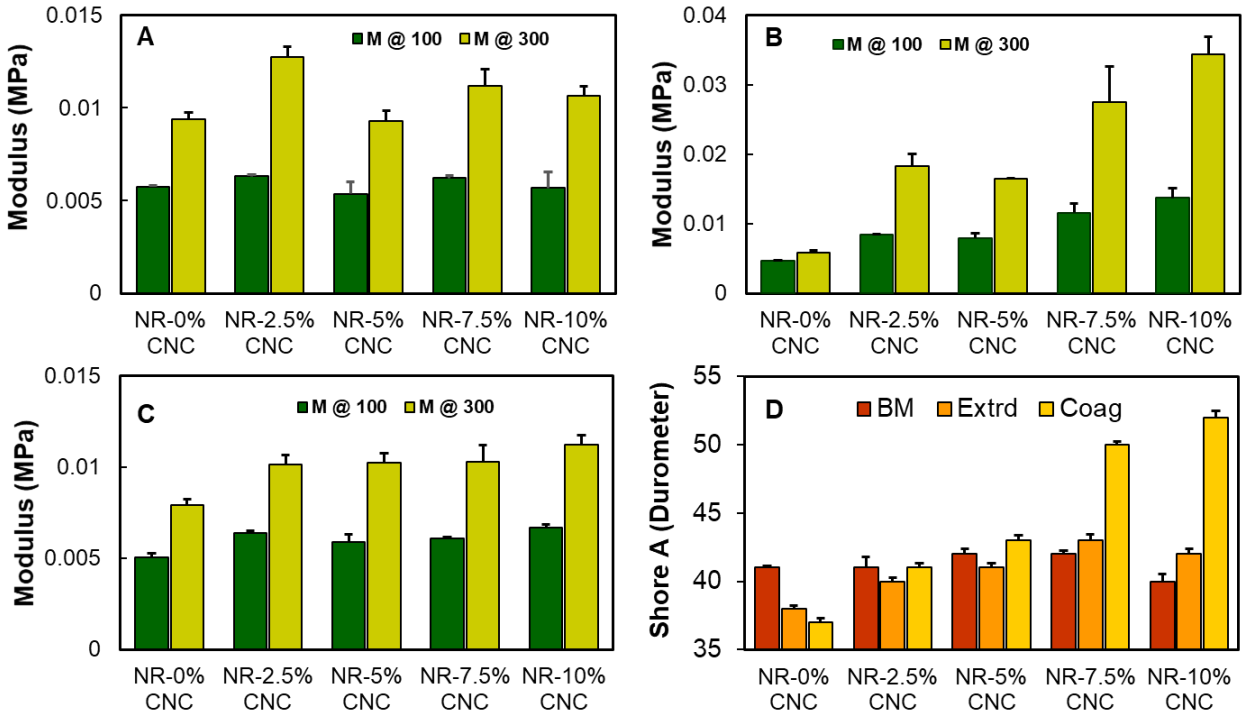

Figure 3.6. Modulus as a function of CNC loading for NR-CNC nanocomposites fabricated by (A) batch mixing, (B) co-coagulation, and (C) extrusion; (D) Hardness test plot of NR-CNC nanocomposites.

3.3.7 Frequency sweep test

The results of the change in modulus with deformation are presented in **Figure 3.7.** The effect of CNCs incorporation (increased stiffness) is shown by the increase in storage modulus G' at low frequencies. According to previous studies, the storage modulus response at low frequencies is dominated by the rubber matrix while at high frequency, the response is dominated by the

concentration and dispersion of CNCs in the nanocomposite[135]. As presented in **Figure 3.7**, except for the NR-10% CNCs samples fabricated by extrusion, all the nanocomposites showed an increase in storage modulus compared to the control. This increase in the storage modulus of the filled nanocomposites can be attributed to the presence of rigid CNC fillers. The lower storage modulus of the extruded NR-10% CNCs sample compared to NR can be associated with possible shear and thermal degradation of the polymer and a decrease in the molecular weight, hence increasing the dissipation of stored energy. This observed trend can be correlated to the Mooney viscosity in the previous section where no statistical change in viscosity with the addition of CNCs attributed to scission of the rubber chain was observed. Finally, the high G' exhibited by the samples prepared by co-coagulation can be attributed to better CNC dispersion in the matrix leading to improved filling of the free volume between rubber chains by CNC nanoparticles.

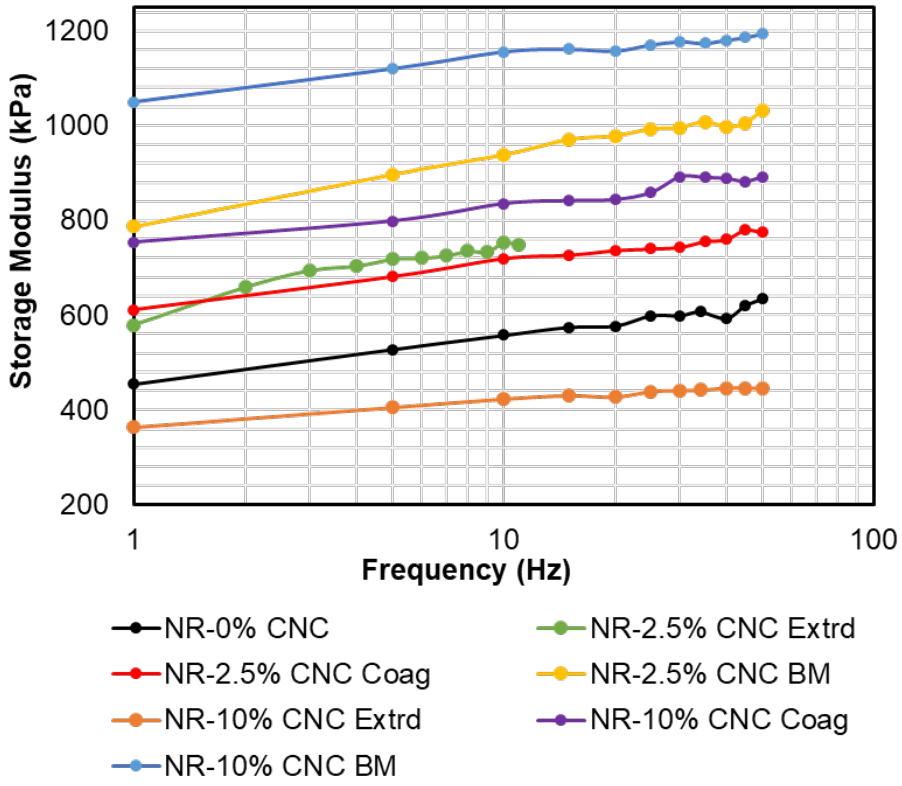

Figure 3.7. Storage Modulus obtained from the frequency sweep test of 2.5 and 10% NR-CNC vulcanizates for all processing methods.

3.3.8 Strain sweep test

Typically, the storage modulus of unfilled rubbers shows no significant change with increasing strain. When fillers are introduced into the rubber, the fillers tend to form a filler-filler network structure prone to softening with increasing strain amplitude, known as the Payne effect[46,109,136]. The change in modulus of the NR – CNCs composites with deformation is presented in **Figure 3.8**. The increased stiffness with CNC incorporation was shown by the increase in G' at low deformations. The unfilled rubber batch mixed samples showed a linear viscoelastic region (LVE) at low strain and a loss in modulus at high strain. Furthermore, the width of the LVE showed a dependence on the filler loading and the processing method. For instance, as the loading of CNCs increased and with improved dispersion, the width of the LVE decreased as shown in the

nanocomposites processed by co-coagulation. A non-linear viscoelastic behavior was observed in the samples prepared by extrusion and even more in the coagulated vulcanizates. Although rather unexpected, no trend was observed with an increase in loading of CNCs except for the coagulated vulcanizates that showed an increase in G' and a higher loss in G' at low deformation. The lower storage modulus of the batch mixed samples compared to NR can be associated with the poor dispersion of CNCs in the rubber matrix and high CNCs agglomerates resulting from the insufficient shear at nanoscale provided by the batch mixer. The extruded vulcanizates showed higher modulus compared to the batch mixed vulcanizates indicating better dispersion emanating from the high shear of the co-rotating twin screws. Similarly, the high G' exhibited by the nanocomposites processed by co-coagulation can be attributed to improved CNCs dispersion in the matrix.

It is well known that CNCs aggregate in non-polar matrices due to their high polarity that results in poor compatibility, and inter-particle hydrogen bond formation. In all the filled vulcanizates, the strain-dependent viscoelastic behavior (Payne effect) can be observed, and it changes with filler loading. Compared to the other processing methods, the Payne effect is the highest in the coagulated vulcanizates due to the high surface area and filler-filler interaction resulting from good dispersion (**Figure 3.8**). Moreover, with good dispersion, the inter-aggregate distance becomes smaller, and the probability of network formation increases. This means that the well-dispersed CNCs being close to each other could form inter-and intramolecular hydrogen networks which start to break down with deformation, hence the non-linear viscoelastic behavior. Fronlich *et al.* [137] compared the Payne effects of carbon black and pristine silica at different loadings and found that while the carbon black network breakdown occurred at 5-7% strain amplitude, that of silica occurred at 42% strain attributed to a stronger filler network formed by

the hydrogen bonds in silica. Additionally, they reported that for silica, a high surface area (smaller particles and well dispersed) showed a higher Payne effect compared to the aggregated vulcanizates.

Payne effect is a very important dynamic property in tires and responsible for the rolling resistance[137]. While the pristine CNCs show network formation, increasing the surface activity decreases the filler network formation as a result of improved filler-polymer interaction and reduced surface hydroxyl groups available for hydrogen bonding formation.

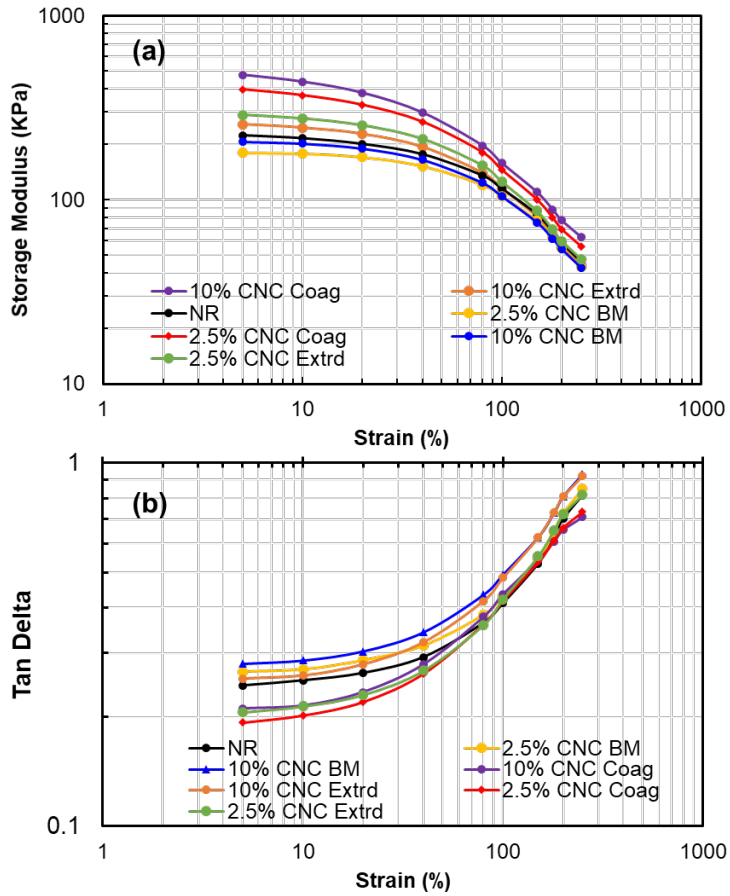

Figure 3.8. Storage Modulus (a) and Tan delta (b) results obtained from the frequency sweep test of 2.5 and 10% NR-CNCs vulcanizates for all fabrication methods.

3.3.9 Process comparison

The dispersion of fillers in NR is a crucial factor to consider when determining processing methods. In addition to the effectiveness of the processing method, other factors such as process energy consumption, process feasibility, processing time, process costs, repeatability, and cleanliness influence the choice of processing systems. NR is supplied in two forms: NR latex and bale rubber. While masterbatch preparation by co-coagulation and mixing with an internal mixer, both batch-mixing processes, can be carried out using NR latex and bale rubber, respectively, as the starting material, the absence of rubber supplied in granular form adds a grinding step to process the composites via extrusion. Co-coagulation, on the other hand, involves mixing a pre-dispersed filler in the latex, followed by coagulation into a masterbatch and drying before roller mill mixing. These processes increase the number of steps and time spent in sample preparation compared to batch-mixing by internal mixing. Also, based on evidence from thermoplastic mixing, extrusion is a continuous process that offers the following advantages over the batch-mixing process: lower capital and operation costs, continuous operation, consistent samples, operational cleanliness, lower mixing energy, lower mixing times, and process simplification[138,139]. Furthermore, the high shear and great temperature control in extrusion process that allows it to breakdown particle agglomerates and aggregates makes it an appealing process for NR-CNC composites.

3.4 Summary of Chapter 3

In this work, CNC was processed by using extrusion, co-coagulation, and batch mixing processing methods to elucidate the dispersion of CNCs in natural rubber. The properties of the resulting composites from the different processing methods were then compared to determine the optimal

processing method. Depending on the employed processing method, various levels of CNCs dispersion in the NR were achieved. It was observed that the reinforcement of the nanocomposite was higher with improved dispersion of the CNCs. Though extrusion showed efficient filler dispersion, co-coagulation presented the strongest CNCs dispersion of all the processing methods. Aside from the batch-mixed processed samples, the tensile strength for the co-coagulated and extruded samples peaked at a loading of 2.5% CNCs with an increase in tensile strength of 26% and 21%, respectively. Beyond that, the tensile strength decreased. The results from the rheology studies corroborated the tensile property observations. The processing method also affected the polymer-filler interaction, rheological properties, and viscosity of the vulcanizates. Based on the findings from this study, it can be concluded that the effect of CNCs in improving the properties of the rubber nanocomposites depends on the employed processing methods that subsequently affect CNCs dispersion. Results of this study indicated that to obtain further enhancement in the nanocomposite properties, especially at higher loading levels, surface modification of either the CNCs or the NR to enhance the compatibility could be required. Future studies will focus on elucidating the impact of surface modifications of CNCs and rubber on the properties of the resulting nanocomposites.

Chapter 4. Batch mixing for the *in situ* grafting of epoxidized rubber onto cellulose nanocrystals[2]

4.1 Introduction

Natural rubber (NR), a renewable biopolymer shows excellent properties like tensile strength, dynamic properties, abrasion resistance, and resilience when crosslinked; however, it is riddled with low strength and poor weathering conditions, which limits its applications in its pristine state. To improve these properties and extend rubber applications, fillers such as silica, mineral fillers, and carbon black are commercially employed. Carbon black is widely used as a filler in rubber, such as in tires and at high concentrations, it has been reported to improve rubber's strength and abrasion resistance. However, carbon black is obtained from crude oil sources, contributes to greenhouse gases, and is a known environmental pollutant. Silica and other mineral fillers typically consume high energy during production while also increasing the weight of the rubber composite due to their high density[95]. Therefore, alternative biobased fillers for rubber composite are of high interest to the industry and research community.

To mitigate the associated issues with carbon black and mineral fillers, biobased filler for rubber such as lignin[140,141], eggshells[142], oil palm ash[143], rice husk[144], cellulose nanofibers[145], starch[146], soy[147], and cellulose nanocrystals[82,95,148] have been investigated. Cellulose nanocrystals are of high interest in all these fillers due to their natural abundance, biodegradability, environmental friendliness, low density, high aspect ratio, high modulus, and high strength[64,95,149,150]. Furthermore, CNCs are structurally uniform as compared to other biomass-

[2] A version of this chapter has been published. Ojogbo E, Tzoganakis C, Mekonnen TH. Batch Mixing for the in Situ Grafting of Epoxidized Rubber onto Cellulose Nanocrystals. *ACS Sustain Chem Eng*. 2022;10(27):8743-8753. doi:10.1021/ACSSUSCHEMENG.2C01054

derived fillers, such as lignin, hemicellulose, plant fibers, etc. Although cellulose nanocrystal (CNC) is an excellent filler, the rich hydroxyl groups on CNC make it highly polar and as such renders it incompatible with mostly non-polar polymers. Therefore, cellulose-filled natural rubber systems suffer poor dispersion and interfacial adhesion leading to voids at the interface of the filler and the rubber, causing premature failure under stress. Efforts to improve the compatibility and dispersion of CNC in rubber, such as modification of CNCs to reduce hydrophilicity[20,151,152] and investigating fabrication approaches[95] to improve dispersion have been studied. These approaches have been shown to improve the compatibility and properties of the CNC-filled rubber composites.

Another approach to improve the compatibility of CNC and rubber is the use of modified natural rubber. Epoxidized natural rubber (ENR), a chemically modified natural rubber with oxygenous reactive epoxides attached to the double bonds of the rubber backbone, introduces polarity and reactive sites on the rubber. This epoxidation of natural rubber introduces other unique properties to the rubber, such as oil resistance, low gas permeability, improved wet grip, and reactive sites on the modified rubber. Of great importance are the reactive sites on ENR which make it amenable to grafting with other polymers, increasing the possibility of incorporating desirable properties in the rubber, therefore expanding its applications. These oxygenous groups also make the ENR more polar than NR, improving the compatibility with polar fillers. For these reasons, ENR is desirable for composites with polar fillers.

Filled ENR composites have improved properties and are receiving much attention. Fillers, such as graphene oxide[153], rice husk[154,155], wood flour[156], lignin[157,158], silica[159], carbon black[160], chitin[161], organoclay[162], and cellulose nanocrystals (CNC)[163] have been reported in the literature. Among them, CNC has received a lot of interest due to its appealing properties, as highlighted above. Furthermore, in addition to the polarity of CNC, the electronegative hydroxyl groups on

CNC can covalently bond with the oxirane group of ENR in a ring-opening reaction, thereby leading to a homogenous dispersion of CNC in ENR. This could create multiple polymer grafts and possible crosslinks in the composite and ultimately improve the properties of the composite. Cao *et al.*[164] investigated the properties of ENR and tunicate CNC composites and reported improved reinforcements based on hydrogen bond and filler entanglements. In another study, the same authors studied the interactions between ENR-CNC and ENR and carboxylated CNCs and concluded improvement in properties based on hydrogen bond formation between ENR and CNC and dual crosslinks and hydrogen bonds between ENR and carboxylated CNCs[165]. Fernandes *et al.*[166] studied the curing and aging characteristics of ENR-cellulose vulcanizates and found that the mechanical properties and solvent resistance improved[166]. Similarly, Ming *et al.*[163] prepared a composite of ENR and CNC for adaptive mechanical behavior. They reported hydrogen bonds and covalent crosslinks between the ENR and CNC; however, toluene swelling experiments to confirm the chemical crosslinks were omitted in their study.

ENR is a specialty rubber with a high cost and employing ENR alone as base rubber is uneconomical for commodity products. Therefore, this research aims to prepare a masterbatch of reinforced ENR-CNC composite by grafting the CNC on ENR via covalent ether bonds to disperse the CNC in the ENR. This work aims to understand how the interactions between ENR and CNC contribute to the CNC reinforcing performance. This was achieved by carrying out a base-catalyzed reaction at varying reaction temperatures in a batch mixer using bale rubber and studying relevant properties, including mechanical properties, swelling studies, and rheological properties of the resulting composite. This ENR-CNC masterbatch with superior properties can be used as fillers for other rubbers such as natural rubber to incorporate desirable properties in the rubber. To the best of our knowledge, the grafting based on oxirane ring-opening of re-processable ENR-

CNC masterbatch has not been reported before. Other authors[161,165] reported crosslinking based on the oxirane ring-opening which renders the ENR composite non-reprocessible, and as a result, presents a limitation in employing the composite as a filler for other polymers. Therefore, in this study, CNC is grafted on the ENR via the oxirane ring-opening to disperse the CNCs in a masterbatch preparation to be reprocessed and employed as a filler in other hydrophobic rubbers. This aims to improve the dispersion of CNCs in these rubbers such as in natural rubber. Furthermore, the properties of the ENR-CNC masterbatch which could be employed as a filler for other rubbers, have not been investigated.

4.2 Materials and methods

4.2.1 Materials

CNCs were supplied as a dried powder by Celluforce Inc (QC, Canada). The length, width, aspect ratio, and sulphur content of the CNCs were 150 nm, 7.5 nm, 20 nm, and 5000-9000 mg/kg respectively. Bale ENR with 50% epoxide content was purchased from Muang Mai public Company Ltd, China. and sodium hydroxide (NaOH) was purchased from Sigma-Aldrich (Oakville, ON, Canada) and a 7 wt.% solution in water was prepared before use.

4.2.2 Methods

4.2.2.1 Preparation of ENR-CNC composites

The ENR-CNC composites were prepared in a batch mixer (Haake Rheocord 90) set to a rotor speed of 80 rpm. 100 g of bale ENR was first added into the batch mixer and 100 g of CNC was added slowly and mixed with the ENR at 140, 180, and 220 ^{o}C and until a homogenous blend was achieved. Then, 60 mL 7% NaOH solution per hundred grams of rubber was added to the

blend as a catalyst and the reaction was carried out for 30 mins. Once mixing was complete, the sample was transferred into cold water to end the reaction. The control samples, neat ENR, and ENR-CNC blend masterbatch composites were prepared without the use of a catalyst and at room temperature. The actual temperature in the batch mixer during the control sample mixing was approximately 50 ^{o}C as a result of the torque. The samples prepared were coded ENR, CNC-ENR blend, CNC-ENR-140, CNC-ENR-180, CNC-ENR-220. All the ENR-CNC masterbatch composite samples were passed through a two-roll mill to make sheets in preparation for characterization.

4.2.2.2 Characterization

Fourier Transform Infrared Spectroscopy (FTIR)

FTIR was recorded on a Thermo Nicolet Nexus 670 FTIR equipped with an attenuated total reflection (ATR) accessory. Each solid sample was placed on the ATR accessory and 32 scans were taken and averaged. The IR spectra were analyzed and smoothed using the Thermo Fisher OMNIC^{TM} spectra software using the Savitzky-Golay algorithm.

X-ray photoelectron spectroscopy (XPS)

XPS was carried out to determine the surface functional group content and chemical compositions of the samples and XPS was carried out using a Thermo-VG Scientific ESCALab 250 microphobe with a monochromatic Al K-alpha x-ray emission source. The samples were cut to 1 cm x 1cm in size and the surface was cleaned thoroughly using ethanol before testing. CasaXPS software was employed to analyze the data.

Injection molding of ENR-CNC samples

Injection molding of samples was carried out using a Haake Minijet Pro injection molding machine (Thermo Scientific) with injection pressure, injection time, injection back pressure, cylinder temperature, and a mold temperature of 700 bar, 10 s, 500 bar, 140 ^{o}C, and 30 ^{o}C respectively. All tensile and dynamic mechanical analysis (DMA) test specimens were prepared using this procedure except for the ENR-CNC blend which had a cylinder temperature of 80 ^{o}C. The samples were conditioned at 23 ^{o}C for 40 h before further testing.

Toluene swelling studies

Specimens weighing approximately 0.2 g were cut from each sample, weighed, and immersed in toluene at room temperature. The final weight of each sample was recorded after 72 h and the degree of swelling was obtained by calculating the swelling index (SI) according to Equation (4.1). Each sample was run in triplicates and the average swelling index is reported. For the ENR, CNC-ENR blend, and ENR-CNC-140 samples, an ENR gel was formed with toluene while the CNC precipitated, hence it was impossible to calculate the swelling index of these samples.

$$SI = \frac{W_2 - W_1}{W_2} \quad (4.1)$$

Where W_1 and W_2 represent the weights of the specimens before and after toluene immersion.

Mooney viscosity

The Mooney viscosity was measured using a rubber processing analyzer (Pioneer MDR 200) as per ASTM D1646-19A. The initial and final Mooney viscosities for all samples were recorded and analyzed.

Morphological analysis

Scanning electron microscopy (SEM) was conducted using a Zeiss Ultra Plus SEM to investigate the dispersion of CNC in ENR. A cross-section of fractured samples was first gold-coated under argon gas for 120 s to introduce conductivity before imaging. Transmission electron microscopy (TEM) (Philips, CM 10) was performed on the neat CNC to obtain the nanoparticle morphology.

Stress-strain properties

The 5tensile properties of the ENR-CNC nanocomposites were measured using a Shimadzu AGs-X tensile testing unit with a load cell of 10 kN and a crosshead speed of 500 mm/min as per ASTM D638. Five replicates were tested and averaged.

Hardness test

The hardness test was carried out using a Shore A digital durometer as per ASTM D2240. Stacked specimens of approximately 6 mm thickness were placed on a flat surface and pressed with the instrument indentor. Data was read immediately after the indentor established firm contact with the specimen. Indentation was done at 3 points on the specimen and averaged.

Rheological properties

The rheological properties for all samples were studied using a Haake Mars III parallel plate rheometer (Thermo-Fisher Scientific Inc., Waltham, MA, USA). Disc-like specimens with a thickness and diameter of 2.5 and 25 mm, respectively were prepared by injection molding. A time sweep test was first performed at 180 ^{o}C for 1 h to evaluate the stability of the specimens, which revealed no change in torque for all specimens. A frequency sweep from 0.1 to 100 rad/s (within the viscoelastic region) was then performed at a 2 mm plate gap.

Strain sweep test

The strain sweep test of the unvulcanized rubber composites was carried out to investigate the filler-filler interactions. This test was carried out using a rubber process analyzer (RPA) (Pioneer MDR 2000) as per ASTM D 6204-99. For this test, 5 g of the sample was loaded into the RPA die and the strain sweep was carried at 120 ^{o}C in the range of 0.3 to 100, from high to low at 1.67 Hz frequency. The storage modulus (G'), loss modulus (G"), and complex modulus (G*) with the change in strain amplitude were measured.

4.3 Results and discussion

4.3.1 CNC grafting on ENR

In this work, the opening of the epoxide ring and grafting with CNCs was carried out in a thermo-mechanical-catalyzed reaction using sodium hydroxide (NaOH) as catalyst and varying the temperature to design an irreversible ENR-grafted CNCs. The reaction was carried out at a constant concentration of CNCs, ENR, and the NaOH catalyst while varying the reaction temperature. Deionized water was employed as a solvent or the NaOH and no other solvents were employed for the reaction process making it green, non-toxic, and environmentally friendly.

Scheme 4.1A illustrates the schematic representation of the plausible grafting of ENR onto CNCs. The resulting supramolecular network could be formed firstly via a reversible physical hydrogen bond between the oxygenous groups in ENR and the hydroxyl groups of CNC; and secondly, an irreversible covalent bond grafting through the opening of the oxirane ring of ENR and ether bond formation with the OH groups of CNCs.

Scheme 4.1B presents the mechanism of the base-catalyzed reaction. The nucleophile (-OH) from the NaOH catalyst first attacks the ENR at the least substituted position (C2) to form an alkoxide (RO-), which leads to an inversion in the stereochemistry at this C2 position. A proton is

then transferred from the CNC to the alkoxide to form a covalent ether bond at this position. This base-catalyzed epoxide ring-opening reaction mechanism was first described by Mayr *et al.*.[167].

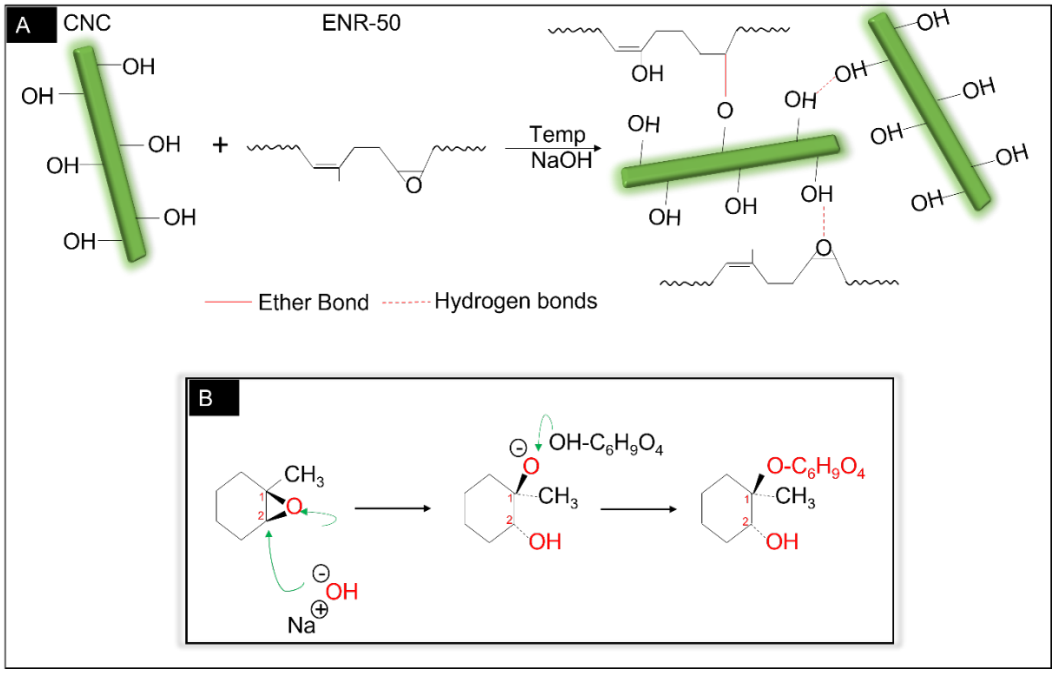

Scheme 4.1. (A) The plausible reaction between ENR and CNC and (B) the mechanism of the reaction

4.3.2 Fourier transform infrared spectroscopy (FTIR)

FTIR was used to investigate the hypothesized chemical reaction between ENR and CNCs. **Figure 4.1. FTIR spectra of neat ENR and ENR-CNC composites.** presents the IR spectra of the baseline and the modified samples. For the CNC spectra, the peaks at 3338, 2981, and 1160 cm^{-1} correspond to the stretching vibrations of O-H, C-H, and C-O respectively while the peak at 1637 cm^{-1} represented the adsorbed water in CNCs[168]. For the ENR, the peaks between 2472 and 3000 cm^{-1} represented C-H stretching vibrations; 1652 cm^{-1}, C=C stretching, 1444 and 1378 cm^{-1}, CH_2 and C-H deformations respectively; 1246 and 870 cm^{-1}, asymmetrical and symmetrical C-O stretching respectively; 838 cm^{-1}, -=CH out of plane vibrations[169]. For the CNC-grafted ENR, an

increase in the broad absorption band between 3000 and 3500 cm^{-1} attributed to the OH peaks of CNC is observed. Additionally, there is a successive reduction in the peak intensity of C-O vibration at 1246 cm^{-1} compared to the neat ENR. This peak is significantly reduced for ENR-CNC-180 and ENR-CNC-220. An associated new peak at 1160 cm^{-1} representing the ether group is observed which confirms the chemical bond formed between ENR and CNC. This peak overlaps with the C-O-C of the CNC and is absent in the neat ENR. Furthermore, compared to neat ENR, a shift to lower wavenumbers in the absorption peaks for the CNC-modified ENR is observed. This shift to the right reflects the formation of intermolecular hydrogen bonds between the unreacted oxygenous groups of ENR and the hydroxyl groups of CNC, and intramolecular hydrogen bonds of the CNC chains as illustrated in **Scheme 4.1**. Nie *et al.*[170] in their study of ENR-Chitin nanocomposites observed similar IR intensities and concluded that chitin was grafted on ENR.

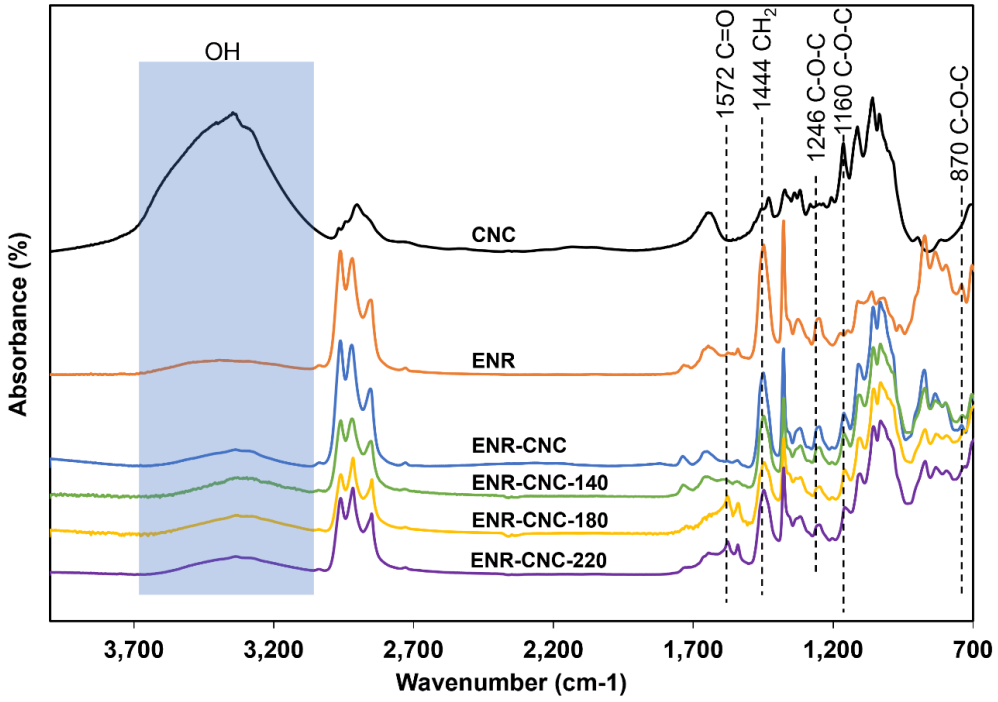

Figure 4.1. FTIR spectra of neat ENR and ENR-CNC composites.

4.3.3 X-ray photoelectron spectroscopy

XPS provides information about the chemical structures of materials by detecting the composition and elements present at the surface of a material. In this study, the C 1s and O 1s spectra for ENR and ENR composites were investigated for the interactions between ENR and CNC, and the results are presented in **Figure 4.2** and **Figure 4.3**. For all samples, the low-resolution XPS spectra presented in **Figure 4.2** showed peaks at binding energies of 105, 285, and 532 eV corresponding to Si 2p, C 1s, and O 1s, respectively. The atomic composition of these elements in the individual samples is presented in **Table 4.1.** An increase in the O/C ratios for all composite samples indicates the presence of more oxygen-containing groups attributed to the presence of CNCs in the ENR-CNC composites compared to the neat ENR. As an example, the ENR-CNC blend prepared in the absence of temperature and catalyst showed a 64% higher O/C ratio than neat ENR. The increase was due to the high oxygen content from CNC and possible hydrogen bonds. It is important to note that the peak at 105 eV (Si 2p) was rather unexpected and could be from additives (e.g., antitack agents) or impurities in the ENR.

Figure 4.2B presents the high-resolution C1s spectra of neat ENR and ENR-CNC masterbatch, which exhibits the four species C-C, C-H, C-O-C, C=C, C=O[171]. A shift in the binding energy from 285 eV in the neat ENR to 283 eV in the composites could be the result of hydrogen bonding[164]. Neat ENR showed a broad C-O-C peak, which became narrower in all the composites except the ENR-CNC-180. This observation could be a result of the participation of C-O-C in hydrogen bond formation in the blend and ENR-CNC-140. The C-O-C peak for the ENR-CNC-180 (**Figure 4.2D**) remained broad and more convoluted indicating that even though these groups participated in possible hydrogen bond formation, more C-O-C groups were formed from the oxirane ring-opening and ether bond formation (**Scheme 4.1**). Finally, the significant

reduction in the C-O-C spectra of the ENR-CNC-220 could be from oxygen bond formation as well as possible thermal degradation of the ENR polymer.

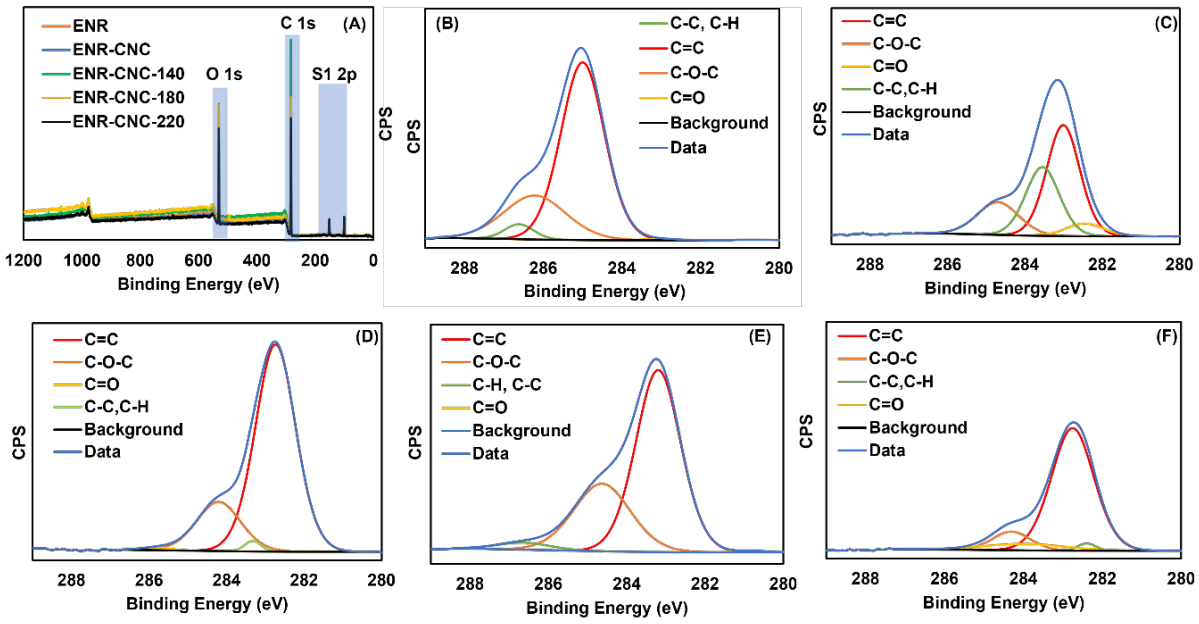

Figure 4.2. (A) Low-resolution XPS spectra of ENR and all ENR-CNC composites and high-resolution deconvoluted spectra of C 1s for (B) ENR, (C) ENR-CNC, (D) ENR-CNC-140, (E) ENR-CNC-180, and (F) ENR-CNC-220

Table 4.1. Atomic compositions and O/C ratios for ENR and ENR-CNC composites

Sample	O 1s (%)	C 1s (%)	Si 2P (%)	O/C ratio
ENR	11.63	83.93	4.44	0.14
ENR-CNC	17.39	75.10	7.51	0.23
ENR-CNC-140	16.43	77.22	6.34	0.21
ENR-CNC-180	18.57	72.92	8.36	0.25
ENR-CNC-220	17.83	71.56	10.62	0.25

The O 1s spectra of ENR presented in **Figure 4.3A** display binding energy at 530.7 eV attributed to the oxirane groups in ENR while the ENR-CNC-180 (**Figure 4.3B**) exhibits three

distinct peaks at binding energies of 530.6, 528.9, and 530.5 upon deconvolution. These peaks can be ascribed to the unreacted oxirane and ether bonds (C-O-C), C-OH, and oxygen in the glucose rings, respectively[164]. Li *et al.*[172] proposed that a 0.3 – 0.4 eV change in hydrogen bonding peaks is indicative of hydrogen bonding. From our results, only a slight shift by 0.1 eV in the binding energy of the ENR-CNC-180 is rather insignificant to conclude the presence of hydrogen bonds. Overall, the C 1s and O 1s results confirm that CNC was grafted to ENR via primary ether bonds and secondary hydrogen bonds.

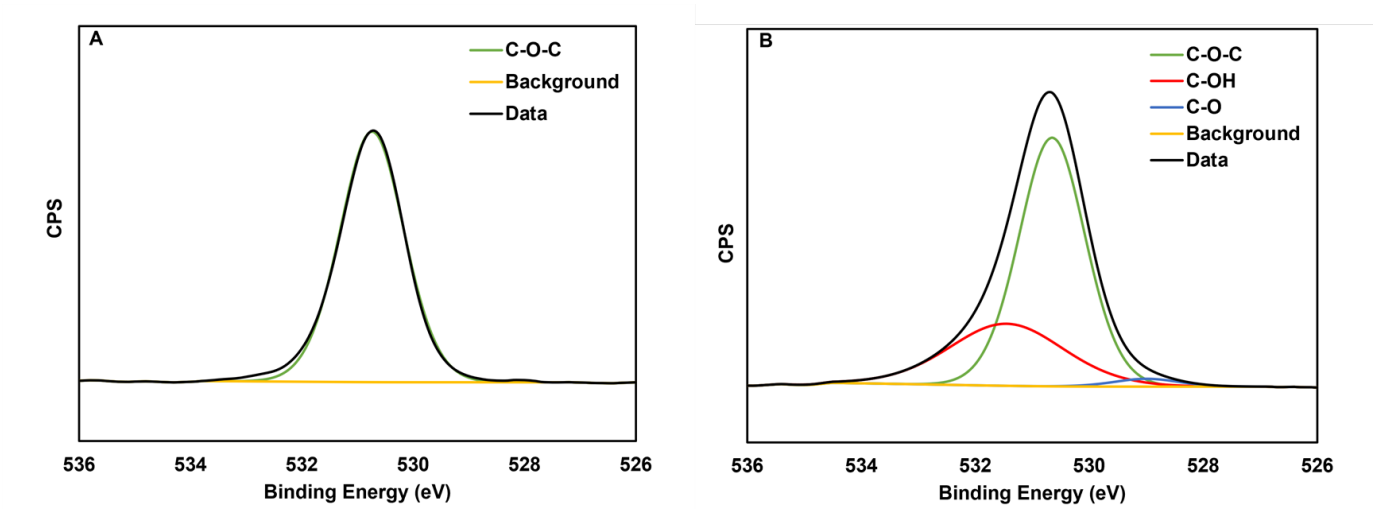

Figure 4.3. Low resolution deconvuloted spectra of O 1s for (A) ENR and (B) ENR-CNC-180

4.3.4 Toluene Swelling

To study the formation of insoluble gel between the ENR and CNC chains, equilibrium swelling tests were carried out on the baseline and masterbatch composites. **Figure 4.4** presents the images of ENR and ENR-CNC composites from the swelling experiments. As observed from **Figure 4.4**, the baseline ENR, ENR – CNC blends, and the ENR – CNC-140 samples were soluble in toluene. While the neat ENR formed a homogenous solution in toluene, the ENR-CNC and ENR-CNC-140 samples were solubilized in toluene with precipitates of CNC settling at the bottom. It is noteworthy to state that the neat ENR disintegrated into a homogenous solution within 3 h while

the ENR-CNC and ENR-CNC-140 samples were slower, taking about 5 h. This increase in dissolution time could be attributed to the presence of intramolecular hydrogen bonds between ENR and CNC or light grafting of the ENR onto the CNCs. Overall, these results suggest the absence of substantial chemical networks between the ENR and CNCs in the ENR – CNC and ENR-CNC-140 samples. On the contrary, the samples treated at 180 ^{o}C and 220 ^{o}C only swelled in toluene suggesting that the ENR and CNCs in these samples formed networks, inhibiting the diffusion of solvent molecules into the ENR composite. The insolubility of the high temperature treated composites could also be a result of the increased molecular weight from grafting as well as light crosslinks within the composite limiting its ability to solubilize. The results from the swelling experiments validate the FTIR study that demonstrates ether bond formation indicating grafted network formation between ENR and CNC.

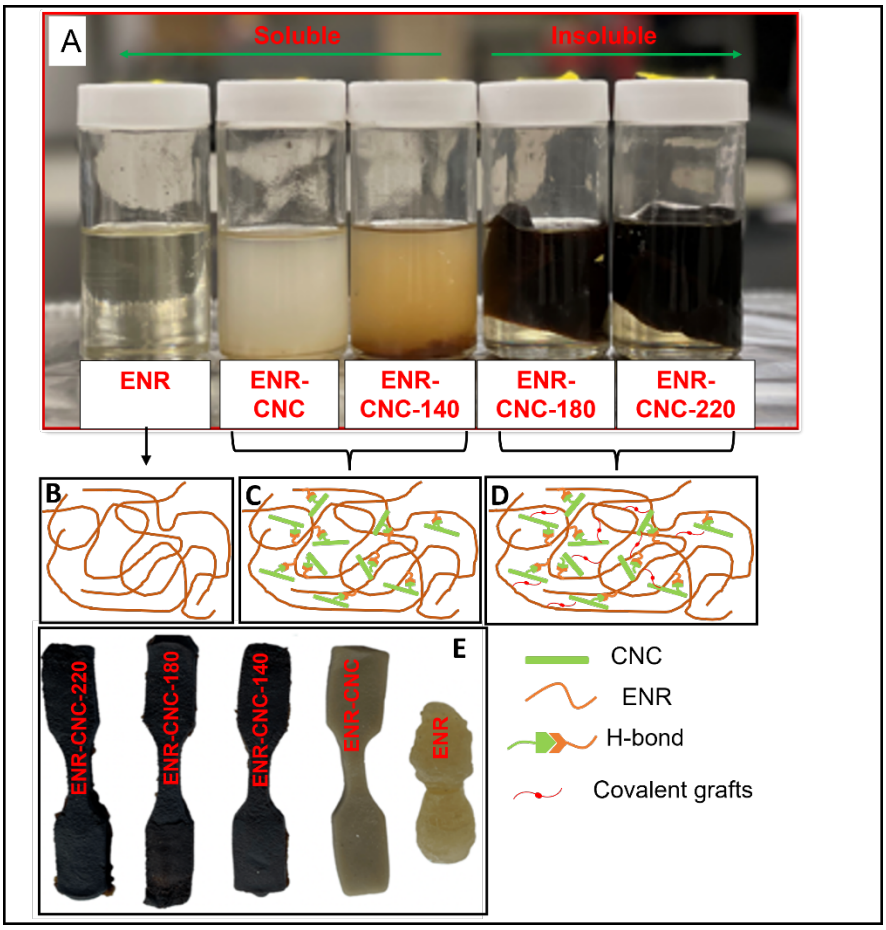

Figure 4.4. Pictures of neat (A) ENR and ENR-CNC nanocomposites in toluene, nature of interactions (B) neat ENR, (C) ENR-CNC and ENR-CNC-140, (D) ENR-CNC-180 and ENR-CNC-220, and (E) injection molded samples of neat ENR and nanocomposites showing the evolution of solubility

Based on the data obtained from the swelling experiments, the swelling index of the composites were calculated and presented in **Table 4.2.** The swelling index of the ENR-CNC-180 sample was lower than the sample processed at 220 °C. This increase in swelling index with an increase in temperature of the sample processed at 220 °C could be a result of thermal degradation and chain scission of the rubber chains and CNCs, lowering the number of covalent grafts and hence more ungrafted ENR available for swelling.

Table 4.2. Swelling index results of samples

Sample	SI (%)	Std Dev
ENR	Solubilized	N/A
ENR-CNC	Solubilized	N/A
ENR-CNC-140	Solubilized	N/A
ENR-CNC-180	346.6	61.9
ENR-CNC-220	450.0	22.8

4.3.5 Morphological analysis

Figure 4.5 presents the TEM micrograph of the neat CNC and the SEM micrographs of the brittle surfaces of all the ENR-CNC composites. The TEM image of the pristine CNC showed the rodlike structure of the CNCs. The ENR showed a flat cross-section while the composites were rough with visible white highlights, revealing the embedded CNCs in the matrix with a layer of rubber covering them. In the composites, the rodlike nature of the CNCs is non-existent as the CNCs aggregate within the composite. Particularly, huge visible surface (circled in red) aggregates of CNC can be observed in **Figure 4.5B** and **Figure 4.5C** revealing comparatively poorer dispersion, which is absent in the other composites. This is an indication that the CNCs in the ENR-CNC-180 and ENR-CNC-220 interacted better with the rubber as evidenced by the more uniform dispersion of the composite. Regardless of the nature of the interaction, no interfacial voids were observed in the composites. This reveals that the CNCs in all the composites had good interfacial interaction with the matrix attributed to the hydrogen bond formation in ENR-CNC and ENR-CNC-140, and the covalent ether bonds in addition to the hydrogen bonds in ENR-CNC-180 and ENR-CNC-220. The absence of voids also indicates that the propagation of the fracture was

through the matrix. Overall, the SEM images reveal the improved network formation with an increase in processing temperature and these results agree with the FTIR, XPS, and solvent swelling results.

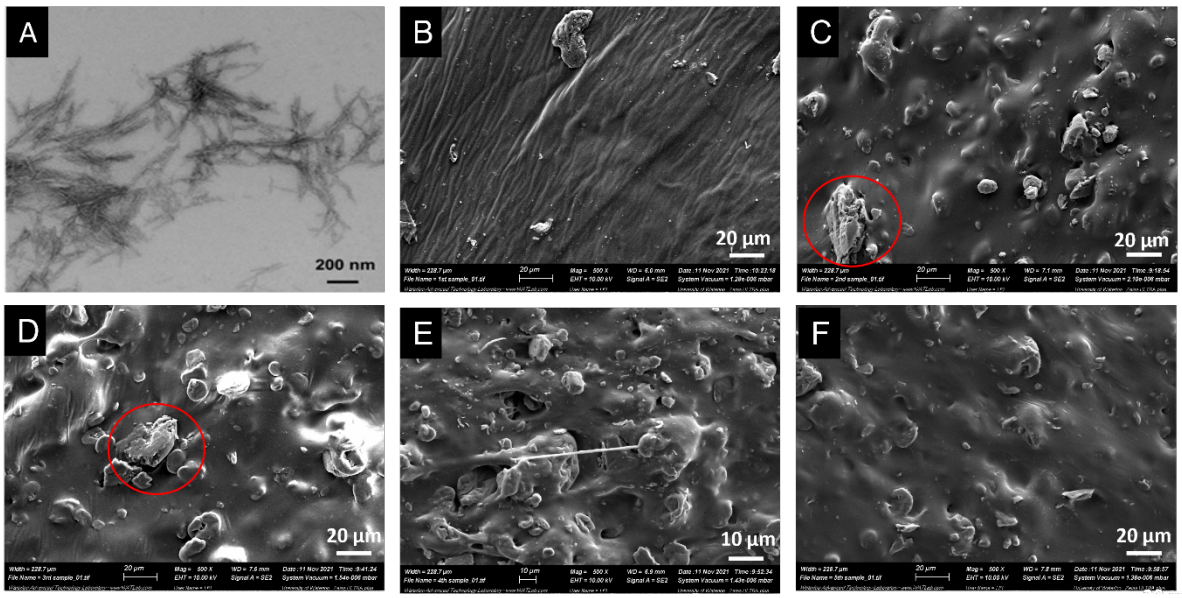

Figure 4.5. TEM micrograph of (A) Neat CNC and SEM micrographs of (B) Neat ENR, (C) ENR-CNC, (D) ENR-CNC-140, (E) ENR-CNC-180, and (F) ENR-CNC-220

4.3.6 Mechanical properties

For filled nanocomposites, the concentration and dispersion of fillers as well as the interactions between the fillers and the matrix impact the reinforcing capability of the fillers. The mechanical properties of the neat ENR and ENR-CNC nanocomposites are presented in **Figure 4.6**. The results of all the mechanical property tests show an overall increase in the CNC-filled nanocomposites compared to neat ENR.

The tensile properties of the baseline and composite specimens are presented in **Figure 4.6 (A – C)**. The tensile strength results (**Figure 4.6)** showed a decrease in tensile strength in the ENR-CNC blend and an increase in all the batch-mixed processed nanocomposites compared to neat

ENR. For all filled and processed nanocomposites, the tensile strain increased compared to ENR. A 49% decrease in tensile strength in the ENR-CNC blend compared to neat ENR was expected as the blend was highly filled (50% CNC) causing substantial aggregation and agglomerations. Such high loading in the absence of chemical bonds could lead to stress concentrators within the nanocomposite, thereby, causing a fracture[96]. This observation corroborates the results from SEM where aggregates of CNCs were observed in the ENR-CNC blend. For the batch mixed processed nanocomposites, although all nanocomposites show superior tensile properties with an increasing trend in the tensile strength up to 180 ºC and a reduction after that. The increase in reinforcing properties of the batch mixed grafted nanocomposites could be attributed to the increased chemical interactions between the ENR and the CNC. Particularly, the ENR-CNC-180 nanocomposite exhibited an 83% increase in tensile strength compared to the neat ENR, the optimum amongst all the studied nanocomposites. This superior reinforcement results from the formation of hydrogen bonds and especially the covalent grafts, which can withstand large stresses and transfer the stresses from the ENR matrix to the CNC fillers. As the reaction temperature increased to 220 ºC for the ENR-CNC-220, the observed decrease in the tensile strength can be attributed to temperature-induced chain scission as well as a decrease in the chemical interactions between the rubber matrix and the filler due to filler and rubber degradation. These results are consistent with the results obtained from the swelling experiments shown in **Table 4.2** where the swelling index was higher in the ENR-CNC-220 compared to ENR-CNC-180.

It is generally known that the incorporation of fillers in the rubber matrix decreases the elasticity resulting from the chain mobility restriction and suppresses strain crystallization in the matrix initiated by the fillers[165,173,174]. However, in this study, for all the nanocomposites, the 50 % CNC filled ENR yielded an increase in the tensile strain compared to the neat ENR as presented

in the typical stress-strain curves (**Figure 4.6B)**. This phenomenon can be explained by the nature of the bonds between the ENR and the CNCs. The ENR and CNC are linked together by the primary covalent bonds of the ENR onto the CNCs and secondary inter-and intramolecular hydrogen bonds. Additionally, within the composite, it is expected that there are combinations of grafted and ungrafted chains leading to varied chain lengths[175]. When strain is applied to the composite, either or all of the following network evolution occurs to fracture the nanocomposite: First, the shorter chains will stretch, rupture, and dissipate energy (**Scheme 4.2A**), followed by the dissociation of the weak hydrogen bonds which synergistically dissipates energy and enables the reorientation of the rubber chains in the direction of the strain, hereby improving elongation (**Scheme 4.2B**). In such situations, the extensibility is still possible due to the interfacial covalent interaction between the ENR and CNC. Finally, with further stretching, the CNCs dissociate from the ENR matrix **(Scheme 4.2C**), and fracture occurs[175,176]. The fracture mechanism described above is illustrated in **Scheme 4.2.**

The elongation at break increased until ENR-CNC-140, decreased for ENR-CNC-180, and increased thereafter. Based on the proposed fracture mechanism, the increase in elongation of the ENR-CNC blend and ENR-CNC-140 compared to neat ENR is a result of the dissociation of the sacrificial hydrogen bonds. A reduction in elongation is observed in the ENR-CNC-180 compared to the ENR-CNC-140 counterpart. Although the fracture mechanism proposes that the covalent grafts improve the elongation, for the ENR-CNC-180 composites, fewer shorter chains are expected due to the higher comparative grafting density. As noted from the characterizations, more epoxide groups participate in the grafting reactions, therefore, reducing the available epoxide groups for intramolecular hydrogen bonding. This leads to a decrease in the extensibility of the composite. Beyond ENR-CNC-180, the increase in elongation could be attributed to the lower

grafting density of the composite. These findings corroborate the swelling results previously discussed. Overall, the simultaneous increase in tensile strength and strain could be attributed to the nature of interactions within the composites.

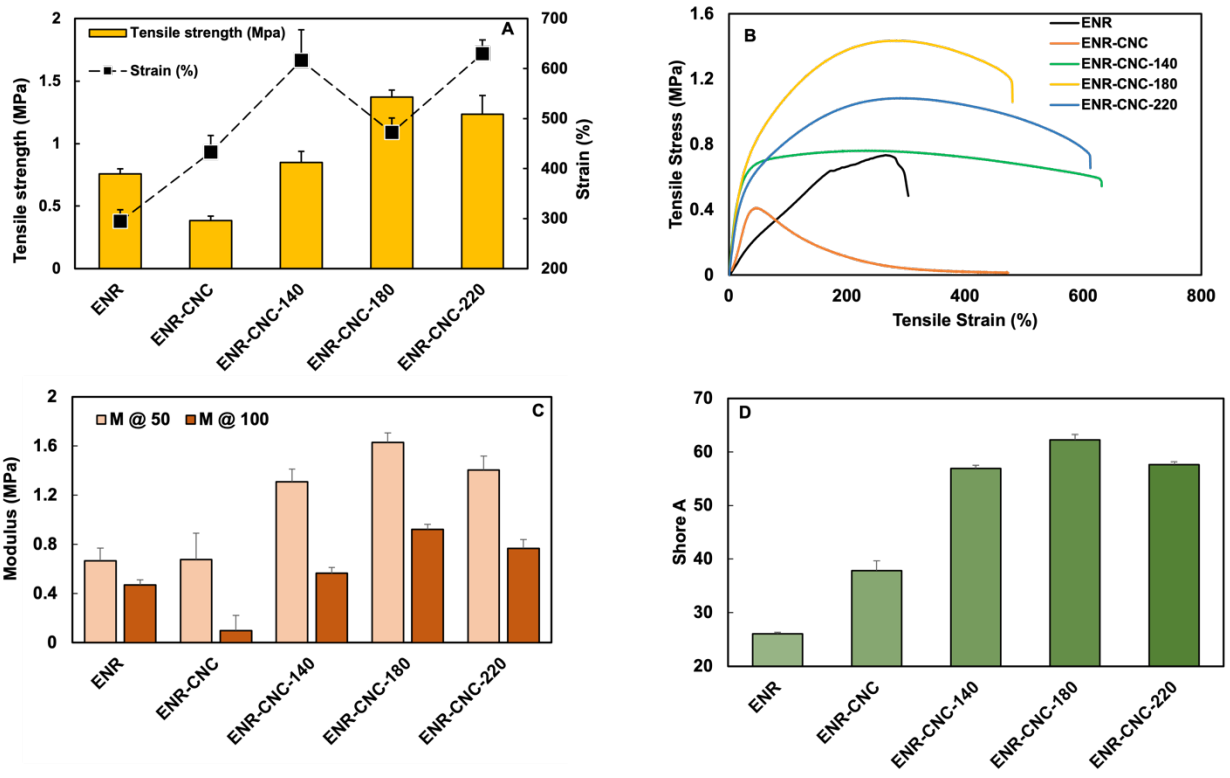

Figure 4.6. (A)Tensile strength, (B) typical tensile strength vs strain plot, (C) modulus at 50 and 100, and (D) shore A hardness test of neat ENR and ENR-CNC nanocomposites

The modulus M50 and M100 are presented in **Figure 4.6C**. Two factors affect the modulus of the filled composites. The first is the extent of dispersion of the CNCs in the ENR matrix and the second, the nature of the chemical interactions within the composite. The modulus M50 follows an increasing trend as the batch mixing processing temperature of the composite increases up to 180 °C. Compared to the neat ENR, the M50 of the ENR-CNC blend showed no significant change in modulus even with 50 % CNC concentration. This could be due to the poorly dispersed CNCs in the blend, as evidenced by the SEM images. For the catalyzed and batch-mixed nanocomposites,

the increase in modulus could be attributed to the formation of filler-filler and filler-polymer networks in the nanocomposites. The reduction beyond ENR-CNC-180 could be attributed to the chain scission of the polymer chains. The M100 follows a similar trend except for the ENR-CNC blend which decreases below the neat ENR. This could result from the aggregation of the CNCs and the encapsulation of the CNCs by the rubber marix[177].

The results from the hardness tests exhibiting the effects of the filler concentrations and chemical interactions within the nanocomposite are presented in **Figure 4.6D**. An increasing trend in hardness was observed for all the nanocomposites up to the optimum ENR-CNC-180 followed by a slight reduction thereafter. The filler concentration and grafts within the composites greatly affect the hardness, therefore, since the same concentration of filler was incorporated in all nanocomposites, the increase in the hardness can be attributed to the network formation in the composite. With increasing processing temperature, the bond formation evolves from hydrogen bonds to hydrogen bonds and covalent grafts. This increases the hardness of the composites. Beyond ENR-CNC-180, a decrease in hardness could result from thermal degradation of the filler and chain scission of the ENR in the composite.

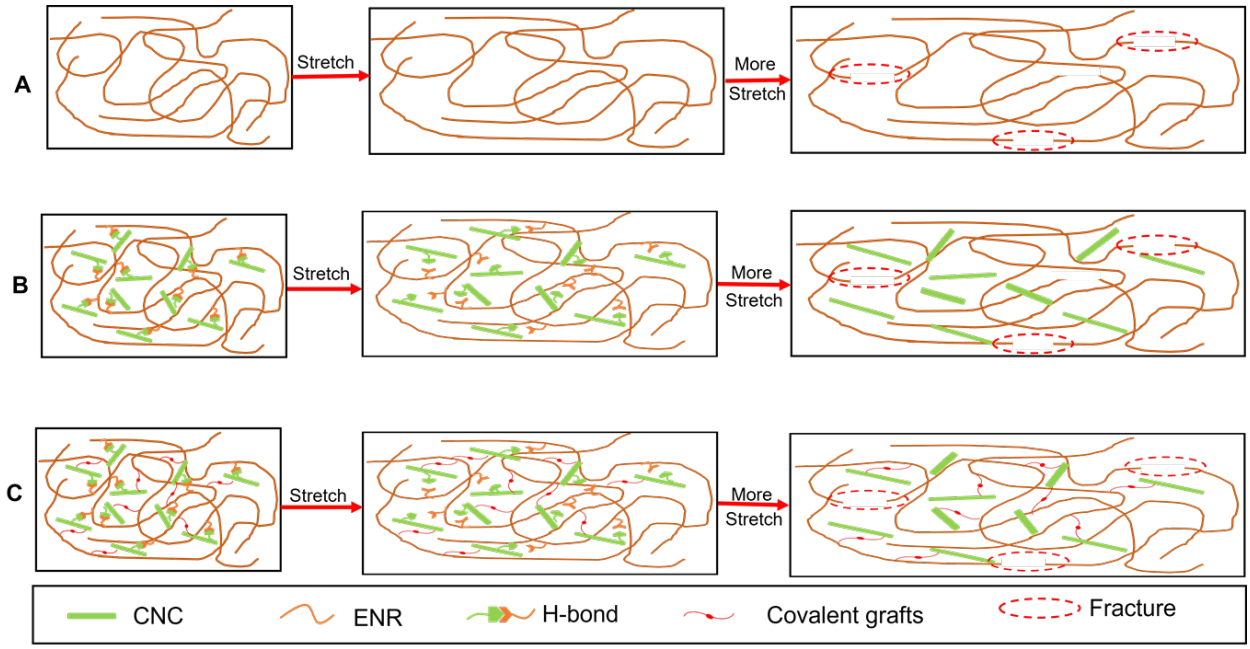

Scheme 4.2. Schematics of fracture mechanism of (A) Neat ENR (B) Low temperature ENR-CNC graft (ENR-CNC, ENR-CNC-140), and (C) High temperature grafts (ENR-CNC-180 and ENR-CNC-220)

4.3.7 Mooney viscosity

The Mooney viscosity characterizes the processability of rubbers and is influenced by the filler-filler and rubber-filler interactions, which has an overall effect on the final properties of the composite**. Figure 4.7A** presents the Mooney viscosity of the ENR-CNC composites at 100 ºC. As seen in **Figure 4.7A**, an increase in the initial Mooney (MI) was observed for all CNC filed ENR composites except for ENR-CNC-220. The increase in MI can be attributed to the presence of fillers, which increases the viscosity of the composite compared to ENR. The composite processed at 180 ºC showed the highest MI while the composite at 220 ºC displayed the lowest. A similar trend was observed for the final torque ML (1+4) which shows an increase in the Mooney viscosity for all composites where ML increased up to ENR-CNC-180 and decreased for the 220

°C treated sample. Particularly, the Mooney viscosity of ENR-CNC-180 increased by 342 % compared to the neat ENR and was higher than all the other composites. This observation can be attributed to the covalent bond grafting of the ENR onto CNC in the composite treated at 180 °C which increases the molecular weight of the composite and hence the Mooney viscosity while the decrease in ML for the 220 °C treated sample could be attributed to possible chain scission resulting from the high-temperature treatment. This result substantiates the insolubility of the composites treated at180 °C and 220 °C from the toluene swelling study as well as the ring-opening of the epoxy ring and the chemical grafting of the ENR-CNC composites. However, it is worthwhile to mention that such a massive increase in Mooney viscosity could cause processing challenges in some applications.

4.3.8 Strain Sweep Test

The strain sweep tests provide information about the amount and nature of rubber-filler interaction from the strain-dependent modulus. Generally, the impact of the filler-filler interactions is evidenced at low strains while the high strain behavior is impacted by the polymer molecular weight as well as polymer-filler interactions.

Figure 4.7B presents the strain sweep test for ENR and CNC modified ENR. The ENR-CNC composites showed an increasing trend in storage modulus with a change in processing temperature. This increased stiffness of the composites can be attributed to the incorporation of CNCs and corroborates the results obtained from the mechanical strength tests. The pristine ENR displays a linear viscoelastic region (LVR) at low strains as is typical for unfilled rubbers and with the incorporation of CNCs, the width of the LVR reduces for all composites. The change in the LVR also known as the Payne effect could be from the following contributions: the destruction of the CNC-CNC and CNC-ENR network, uncoupling of ENR chains, and interfacial adsorption and

desorption of the rubber chains[173]. Furthermore, comparing the storage modulus with strain for all filled composites, no change in the width of the LVR was observed with a change in processing temperature. This provides information about the ENR-CNC covalent grafting starting with ENR-CNC-180 as some of the hydroxyl groups of the CNCs participated in the reaction increase the stiffness of the composite and leave limited OH groups for CNC-CNC interactions. Also, ENR-CNC-220 showed reduced storage modulus compared to ENR-CNC-180 which could be attributed to thermal degradation at that temperature. It is worth noting that although the LVR of the composites is reduced, the change is less rapid when compared to carbon black[178] due to the superior filler-filler hydrogen bonds in CNC compared to the weak Van der Waals forces in carbon black.

At high strain, the storage modulus of all the CNC-ENR composites remained higher than the pristine ENR. As the high strain behavior is impacted by the polymer-filler interactions and the polymer molecular weight, the higher high strain modulus could be attributed to the CNC-ENR hydrogen bonds in the ENR-CNC blend and ENR-CNC-140, and the hydrogen bonds and chemical grafts in ENR-CNC-180 and ENR-CNC-220 (**Scheme 4.1A**). In comparison to ENR-CNC-180, ENR-CNC-220 showed a higher storage modulus slope at high strains. This could be the contribution of molecular weight reduction from thermal degradation.

4.3.9 Rheology

Rheology tests were carried out to study the microstructure of the composites. **Figure 4.7 C&D** presents the viscosity, storage, and loss modulus of CNC- filled ENR. As expected, all the samples exhibit a shear-thinning behavior initiated by microstructural changes within the composites and disentanglements of the rubber chains during flow. This leads to an increased free volume within the ENR polymer and hence, a reduction in the viscosity with shear. According to Peng *et al.*[179],

the viscosity, whether shear thinning or otherwise depends on how the viscosity is measured and calculated. As seen in **Figure 4.7C**, except for the ENR-CNC-180, the viscosity follows an increasing trend with processing temperature, the neat ENR being the lowest. Compared to the neat ENR, the CNCs in the composite occupies the free volume of the ENR matrix, thereby, increasing the viscosity. It is observed that the processing temperature of the filled sample impacts the viscosity of the composite as evidenced by the increased viscosity with temperature. This could be attributed to the chemical interactions between the ENR and the CNC – hydrogen bonds in the blend and ENR-CNC-140, and grafts in the other samples. Among all the samples, ENR-CNC-180 showed the highest viscosity attributed to the irreversible ether bond grafting of the ENR onto the CNCs. The grafting and possibly some crosslinking in the composites increase the molecular weight and inhibit the disentanglement of the polymer resulting in significantly higher viscosity compared to the neat ENR[180]. Although the viscosity increases with an increase in the processing temperature, the ENR-CNC-220 exhibited lower viscosity compared to ENR-CNC-180. This observation substantiates the grafting density of the ENR-CNC-180 was highest.

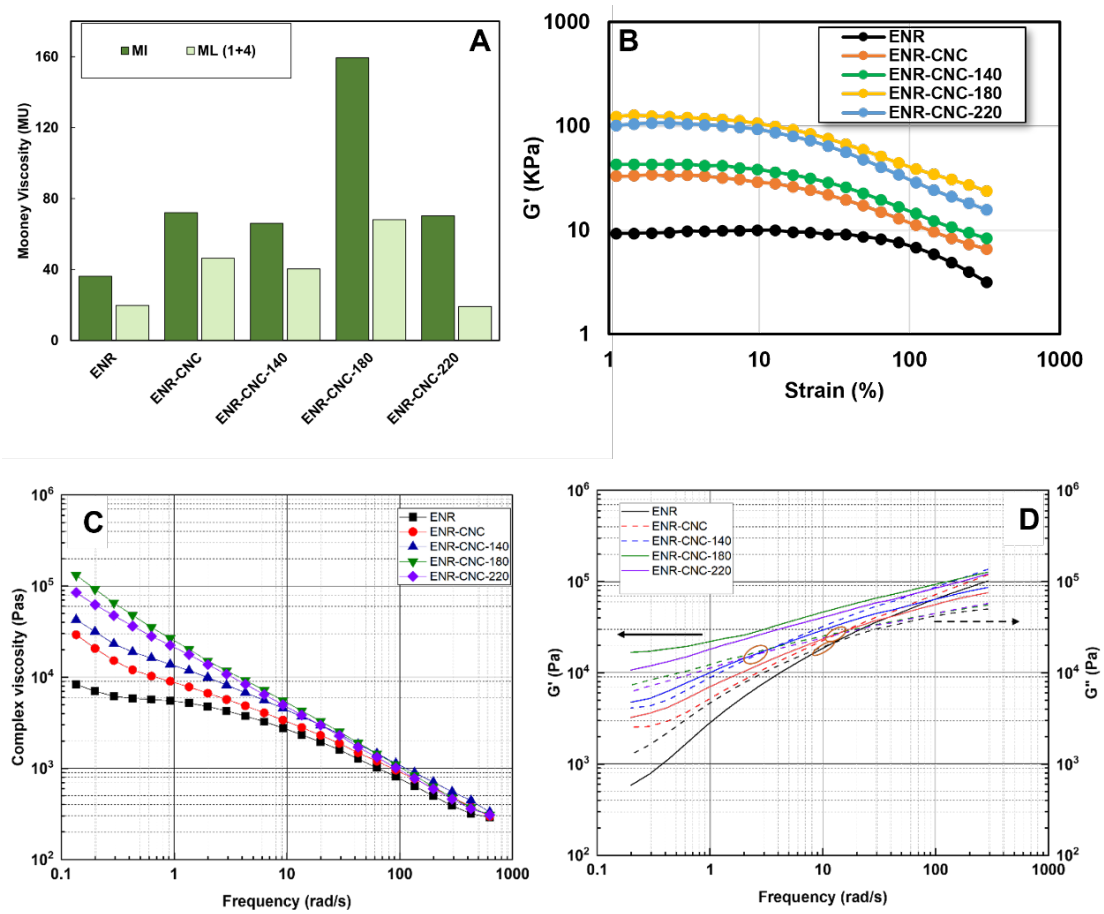

Figure 4.7. (A) Mooney Viscosity of CNC-filled ENR at different temperatures, (B) Strain dependence of storage modulus for ENR and ENR-CNC composites (C) Complex Viscosity, and (D) storage modulus and loss of neat ENR and ENR-CNC nanocomposites.

The storage and loss modulus of the samples are presented in **Figure 4.7D**. The storage modulus displays an increasing trend with increasing temperature up to ENR-CNC-180 and decreases beyond that. The positive correlation of the storage modulus with temperature proves the interactions within the CNC-filled composites strengthen with increased temperature. This means that the increased rigidity of the composites is affected by the presence of the CNCs and the molecular network within the composite. Analyzing the individual samples, a crossover frequency is observed in the ENR, ENR-CNC, and ENR-CNC-140 composites. This implies that the shear forces overtake the intermolecular interactions of the composites, which collapse the

microstructure and the composite yields. The loss modulus then becomes larger than the storage modulus and the rheological behavior transitions from being filler dominated to matrix dominated. In contrast, the ENR-CNC-180 and 220 composites lacked a crossover frequency revealing the ability of the composites to withstand the applied external forces without yielding. This can be explained in terms of the relaxation time, calculated from the inverse of the cross-over frequency. As the interactions in the composite improve, the crossover frequency moves to lower frequencies, and the relaxation time increases. When the interactions become so high, as in the case of the grafted samples, the cross-over frequency is absent, which means that G' is always higher than G" and hence the composite behaves more like an elastic solid[181,182]. The relaxation time for ENR, ENR-CNC, and ENR-CNC-140 was calculated as 0.07, 0.11, and 0.23 s, respectively. This establishes that the change in the macromolecular architecture of the composite was dependent on the physical and chemical interactions induced by a change in the processing temperature of the composite. This agrees with the swelling results and confirms the grafting of ENR onto CNCs. It is widely reported that molecular chemistry has a positive correlation with the storage modulus and our results agree.

4.4 Summary of Chapter 4

This study aimed to prepare a masterbatch of CNC filled ENR to be employed as a filler for other hydrophobic rubbers to improve filler dispersion in the rubber matrix. CNC was used as a reinforcing filler in ENR to prepare ENR-CNC masterbatch in a base-catalyzed batch-mixed *in situ* reaction at varying temperatures. The investigated process avoids the use of toxic and ecologically undesirable solvents. The processed composites displayed excellent interaction due to covalent ether bond and hydrogen bond formation between the ENR matrix and CNC fillers, which were confirmed from FTIR, XPS, and rheology investigations. Toluene swelling and

Mooney viscosity evaluations revealed that grafting started at 180 ºC for the processed samples, and below that, the ENR solubilized, leaving precipitates of CNCs. From tensile testing, an initial decrease in tensile strength was observed with the addition of fillers, but the composites showed a progressive increase in tensile strength, strain, modulus, and hardness as a result of the thermo catalyzed batch mixed processing. Viscosity and storage modulus tests displayed a similar trend. Finally, the strain-sweep experiments revealed Payne effects at low strains for all composites, but even with the high composition of fillers, the composites showed the presence of an LVR. For all experiments, the properties of the ENR-CNC-220 deteriorated compared to the lower temperature processed counterparts due to thermal degradation. Overall, the grafting of ENR onto CNCs exhibited improved properties compared to neat ENR even at high filler loading. It is noteworthy that pristine CNC was employed, and no external crosslinking agents were incorporated to achieve these properties. The composite demonstrated in this study can be utilized as a masterbatch reinforcing filler in other hydrophobic rubber systems such that the ENR is compatible with the rubber while carrying the CNC.

Chapter 5. Silane-modified cellulose nanocrystals (CNCs) based natural rubber composites[3]

5.1 Introduction

The resilience and flexibility of rubbers are distinctive features that render them desirable for many applications (e.g., automotive, electronics, marine, and commodity products such as shoe soles, gloves, vehicle tires, etc.). At the same time, rubber, in its pristine form, lacks the strength required for practical applications. While introducing chemical crosslinks between the long chains of rubber by vulcanization improves its mechanical properties, the incorporation of fillers ensures desirable physical and chemical properties and, in some cases, reduces cost [95,183] Both organic and inorganic fillers have been explored for rubber applications, but carbon black remains the commonly used and commercialized filler for rubber. Although commonly used, carbon black is extracted from fossil fuel sources, thus contributing to greenhouse gas generation. Also, it is a reported carcinogenic substance[184] and requires high energy during production. Due to the recent interest in material sustainability, green and environmentally friendly fillers derived from sustainable and abundant nature are vital to industry and the research community.

Different natural fillers have been studied and reported in the literature, but among these fillers, cellulose nanocrystals (CNC) have gained significant attention because it is abundant, able to degrade in the natural environment, sustainable, has low density, and high strength. Also, it is rich in hydroxyl (-OH) groups, making it amenable to functionalization to extend its properties. While the features of CNCs are desirable, the rich -OH groups render it hydrophilic, making it difficult to disperse homogenously in hydrophobic matrices, such as rubber. Therefore, a composite of

[3] A version of this chapter has been submitted for peer-reviewed publication.

natural rubber and CNC suffers from poor filler dispersion, aggregation of the CNCs, and poor interfacial bonding within the matrix. These aggregates create stress and weak points within the composite, leading to poor mechanical properties of the composite, which limits the reinforcing effect of the filler. Due to the criticality of filler dispersion in composite reinforcement, different approaches to better disperse the CNCs in hydrophobic matrices have been investigated. Both physical methods, such as optimizing the fabrication methods[95] and chemical methods (functionalization)[17,185–187] have been explored.

The chemical modification of cellulose nanocrystals (CNCs) involves altering their surface properties through various chemical reactions, enabling improved compatibility with different matrices in composite materials. Several methods have been explored for this purpose, including esterification[151,188], acetylation[189–191] and silane coupling agents[19,192,193] among others. Trialkoxylsilanes are widely used as coupling agents to improve filler dispersion in polymer matrices because they readily partake in hydrolysis and condensation reactions [194]. Silanes with organic functional groups such as amine can improve adhesion or even form copolymers with matrices, thereby improving dispersion. Pei *et al.*[195] partially modified CNC using *n*-dodecyldimethylchlorosilane (DDMSiCl) for composition in poly (L-lactide) and their results showed that the modified CNCs were stable in non-polar solvents and improved the mechanical properties of the nanocomposite compared to when unmodified CNCs was employed in the composition. Raquez *et al.* [196] modified cellulose nanowhiskers using methacryloxy propyltrimethoxy silane (MPS) to be used as a reinforcing filler. As is typical with alkoxysilanes, their procedure involved a hydrolysis step, which is rather time-consuming. Taipina *et al.* [197] modified cotton nanocrystals using 3-isocyanotopropyltriethoxysilane (IPTS), they reported

promising results with modification on the surface of the cotton nanocrystals while maintaining the structural integrity as their x-ray diffraction results showed.

The major challenge with the chemical modification of CNCs is restricting the modification to the surface while preserving the morphology of the CNCs to retain their crystal structure. The high strength of CNCs originates from its crystal structure and morphological changes in the crystal structure due to solvent swelling and chemical modification give rise to inferior mechanical properties, defeating the purpose of using CNC as a reinforcing filler. This means that while modifying the CNCs to improve dispersion in the hydrophobic rubber, restricting the chemical modification to the surface of the CNCs is also important to maintain the integrity of the CNCs.

This research hypothesizes that controlled surface modification of CNCs brings about enhanced rubber composite properties desirable for practical applications, while maintaining ease of processability with the existing rubber processing technology. In this research, IPTS was employed to modify the surface OH groups of the CNC. IPTS was chosen because the isocyanate group is highly reactive. Furthermore, while functional alkoxysilanes require a hydrolysis step to form silanol groups, which is time-consuming, the highly reactive isocyanate group reacts directly with the -OH groups in CNC. To restrain the modification to the surface hydroxyl groups, dimethylformamide DMF was used as a solvent for the reaction because of its relative performance over other solvents in retaining CNC crystal structure while simultaneously dispersing the CNC[198]. This research aimed to promote the dispersion and interfacial adhesion of the CNCs in the rubber polymer matrix by modification and to study the resulting properties of the nanocomposite of rubber and modified CNCs.

5.2 Materials and methods

5.2.1 Materials

CNCs were supplied as a dried powder by Celluforce Inc (QC, Canada). The length, width, aspect ratio, and sulphur content of the CNCs were 150 nm, 7.5 nm, 20 nm, and 5000-9000 mg/kg respectively. Natural rubber slab was received from AirBoss Rubber Solutions (Kitchener, ON, Canada). Zinc oxide, stearic acid, N-tert-2-benzothiazyl sulfonamide (TBBS), Sulfur, Tin (II) 2-ethylhexanoate, N, N-dimethylformamide (DMF), and ethanol were supplied by Sigma-Aldrich. 3-(Triethoxysilyl)propyl isocyanate (IPTS) was supplied by Hubei Co-Formula Material Tech Company, Ltd (Wuhan, China).

5.2.2 Methods

5.2.2.1 IPTS modification of CNCs

Oven-dried CNC weighed using an analytical balance (Mettler Toledo AG205) was dispersed in DMF (1:10 (wt./wt.) ratio of CNC to DMF) for 30 mins using a probe sonicator (Fischer Scientific Model-CL18). After sonication, the DMF/CNC was transferred to a 500 mL three-headed flask equipped with a thermometer, condenser, magnetic stir bar, and nitrogen inlet and submerged in an oil bath. The reaction mixture was left to stir until the desired temperature according to the experimental design (**Table 5.1**). Once at temperature, 0.2 molar ratio of Tin (II) 2-ethylhexanoate catalyst with respect to CNC was added and stirred in, then a calculated amount of IPTS in mol % (corresponding to the concentration of surface hydroxyl groups based on the chain ratio in accordance with Eyley and Thielemans[18]) according to the design of experiment in **Table 5.1** was added slowly using transfer pipettes. The reaction was then conducted according to the

temperatures in **Table 5.1** for 2h. Once the reaction was complete, the product was cooled, isolated by centrifugation, washed three times in ethanol, and dried overnight (80 ^{o}C).

Table 5.1. Design of experiments for modification of CNCs

Sample Name	Temperature	Mole Ratio
2 mol 50	50	2
6.5 mol 50	50	6.5
2 mole 65	65	2
6.5 mol 65	65	6.5
4.5 mol 57.5-c1	57.5	4.5
4.5 mol 57.5-c2	57.5	4.5
4.5 mol 57.5-c3	57.5	4.5

For this experimental design, a 2^2 factorial design of experiments to vary the mol ratio of IPTS to CNC and temperature were performed. For the mole ratio, the low and high values were chosen to correspond to the concentration of surface hydroxyl groups of cellulose, and the temperatures were chosen to be high enough for the reaction and low sufficient to retain the crystalline structure of the CNC. The reaction time was chosen based on preliminary studies, and 2 h was determined to be the maximum feasible time to carry out the reaction without destroying the crystalline structure of the CNCs.

5.2.2.2 Characterization of modified CNCs

Fourier transform infrared (FTIR) spectroscopy

Sample pellets for FTIR were prepared by crushing 10 mg of the individual modified CNC samples with 300 mg of KBr powder and pressing them into a pellet at approximately 12,000 psi for 2 min

using a Carver hydraulic press. CNC pellets used as control, and KBr pellets used to collect background were also prepared using the same method. FTIR analysis was then performed on the pellets using a Fisher Scientific Nicolet 6700 FT-IR spectrometer, where 32 scans were collected and averaged.

Nuclear Magnetic Resonance (^{1}H-NMR)

Proton NMR analysis was conducted using a Bruker 500 MHz high resolution MNR (Bruker spectrospin 500 MHZ Ultrashield, Bruker Corporation, MA). The samples were prepared by either dissolving/dispersing 10 mg of individual samples in 10 ml deuterated DMSO or chloroform based on solubility. The dispersion was then heated overnight at 80℃.

Elemental analysis

The carbon and nitrogen content in the samples was determined using a 4010 Elemental Analyzer (Costech Instruments, Italy) equipped with a Delta Plus XL (Thermo-Flannigan, Germany) continuous flow isotope ratio mass spectrometer. 1 mg of each sample was weighed and analyzed.

X-ray diffractometry (XRD)

XRD patterns of the pristine and modified CNCs was conducted using a Bruker D-8 focus X-ray Diffractometer operated at 40 kV and 40 mA with Cu Kα and data between 2Θ at 5^o and 40 ^{o} at a 1 s/step and increment of 0.02 were collected using the powdered samples.

Contact angle measurements

CNC and modified CNC samples were dispersed in water to prepare 20 mL of 0.15 wt.% sample dispersion using a probe sonicator. Small amounts of the dispersed samples were then dropped on glass plates at four points using disposable pipettes. These points were referred to as sample points. The glass plates were then placed in an oven at 80 ^{o}C for 30 min to dry. Once dried, another set of

droplets were layered on the initially dried sample points and dried again. This process was repeated until four layers of samples were present at each sample point. The final set of sample points were air-dried to promote a gentle drying process. Finally, the glass plates were placed in a vacuum oven (Shell lab) set to 35 ^{o}C and under vacuum for 45 min.

Contact angle measurements were conducted using a custom-built sessile drop system fitted with new-era pump systems and a high-power camera to capture images of the droplets. For the test, 3 μL of water was dropped on the surface of the samples, and the images were captured at 0 s (right after the water contacted the sample). The contact angle of the images was measured using Matlab software.

Dispersibility studies

The dispersion of the modified CNCs was studied in water, ethanol, DMSO, acetone, THF, chloroform, and toluene to study the change in polarity of the samples. About 10 mg of each sample was added to 10 mL of solvent and dispersed using a probe sonicator for 5 minutes. After sonication, pictures were immediately taken and termed 0 hours. The samples were left undisturbed for 24 h and photographs were collected.

5.2.2.3 NR-mCNC nanocomposite fabrication

Modified CNC ranging from 2.5 to 20% was mixed into bale rubber using a two-roll mill for approximately 20 minutes. The mixing time was the same for all samples. The rubber composite sheets were then cut into thin strips in preparation for extrusion. Extrusion was performed using a mini twin-screw extruder (Prism USALAB 16 mini extruder) equipped with five heating zones configured to a screw speed of 200 rpm, screw temperature of 80 ^{o}C, and die temperature of 100 ^{o}C (actual temperature in screws ranged from 90-100 ^{o}C and 110 ^{o}C in the dies). The rubber composite was fed manually to the extruder, and 3 extrusion passes were carried out.

For control, unfilled NR and NR filled with 10% pristine CNC were subjected to the same processing as the modified rubber composites. The samples were coded NR, NR-2.5 mCNC, NR-5 mCNC, NR-10 mCNC, NR-10CNC and NR-20 mCNC as shown in **Table 5.2.** The samples were cooled and divided into two parts; half were compounded with curatives for vulcanization, and the other half was used as is for further analysis. The nanocomposites were passed through the two-roll mill, where curative recipes were mixed in (**Table 5.2)**.

Table 5.2. Formulation for NR-mCNC nanocomposite

Materials	**Sample Name**					
	NR (Control)	NR-2.5 mCNC	NR-5 mCNC	NR-10 mCNC	NR-10 CNC	NR-20 mCNC
NR	100	100	100	100	100	100
Sulfur	1.5	1.5	1.5	1.5	1.5	1.5
Stearic acid	1	1	1	1	1	1
TBBS	1.5	1.5	1.5	1.5	1.5	1.5
Zinc oxide	3	3	3	3	3	3
mCNC	0	2.5	5	10	0	20
CNC	0	0	0	0	10	0

5.2.2.4 Rubber composite vulcanization

The rubber was vulcanized in an electrically heated hydraulic press (Pasadena Hydraulics Inc., model. P-215C, CA, USA) equipped with a 45 cm × 45 cm platen, at 185 ^{o}C and 1.2 MN using 70 g of samples. Cure property tests predetermined the vulcanization time carried out on the

respective samples (results presented in **Table 5.3**) and individual samples were vulcanized to optimum cure time (T_{C90}) for each sample from the cure property test. Once the cure time was attained, the samples were immediately submerged in deionized water to end the reaction. This was followed by room temperature condition for 24 h to prepare the rubber sheets for further testing. The mCNC modified using 6.5 mol IPTS at 65 ^{o}C was chosen for the composition, and a control sample using 10% unmodified CNC was also prepared.

Table 5.3. Cure characteristics of NR-mCNC vulcanizates.

Property	**NR (Control)**	**NR-2.5% mCNC**	**NR-5% mCNC**	**NR-10% mCNC**	**NR-20% mCNC**
ML (lb-in)	0.29	0.22	0.27	0.27	0.2
Ts2 (min)	1.26	1.28	1.29	1.22	1.13
Tc90 (min)	1.58	1.61	1.65	1.56	1.47
MH (lb-in)	4.93	4.93	5.29	5.68	6.73

5.2.2.5 Rubber composite characterization

Transmission electron microscopy (TEM)

Transmission electron microscopy (TEM) (Philips, CM 10) was done to visualize how the mCNCs dispersed in the composite. Representative unvulcanized samples (NR, NR-10 mCNC and NR-CNC) samples were placed into a cryo-holder and frozen at -140 ^{o}C, then sections (100-150 nm thickness) were cut with a diamond knife on a cryo-ultramicrotome (Leica, EM FC7) and placed onto 100 mesh Formvar-coated Cu grids for analysis. Transmission electron microscopy (TEM)

micrographs were taken from the sections with a JEOL 1200EX TEMSCAN equipped with an AMT Digital Camera (4 megapixels) using an acceleration voltage of 80 kV.

Scanning electron microscope (SEM) with Energy Dispersive X-ray (EDX) mapping

A scanning electron microscope (Oxford Instruments INCAx-act) with EDX capability was used to study the distribution of the additives, particularly zinc oxide, in the rubber composite. For this study, the samples were gold coated.

Cure Characteristics

A rubber process analyzer (Pioneer MDR 2000) was used to determine the cure characteristics as per ASTM D 2084. Sample weighing 5 g was lodged in the bottom die and tested at 185 ^{o}C. The torque transducer recorded the torque charted as a time function on the cure graph. The scotch time (T_{S2}), and optimum cure time (T_{c90}) were recorded and is presented in **Table 3**.

Mechanical properties

The tensile test was carried out using a Shimadzu- AGS-X (Shimadzu Corp, Kyoto, Japan) tensile testing instrument equipped with a 2 kN load cell at 500 mm/min according to ASTM D 412. Test samples were slit in the direction of the mill grain from the vulcanized samples, and five replicates were tested. The hardness test was done using a Shore A digital durometer and according to ASTM D2240. Test specimens stacked to approximately 6 mm thickness were put on a flat surface, and the instrument's indentor was released and pressed upon the specimen. Data was collected with 1 s of firm contact between the indentor and specimen. Readings from three points were taken and averaged.

Toluene swelling studies.

Swelling tests was carried out according to the method described by Ojogbo *et al.* [173] For this test, 0.2 g of specimen from each sample was submerged in toluene until there was no change in swelling (72 h). The specimens were weighed at intervals of 24 h after wiping off the toluene on the surface. The Kraus equation was then used to estimate the effect of CNC on vulcanization. vulcanizate was then calculated[199–201].

Rheological properties

Mooney viscosity

The Mooney viscosity was measured using an Alpha MV 2000 Mooney viscometer and the test was performed as per ASTM D1646-19A using 25 mg of sample. The initial and final Mooney viscosity for all samples were recorded and analyzed.

Frequency sweep

Rheology was studied using a Haake Mars III parallel plate rheometer (Thermo-Fisher Scientific Inc., Waltham, MA, USA). Disc-like specimens, 2 mm thick and 25 mm in diameter were injection molded using a Haake Minijet Pro injection molding machine (Thermo Scientific). The injection pressure, injection time, injection back pressure, cylinder temperature, and mold temperature were 700 bar, 10 s, 500 bar, 100 ^{o}C, and 30 ^{o}C, respectively. A frequency sweep was performed within the linear viscoelastic region from 0.1 to 100 rad/s at a plate gap of 2 mm.

Strain sweep

The strain sweep to investigate the filler-filler interactions within the rubber composite was carried out using a rubber process analyzer (RPA) (Pioneer MDR 2000) as per ASTM D 6204-99. The RPA die was loaded with 5 g of the uncured rubber composite sample and a strain sweep from

0.3 to 100 at 1 rad/s frequency was carried out at 60 ºC. The storage modulus, loss modulus, and complex viscosity were recorded.

5.3 Statistical analysis

A one-way analysis of variance (ANOVA) was carried out to establish the significance of the difference in means of the samples ($p < 0.05$).

5.4 Results and discussion

5.4.1 IPTS modification of CNC

To utilize CNCs as effective reinforcing fillers of non-polar matrices, such as rubber, surface modification to increase the CNCs hydrophobicity is employed to enhance their interaction and dispersion in such matrices. While the surface chemical modification to bring about the hydrophobicity is beneficial, it is also important that the surface modification be carried out under mild reaction conditions to prevent the destruction of the crystal structure of the CNCs responsible for their reinforcing capability. In this work, IPTS was chosen as a modifier because of the high reactivity of the isocyanate groups and the hydrophobicity of the residual silane groups. The importance of choosing a silane with high reactivity towards the OH groups of CNCs was to ensure the surface reaction proceeded under mild reaction conditions using dispersed CNCs and at low temperatures. On the contrary, isocyanate groups could also be reactive with water (from humidity in the environment) that caps the IPTS and limits its reaction with CNCs. This was prevented by carrying out the reaction in a dry system under nitrogen inlet purge.

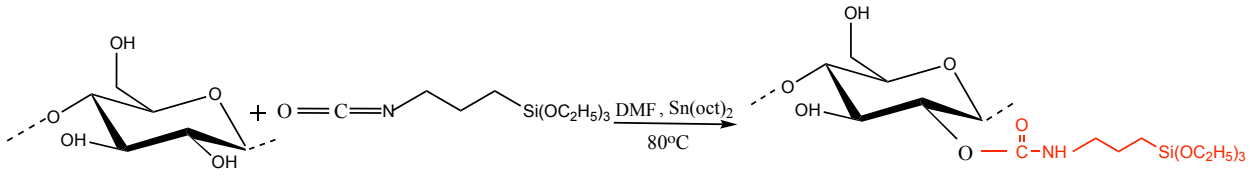

Scheme 5.1. Reaction scheme for the modification of CNC using IPTS

Scheme 5.1 presents the reaction mechanism for the surface hydrophobic modification of CNCs with IPTS. The catalyzed reaction ($Sn(Oct)_2$ catalyst) was performed using DMF as a solvent at varied temperatures and mole ratio of IPTS to the concentration of surface hydroxyl groups in CNCs according to the DOE in **Table 5.1.** The use of DMF as a solvent in this reaction limits the swelling of the cellulose nanocrystal chains, hence limiting the reaction to only the surface of the CNC, which was desired. For this reaction, the isocyanate group (N=C=O) reacts with CNC's hydroxyl group (-OH) to form urethane covalent bond with the IPTS molecules.

5.4.2 Fourier Transform Infrared Spectroscopy (FTIR)

The FTIR spectra of pristine CNC and the various modified CNCs are presented in **Figure 5.1.** The CNC spectrum is characterized by a broad band at 3600 – 3000 cm^{-1} corresponding to the -OH stretching vibrations, a band at 2880 and 1430 cm^{-1} attributed to the asymmetric and symmetric -CH- stretching while the peak at 1164 cm^{-1} corresponds to the glycosidic bond C-O-C stretching. For IPTS, the spectrum shows two characteristic isocyanate peaks: one high-intensity peak at 2270 cm^{-1} and a low-intensity peak at 1700 cm^{-1} corresponding to the N=C=O asymmetric and symmetric stretching, respectively[197]. The absence of the high-intensity N=C=O peak in the mCNCs suggests the consumption of this group during the reaction. As a result of this, the IR spectra for the mCNCs show a slight reduction in the -OH broad band where the proposed grafting reaction occurs and the appearance of three new peaks: C=O peak at 1700 cm^{-1} corresponding to the carbonyl peak, the NH bending from the imino group OOCNH[192] at 1530 cm^{-1} and the C-N peak at 760 cm^{-1}.

Furthermore, there could be a possible formation of polysilsesquioxane (Si-O-Si) from the crosslinking of the silane resulting from the condensation of the silanol groups. This peak at 760 cm^{-1} overlaps with the C-O-C peak in CNC and Si-O-C peak from the grafting reaction, making it

difficult to detect using the IR technique [188,202,203]. Therefore, the IR technique alone is inconclusive in determining the formation of the polysilsesquioxane. The appearance of these new peaks in the mCNC samples results from the opening of the urethane group and the grafting reaction.

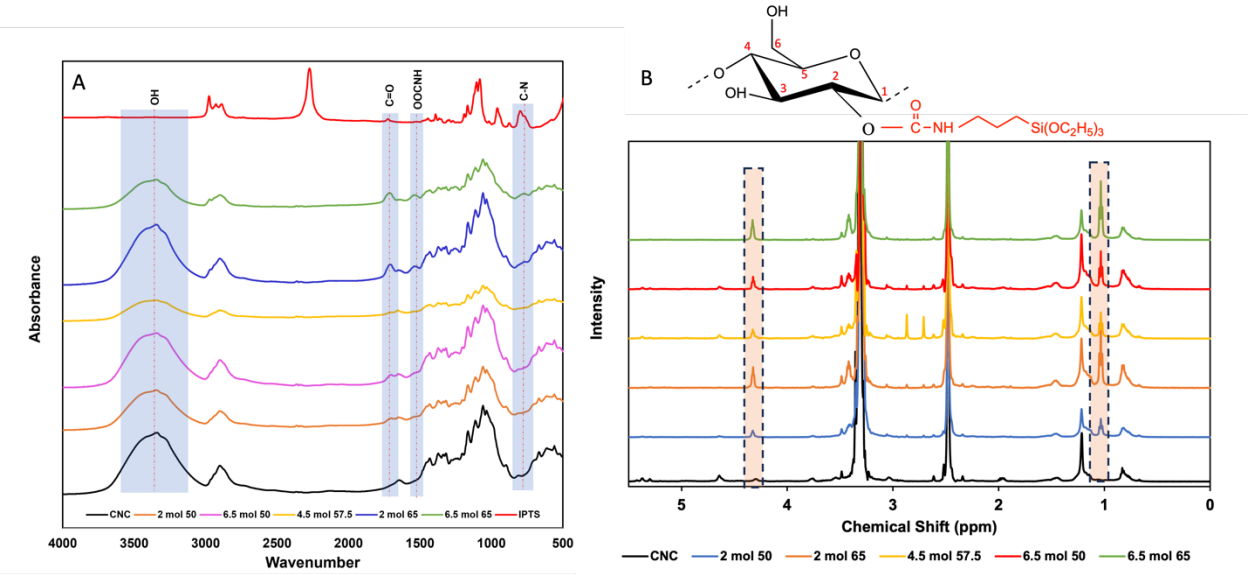

Figure 5.1. (A) FTIR spectra (B) H-NMR spectra of CNC and IPTS modified CNCs at various design conditions.

5.4.3 Proton nuclear magnetic resonance (^{1}H-NMR)

NMR analysis was employed to verify the modification of IPTS on CNCs and the spectra are presented in **Figure 5.1B.** The spectra of pristine CNCs showed peaks clustered at chemical peak 3.8-3.1 ppm attributed to the protons in position 2-6 in the AGU and OH peaks at 4.3 ppm at position 6 and an OH peak overlap at 5.3 ppm at positions 2 & 3[204]. Furthermore, the peak at 4.6 ppm corresponds to the equatorial proton at the α-1,4 linkage[205]. Upon modification with IPTS, two new characteristic peaks are present in the IPTS modified samples; one at 1 ppm attributed to the methylene group from IPTS and the other at 4.3 ppm from the amino group overlaps with the

OH group from CNC. This appearance of these new peaks indicates successful modification with CNCs.

The degree of substitution (DS) presented in **Table 5.4** was then calculated using the integrated signals of the methyl groups from the mCNCs and the signals from the protons of the AGU according to equation 5.1.

$$DS = \frac{\frac{Isignal}{9}}{\frac{IAGU}{7}} \quad (5.1)$$

Where $Isignal$ corresponds to the integral of the methylene signal at 1 ppm and I_{AGU} refers to the integrals of the protons from CNCs that appeared between 3.1 -5.3 ppm.

The DS values obtained showed the impact of temperature on the modification reaction. The DS is observed to increase significantly when the reaction temperature is increased from 50 to 65 ºC revealing that temperature influences the reaction efficiency. Furthermore, the low DS values indicate restriction of the IPTS modification to the surface of the CNCs.

5.4.4 Elemental analysis

The mass percentages of carbon and nitrogen determined by elemental analysis (EA) are presented in **Table 5.4**. The CNC contains 41.86% carbon and showed an absence of nitrogen which was expected. With modification, the introduction of nitrogen, accompanied by a decrease in carbon confirms that CNC forms a covalent bond with the IPTS. This can be seen from the reaction scheme in **Scheme 5.1,** where the CNC and IPTS reaction product forms a new molecular structure containing nitrogen. This decrease in carbon was rather unexpected as IPTS contains 10 carbon atoms, which was expected to increase the carbon percentage of the reaction product. Also, comparing the experimental and theoretical values (not shown), assuming a degree of substitution of either 1 or 3 (assuming the IPTS reacted with one or three OH per anhydroglucose unit (AGU),

the theoretical percent carbon is calculated to be significantly higher than the experimental value. A plausible explanation for this could be the formation of polysilsesquioxane (Si-O-Si) during the reaction, leading to the loss of one or more ethyl groups from the reaction product, crosslinking of the silane, and hence loss of carbon (**Scheme 5.2**). This carbon loss is shown in the lower percent carbon in the modified CNCs compared to the pristine CNCs. Taipina *et al*. [197] in their surface modification of cotton nanocrystals with silane, used ^{29}Si NMR to confirm the formation of the siloxane network and reported peaks corresponding to $Si(OSi)_3$ and $Si(OSi_2)$.

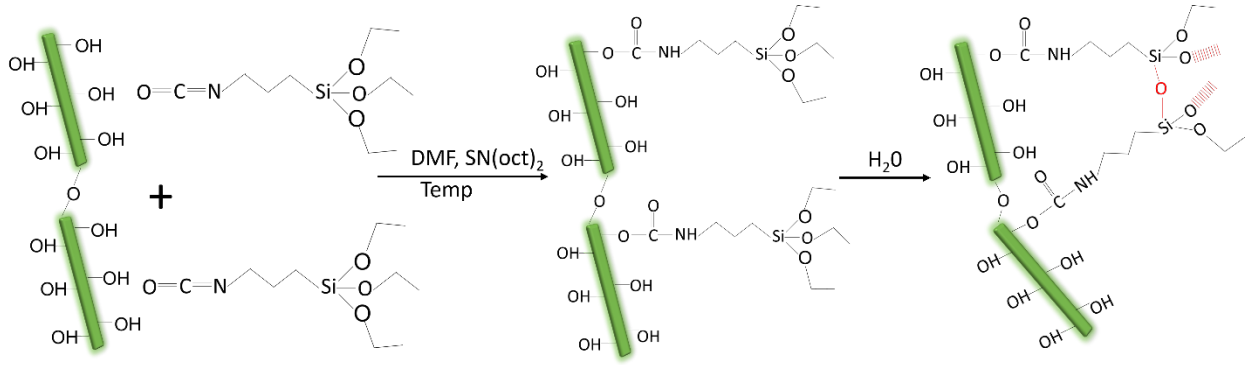

Scheme 5.2. Reaction scheme for possible polysilsesquioxane formation during IPTS modification of CNC

For the same moles of IPTS and with an increase in temperature from 50 to 65 °C, the percent carbon (%C) decreases while the percent nitrogen (%N) increases for all modified CNCs. When the mole ratio increases to 6.5, the change in %C is rather insignificant as compared to the 2 mol at the same temperatures. However, as presented in **Table 5.4**, even while no change in %N is observed as the mole ratio increased from 2 to 6.5 at 50 °C, the change in %N for 6.5 mol at 65 °C is very significant compared to the same temperature using 2 mol IPTS. This indicates that increasing the reaction temperature facilitates IPTS modification of CNCs. Interestingly, while the

other experimental conditions showed the effect of temperature on the %N, except for one, the three center points (4.5 mol 57.5 ºC) had the lowest %N. This was rather unexpected as an increase in temperature had an effect on the reaction.

Table 5.4. Percent Carbon and Nitrogen determined by elemental analysis; and DS from NMR

Sample	**% Carbon**	**% Nitrogen**	**DS from NMR**
CNC	41.86	**0**	**0**
2 mol 50	40.04	0.25	0.12
2 mol 65	38.90	0.74	0.61
4.5 mol 57.5 - 1	40.95	0.19	0.08
4.5 mol 57.5 - 2	40.90	0.11	0.07
4.5 mol 57.5 - 3	40.18	0.27	0.18
6.5 mol 50	40.57	0.25	0.19
6.5 mol 65	38.71	1.21	0.97

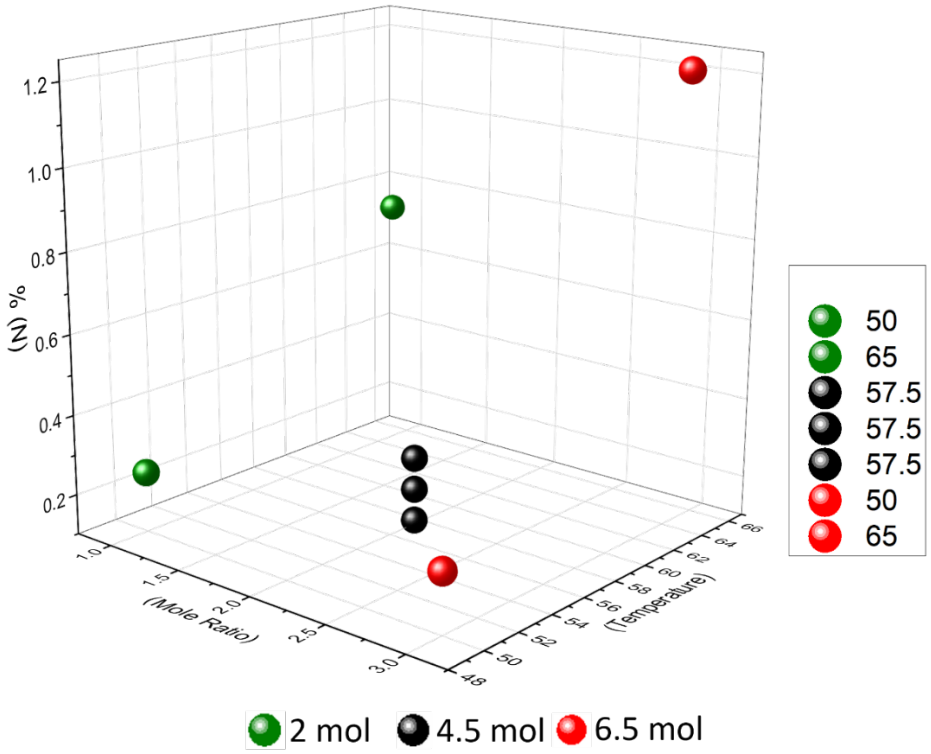

Figure 5.2. Plot of % Nitrogen in modified CNC against the reaction parameters-mole ratio and temperature

The ANOVA table presented in **Table 5.5** further corroborates the effect of temperature on the CNC modification reaction. Using the conventional significance level of α=0.05, the two main effects, mole ratio and temperature with P values of 0.022 ($P \leq 0.05$), are significant. The interactions of the main effect with P value of 0.099 are statistically insignificant. This can be seen in the %N of the center point reactions when a change in both the temperatures and mole ratios had no significant change in the %N of the modified CNC. Also, the curvature with a p value of 0.02 is considered significant because considering the main factors, the temperature is positive, which indicates the positive effect of the change in temperature while the mole ratio and the interaction are negative. This is evidenced in **Table 5.3,** where increasing the mole ratio from 2 to 6.5 at 50 ^{o}C had no effect in the change of %N while increasing the temperature significantly

increased the %N. As a result of this curvature, a linear regression model cannot be produced from this data.

Table 5.5. ANOVA Table for %N from CNC modification

Source	DF	Seq. SS	Adj. SS	ADJ. MS	F	P (α=0.05)
Main effects	2	0.580850	0.580850	0.290425	45.38	0.022
2-way interactions	1	0.055255	0.055255	0.055225	8.63	0.099
Curvature	1	0.306011	0.306011	0.306011	47.81	0.02
Residual error	2	0.012800	0.012800	0.006400		
Pure error	2	0.012800	0.012800	0.006400		
Total	6					

5.4.5 X-ray diffraction (XRD)

XRD measurements were performed on the unmodified and all modified CNCs to explore the impact of surface modification on the crystallinity of the CNCs. **Table 5.3** presents the X-ray diffraction patterns and calculated percent crystallinity of CNC and modified CNCs. For the modified CNCs, although there are no significant changes in the spectra of the mCNCs compared to the CNCs, a slight reduction in the crystalline diffraction peaks at I_{22} and I_{18} is observed. As a result of this reduction, the percent crystallinity of the modified CNCs range from 56- 64 %, an 18% reduction in crystallinity compared to the pristine CNC. This suggests that no obvious changes occured in the crystalline structure from the IPTS modification and the modification occurred at the surface thereby preserving the crystalline structure of the backbone CNCs.

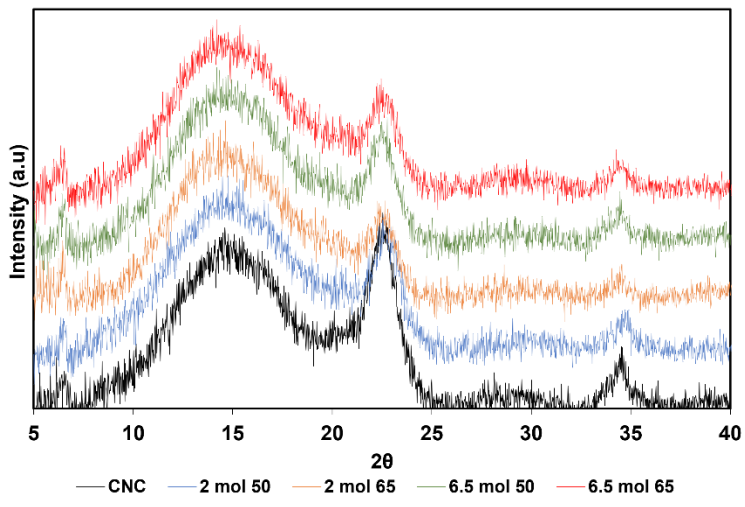

Sample	% Crystallinity
CNC	68
2 mol 50	64
2 mol 65	57
6.5 mol 50	62
6.5 mol 65	56

Figure 5.3. XRD of CNC and modified CNC

5.4.6 Wettability test

The wettability of a material, which provides information about the hydrophilicity or hydrophobicity of the material can be studied by measuring the contact angle formed by sessile liquid drops and the surface of the material[205,206]. Typically, a 0º contact angle indicates complete wetting and an increase in the contact angle indicates an increase in the hydrophobicity of the material surface[207]. In this study, deionized water was employed as a solvent to study the wettability of the CNCs and mCNCs and the results are presented in **Figure 5.4**. Due to the rich -OH surface moieties, pristine CNC is fundamentally hydrophilic and has a high affinity for water, hence, forms a low contact angle of 29.6º. After low temperature modification with IPTS (6.5 mol 50 mCNC), the contact angle increases by up to 32% compared to the CNCs. This increase in hydrophobicity can be attributed to the replacement of some surface -OH groups with the silane groups. Likewise, the 65 ºC modified samples (2 mol 65 and 6.5 mol 65) displayed even higher contact angles up to a maximum of 151% increase in hydrophobicity compared to pristine CNC. For the same temperatures, a slight increase in contact angle is observed as the mole ratio of IPTS

increases. This increase in contact angle with increased reaction temperature is attributed to higher grafting efficiency at this temperature. These results agree with the results obtained from EA where the %N is seen to substantially increase with the increase in grafting temperature indicating more -OH groups are replaced by the silane groups.

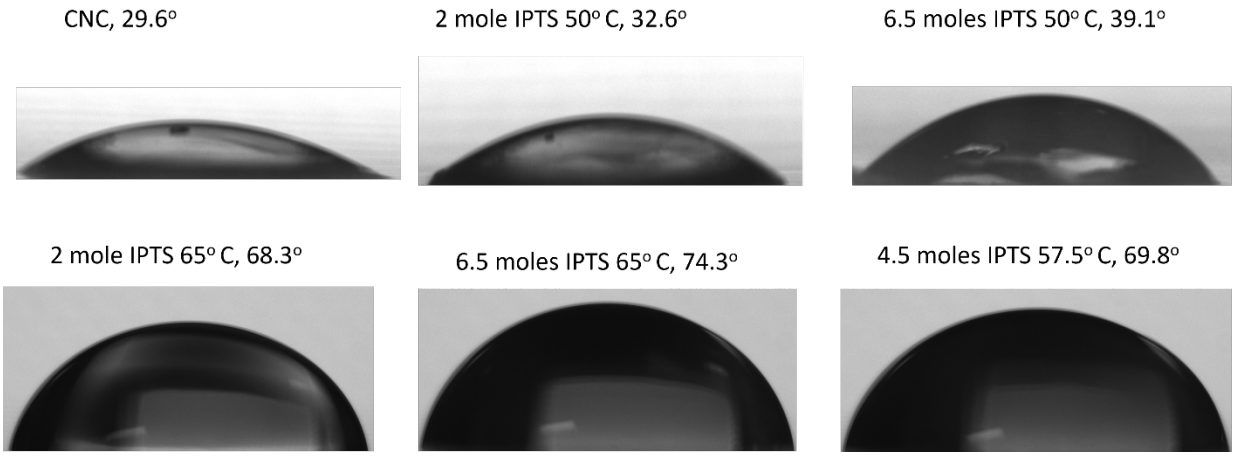

Figure 5.4. Water contact angle images of CNC and mCNC.

5.4.7 Dispersibility studies

The change in the polarity of materials can be analyzed using a solvent dispersibility test. Based on the polarity of the particles, they could be dispersed in polar solvents like DMSO if hydrophilic or non-polar solvents like toluene if hydrophobic. **Figure 5.5** presents the dispersion of CNC and mCNC in different solvents in order of reducing polarity. CNC is a polar nano particle and disperses well in polar solvents like water and DMSO. As the polarity increases, the dispersion changes to poor interaction in the polar solvents and improved dispersion in non-polar solvents. The change in dispersion is an indication of the grafting of IPTS on CNC. Upon dispersion, CNC disperses well in water and DMSO to give a slightly turbid solution. As the polarity of the solvent decreases, the turbidity of the solution increases indicating poor comparative dispersion. The IPTS-modified CNCs on the other hand show a reverse trend. Poor dispersion with very turbid

solution in polar solvents and improved dispersion with clearer solutions in the non-polar solvents which indicate better compatibility with these solvents. It is important to note how the turbidity of the solution for all modified CNCs changes with mole ratio and temperature. As the mole ratio and temperature change according to the experimental design, the dispersion in the polar solvents reduces indicated by increasing turbidity in the solutions. A reverse trend is observed in the non-polar solvents which show clearer solutions with improved dispersion with IPTS modification. Furthermore, although not shown by the picture, the IPTS modified CNCs swelled in the non-polar solvents with increasing swelling with mole ratio and temperature. For all mole ratios, the higher temperature modified temperature showed gradual reducing turbidity especially in toluene indicating the effect of temperature on the modification. In a similar functionalization of cellulose with epoxide functionalized silane, Mekonnen *et al*.[203] observed an improvement in dispersion in non-polar solvents with modification. These dispersibility results also agree with the water contact angle measurements where an increase in hydrophobicity with modification is observed. This further substantiates the modification of CNCs with IPTS.

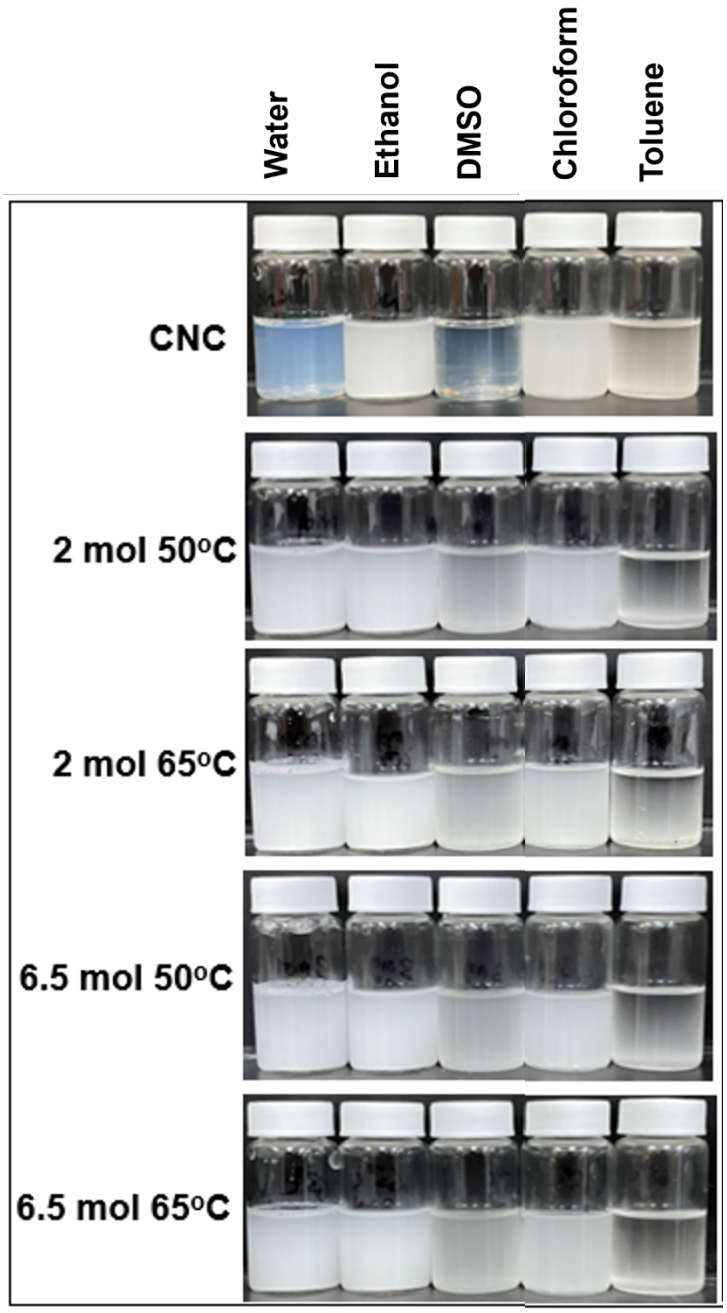

Figure 5.5. Dispersibility of CNC and mCNCs in different solvents

Nanocomposite characterization

5.4.7.1 Transmission Electron Microscopy (TEM)

TEM images were employed to demonstrate the dispersion of the pristine CNC and mCNCs in rubber. For this study, images of pristine CNCs, unfilled NR, NR-10 CNC and NR-10 mCNC were taken and compared. As presented in **Figure 5.6**, the TEM image for pristine CNC (**Figure 5.6A**) showed rodlike structures of the connected CNCs. This connected network results from the strong intramolecular hydrogen bonds in the CNCs. When 10% mCNC was added to the rubber (**Figure 5.6C**), the mCNCs were observed to be evenly distributed in the rubber and formed a network evidenced by the filler connection from one end of the composite to the other. On the other hand, the NR – 10 CNC shows a non-percolated distribution of the CNCs in the composite, as presented in **Figure 5.6D**. While the same concentration of CNC and mCNC are employed in the rubber composition, the non-percolated network formation of the CNCs could be the result of aggregation of CNCs in the composites, leaving insufficient CNCs available to form a percolated network.

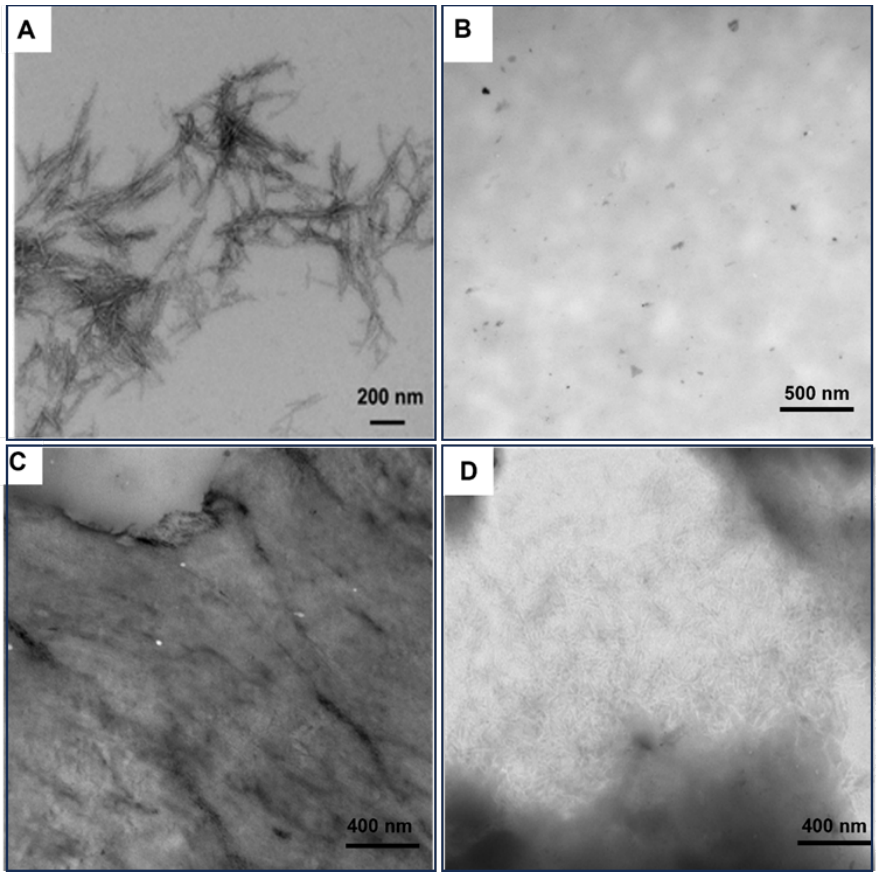

Figure 5.6. TEM images of pristine CNC (A), Natural rubber (B), NR-10 mCNC (C), and NR-10 CNC (D)

5.4.7.2 Cure properties

Cure property experiments provide information about the effect of the fillers on the sulphur crosslinking of the rubber vulcanizates. **Figure 5.7A** illustrates the optimum cure time (T_{c90}) and maximum torque (M_H) of rubber vulcanizates with varying filler loadings. The maximum torque showed a progressive increase with filler loading. This was expected as the presence of the rigid fillers increases the stiffness of the composite and restricts the rubber chain mobility leading to more torque and increased MH. The optimum cure time T_{c90} showed an increasing trend with filler loading up until NR-5mCNC and a successive decrease beyond that. One plausible reason for this could be that for the 2.5 and 5% mCNC composites, the mCNCs were not uniformly dispersed and

aggregated in areas within the rubber matrix. On the other hand, at a loading of 10% and beyond, mCNC disperses throughout the rubber matrix and reaches a percolated filler-filler network. Another plausible reason could be the dispersion and distribution of the Zinc oxide (ZnO), which is responsible for activating sulphur during the curing process and reducing the vulcanization time.

SEM with EDX mapping was carried out on the samples to understand the dispersion of the ZnO within the composite. EDX was used to map zinc and show the presence and nature of the zinc aggregates. As presented in **Figure 5.7B**, the SEM image of the unfilled natural rubber and NR-2.5mCNC showed multiple white agglomerates revealed to be Zn on the EDX map. As the CNC concentration increases to NR-5mCNC, the white agglomerates reduce and is absent in NR-10mCNC and NR-20mCNC. In the EDX maps for NR-5mCNC, only tiny agglomerates of zinc are observed. As the concentration of CNC increases in the samples beyond 5%; no visible agglomerates of zinc are seen in the EDX maps. This means that as the concentration of CNC increases in the rubber composite, the dispersion of the ZnO within the composite improves.

It has been reported that CNCs could form complexes with ZnO, the activator for this vulcanization reaction[208]. Since 10% CNC/mCNC concentration and beyond in the rubber composite forms a network through the matrix while carrying the ZnO, this network of mCNC-ZnO complex activates the sulfur in the entire matrix, promoting sulfur crosslinking, and shortening the curing time. The TEM results where the mCNCs in the NR-10mCNC were well-dispersed and showed the formation of CNC network within the matrix corroborates these findings.

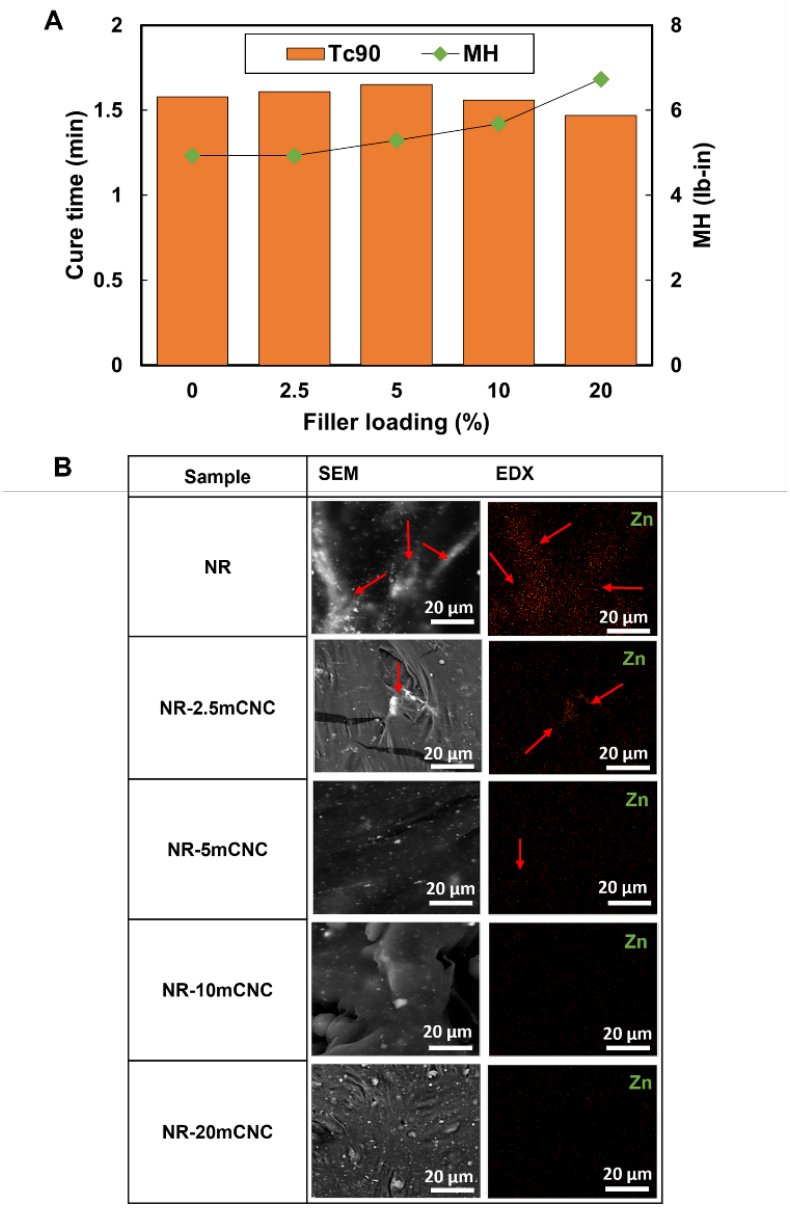

Figure 5.7. (a) Optimum cure time and maximum torque of mCNC-filled NR (b) SEM and EDX of all samples showing the distribution of Zn from ZnO within the composite.

5.4.7.3 Crosslink density

The physical performance of rubber can be improved by introducing crosslinks between the rubber chains to enhance its toughness and mechanical properties. In rubber vulcanization reaction, sulfur reacts to form crosslinks between the individual unsaturated rubber chains, and the

density of these crosslinks is affected by the type and loading of fillers and the rest of the rubber compounding ingredients[209]. **Figure 5.8** shows the plot of Kraus equation for the filled rubber vulcanizates, which correlates the rubber swelling to the rubber-CNC interaction. According to Kraus, the swelling ratio V_{ro}/V_r reveals how much the rubber restricts the toluene absorption due to rubber-CNC interaction[210]. The ratio of true volume (Vro) to apparent volume fraction (Vr) equals unity due to the absence of filler effects for unfilled rubber systems.

As seen from **Figure 5.8**, as more fillers are added in the rubber at increased amounts, the molecular restriction increases, swelling reduces, and Vro/Vr increases for all mCNC-filled vulcanizates up to NR-10 mCNC. Beyond that concentration, a decrease is observed. For the filled rubbers, the increase in swelling could be attributed to several factors, including the filling up of the voids caused by the dewetting of the mCNCs. Amongst the filled composites, the decrease in swelling beyond 10% mCNC loading could be attributed to increased sulfur crosslinks, as explained by the cure property results.

Comparing the vulcanizates of 10% pristine and mCNC, the swelling ratio is lower in the 10% CNC than in the 10% mCNC. This was expected and is due to the CNC aggregates formed within the rubber, leading to lower molecular restrictions or the filling of voids in the composite. These voids, which form from the dewetting of CNCs during rubber gum swelling, then increase solvent uptake and swelling, hence a decrease in swelling ratio[95]. On the other hand, the IPTS modification of the CNC improved the interfacial adhesion and the dispersion of the CNCs within the matrix. These results agree with the TEM results, where improved dispersion and percolation of the CNCs were observed.

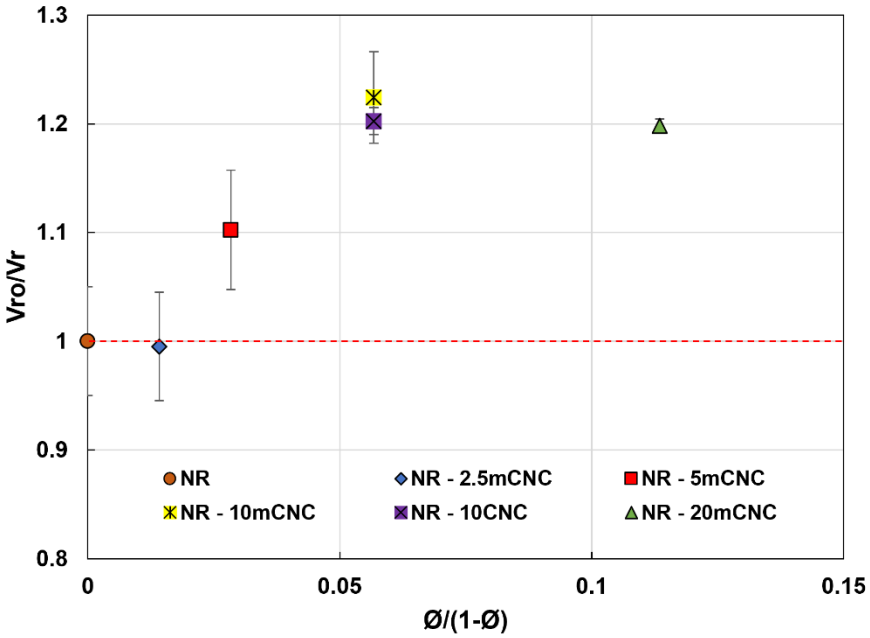

Figure 5.8. Kraus equation plot for swelling tests of filled rubber vulcanizates.

5.4.7.4 Mechanical properties

Tensile strength tests were carried out to determine the effect of mCNC on the mechanical properties of rubber. 10% CNC-filled vulcanizate was used as a control to elucidate the effect of the IPTS modification of CNC on the mechanical properties. The plot of mechanical properties is presented in **Figure 5.9.** The reinforcing effect of the mCNC is evidenced by a positive correlation between the tensile strength and the filler concentration (**Figure 5.9A**) up to 10% mCNC. Beyond that concentration, a decrease in strength is observed which could be attributed to aggregation. This result can be correlated to the crosslink density results where the swelling ratio increased beyond 10% mCNC, indicating fewer crosslinks. The strain on the other hand, displayed an initial decrease with the filler at 2.5% concentration, and beyond that, the strain increased up to 10% mCNC and decreased thereafter. A possible explanation for this effect could be that the IPTS provides a plasticizing effect[211] in the CNCs and increases the elongation; however, when the concentration increases to 20% and aggregates form, these aggregates limit the interaction between

the rubber and filler, acts as stress concentrators in the composites, and serve as weak points within the composite causing it to break[82,212].

To elucidate the effect of the IPTS modification on the reinforcing properties of CNC, the tensile properties of NR with 10% CNC and 10% mCNC were compared to that of NR. As presented in **Figure 5.9B**, while the 10% pristine CNC composite showed a 36% increase in the tensile strength compared to that of NR, the same concentration of mCNC improved the tensile strength of the rubber by 71%. Furthermore, a 25% increase in tensile strength was observed between the CNC and mCNC-filled composites. This significant improvement with the mCNC filler could be due to the following factors: the improved dispersion of the CNC resulting from hydrophobic modification, thereby increasing the interfacial bonding and compatibility of the CNCs and the rubber, the reduction in the formation of aggregates and agglomeration due to the reduced amount of -OH groups available for hydrogen bonding, the formation of a filler network of the mCNCs within the composite leading to effective stress transfer across the composite, crosslink density of the polymer chains, and the likely formation of the silane crosslinks within the filler particles. These results are consistent with the TEM and swelling results. On the other hand, the tensile strain at break decreased with the addition of CNCs and increased when mCNC was added. As previously stated, this could be due to the plasticizing effect of the IPTS. It is interesting that the addition of mCNC increases both tensile strength and elongation at break compared to the addition of CNC.

Figure 5.9C and **D** present the modulus for strains at 100% (M_{100}) and 300% (M_{300}) of the composites. Generally, adding stiff materials to the rubber increases the modulus of rubbers. The mCNC-filled vulcanizates steadily increased moduli at 100 and 300 until 10% mCNC. Beyond this mCNC content, the modulus slightly decreased. This was because the filler concentration

governs modulus hence, the increase in modulus was in line with the increase in the filler loading levels. The decrease in the modulus with 20% mCNC was consistent with the crosslink density reduction.

As presented in **Figure 5.9D,** no visible change in the moduli was observed in the pristine and modified CNC-filled vulcanizates when comparing the pristine and modified CNC-filled vulcanizates. This reveals that the CNC modification did not affect the modulus. The concentration of the fillers generally dominates the change in modulus; therefore, the results obtained were expected due to the equal concentration of fillers in both vulcanizates.

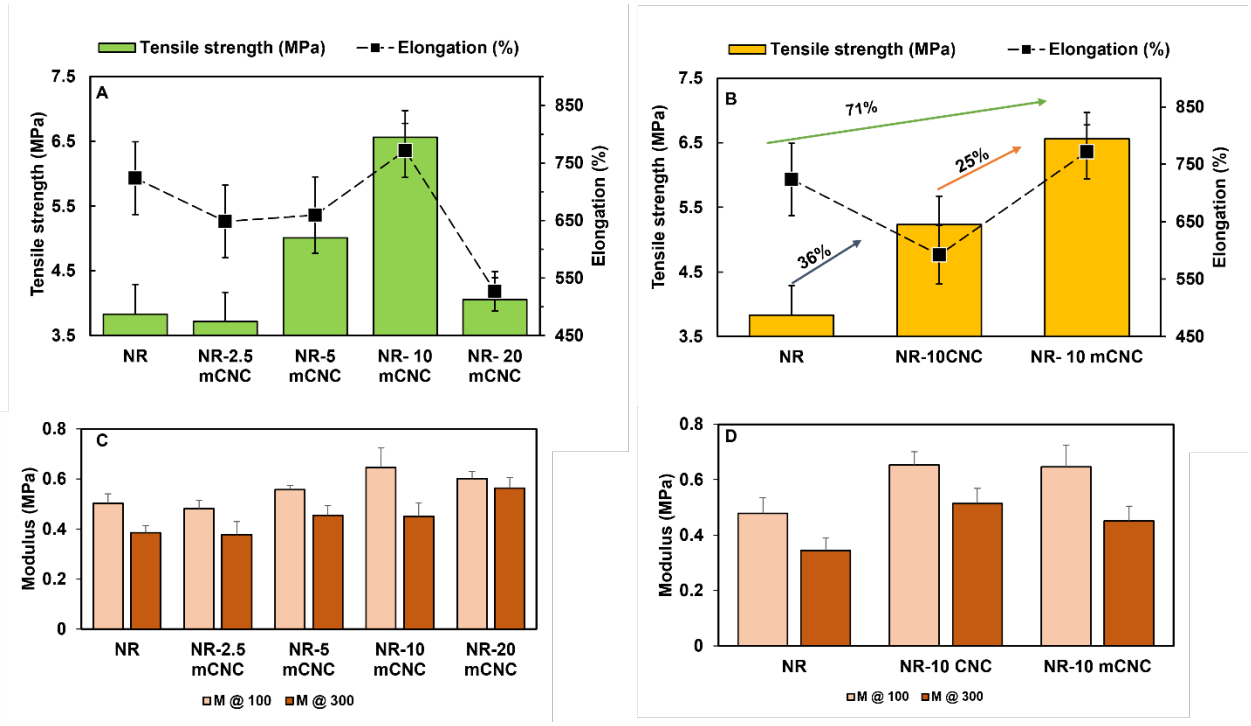

Figure 5.9. Tensile strength of (A) mCNC-filled rubber vulcanizates, (B) the comparison of vulcanizates filled with 10% pristine and mCNCs, and modulus of (C) mCNC-filled rubber vulcanizates, and (D) comparison of 10mCNC-filled vulcanizates.

5.4.7.5 Rheological properties

Incorporating fillers in rubber could change rubber processability; therefore, rheological testing was carried out to understand the processibility of the rubber composites. **Figure 5.10** presents result from Mooney viscosity (MV), strain sweep, and frequency sweep experiments of the filled rubber composites. **Figure 5.10A** shows the torque recorded in Mooney units (MU) of the rubber composites (measured at 100 ^{o}C). It is well-known that fillers increase the viscosity of rubbers, and this is evidenced by the steady increase in Mooney viscosity with mCNC concentration. The MV increased by 88% compared to the unfilled rubber for the 20% mCNC-filled rubber composite. This could be from the filler concentration contribution and possibly silane crosslinking **(Scheme 5.2**) as the Mooney viscosity typically depends on the molecular weight and distribution, molecular structure such as branching, crosslinks, and non-rubber constituents such as presence and type of fillers.

The polymer-filler and filler-filler interactions can also affect the rheological properties. This was studied by a strain sweep test with results showing the plots of storage modulus and complex viscosity as a function of strain, presented in **Figure 5.10B**. All filled composites exhibited a trend of increased stiffness with increased filler loading, which was attributed to the addition of CNCs. It is well known that adding rigid fillers to rubber increases its stiffness. As is typical for rubbers, the unfilled rubber demonstrated a linear viscoelastic region (LVR) at low strains. This characteristic LVR was maintained in the filled rubbers up to NR-10mCNC, similar to the behaviour observed in the unfilled rubber. However, when the filler concentration was increased to NR-20mCNC, a noticeable decrease in the storage modulus (G') at low strains was observed. This reduction in G', evidenced by the reduction of the LVR, is a phenomenon known as strain softening or the Payne effect.

This strain softening phenomenon was significantly influenced by the filler contribution[95]. As the concentration of CNC increased, there was a corresponding rise in the availability of hydroxyl groups for inter- and intra-molecular hydrogen bonds. Consequently, the strain softening observed could be attributed to the disruption of the CNC-CNC network due to the increased presence of these hydroxyl groups.

To understand the impact of CNC modification on the Payne effect, a strain sweep test was conducted on a composite with 10% unmodified CNC (10-CNC) filled rubber prepared under the same conditions. Comparing the results of NR-10CNC and NR-mCNC displayed in **Figure 5.10B**, while the NR-10mCNC displayed LVR, the unmodified CNC composite displayed non-linear viscoelastic behavior indicated by a sudden change in G' at low strains. This non-LVR behavior could be attributed to the dissociation of the hydrogen bond formation of the CNCs. This corroborates the FTIR and elemental analysis results and provides evidence that the IPTS modification of the CNC was successful. Furthermore, it reveals that the IPTS modification of CNC impacted the Payne effect of the composite.

Overall, CNC modification and the concentration of the modified CNCs contributed to the reduction of Payne effect of the rubber composites. IPTS modification of the CNCs limited the availability of -OH moieties for hydrogen bonding within the rubber composite and, hence, the Payne effect. However, as the composition of the modified CNCs increased beyond 10% mCNC, the Payne effect began to appear. Similarly, for the same concentration of CNCs, the unmodified CNC-filled composite showed a high Payne effect. **Figure 5.10C** and **D** present the results from the frequency sweep tests for all samples. As shown in **Figure 5.10C**, the complex viscosity for all rubber composites displayed a shear thinning behavior demonstrated by a decrease in complex viscosity with increasing frequency. Furthermore, comparing the complex viscosity for all

composites, an increase in viscosity is observed with increasing filler loading, with the NR-20 mCNC being the highest. Although this increase could impact the flowability of the composite, the rubber nanocomposites maintained processability. This can be attributed to the improvement in the dispersion of the CNCs in the rubber matrix due to IPTS modification.

The storage and loss modulus as a function of frequency is shown in **Figure 5.10D**. For all composites, as the filler loading increased, the storage modulus (G') increased, indicating that adding the filler increased the rigidity of the rubber. The loss modulus (G") also followed a similar trend. Because rubber is a viscoelastic material G'> G" at higher test frequencies and the reverse is the case at lower frequencies. Moreover, the crossover frequency and modulus where G'=G" provides information about the transition from liquid-like to solid behavior of the rubber. **Figure 5.10D** shows that the cross-over modulus occurs at lower frequencies as the filler loading is increased (NR>NR-2.5mCNC> NR-5mCNC, NR-10mCNC, NR-20mCNC). This indicates that as the filler increased, the samples exhibited solid-like behavior faster, which can be attributed to increased modulus with the incorporation and increase in filler concentrations.

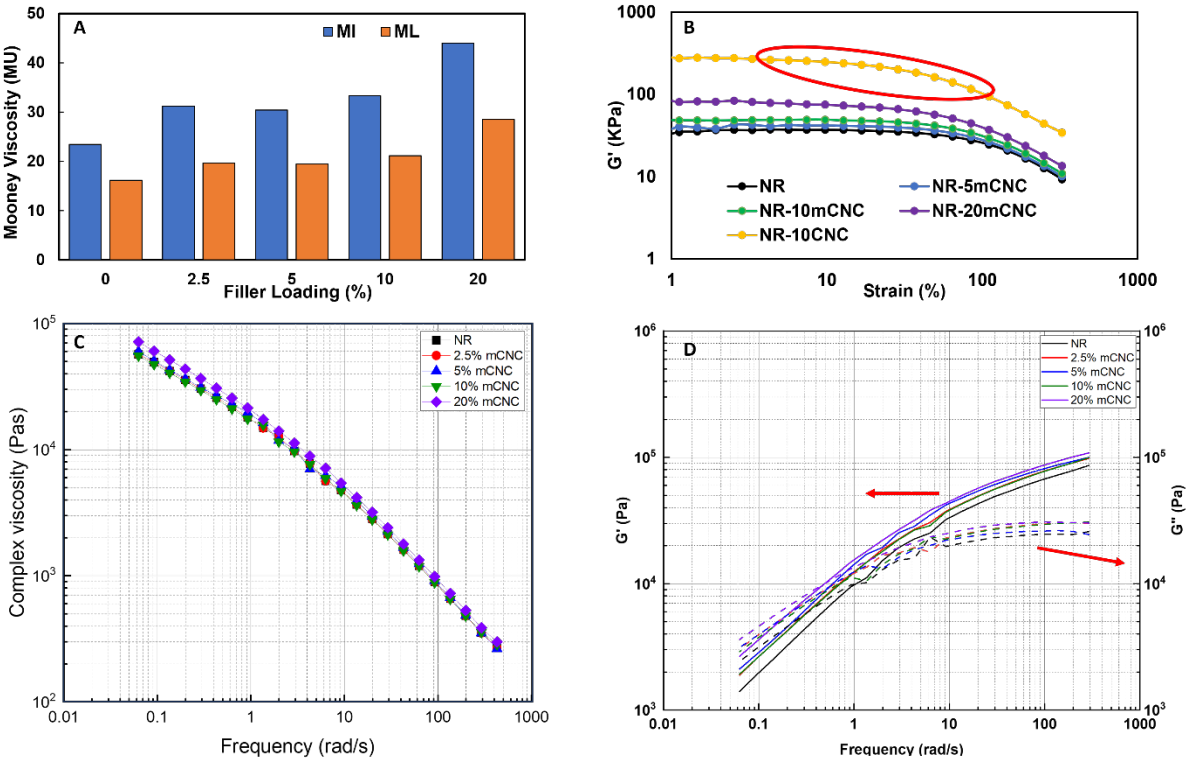

Figure 5.10. (A) Mooney Viscosity, (B) strain dependence of storage modulus, (C) complex viscosity, and (D) storage and loss modulus of NR and mCNC-filled NR nanocomposites

5.5 Summary of Chapter 5

In this study, modified CNC was incorporated into natural rubber to produce rubber nanocomposites. First, CNC was modified using IPTS and confirmed using elemental analysis and FTIR. This substitution of silane groups on the hydroxyl groups of the CNCs introduced hydrophobicity to the CNCs. Elemental analysis showed the introduction and increase in percent nitrogen in the modified CNCs from the IPTS. XRD studies showed an 18% decrease in crystallinity of the highest modified CNC compared to the pristine CNC. Contact angle measurements revealed an increase in contact angle indicating an increase in hydrophobicity and wettability studies showed improved dispersion of the mCNCs in non-polar solvents. The rubber

nanocomposite was then prepared using the mCNC modified using 6.5 mol IPTS at 65 ºC at varied loadings and 10% pristine CNC as control, and characterized. TEM studies showed that mCNC formed a network in the rubber matrix at 10% filler loading, reducing the optimum cure time as CNC was shown to improve the dispersion of the sulfur vulcanization activator, ZnO. Swelling and crosslinking studies showed an increase in swelling up to 10% and a decrease thereafter. Mechanical property analysis indicated higher modulus and tensile strength with increased filler loading, reaching a 71% increase in tensile strength at 10% modified CNC loading compared to pure natural rubber. Comparatively, a 25% increase in tensile strength was observed in the 10% modified CNC compared to the 10% pristine CNC, highlighting the positive impact of the modification on composite strength. The nanocomposites up to 10% mCNC-filled showed similar LVR as the unfilled NR composite, and beyond 10% filler loading, the Payne effect becomes noticeable. The rheological properties revealed that the incorporation of fillers did not negatively impact rubber processing. Based on these studies, it can be concluded that the optimal properties of the nanocomposite are obtained with the 10% filled mCNC.

Chapter 6. Conclusions and Recommendations for Future Work

6.1 Conclusions

In this doctoral thesis, various methods were employed to overcome the limitations of employing CNC as a filler for natural rubber. The methods to improve the dispersion and compatibility of CNC in natural rubber studied in this thesis include optimization of processing methods, masterbatch preparation with functionalized rubber, and CNC surface modification using silane. The CNC-filled rubber composites were then characterized.

In the first experimental study, results showed that despite the fabrication methods, CNC reinforced the composite as noted from the improved mechanical properties. Comparing all three fabrication methods, the co-coagulation process provided the optimal dispersion of the CNCs and improvement of the physical properties. This processing method also impacted the filler-filler interactions and rheology of the composite; therefore, it can be concluded that the properties of the nanocomposites depend on the employed processing method. Furthermore, it was also found that the tensile strength of the rubber composite showed an increasing trend with CNC loading up to a maximum, and then declined. These results indicate that to obtain further enhancement in the nanocomposite properties, especially at higher loading levels, surface modification of either the CNCs or the NR to enhance the compatibility could be required.

In the second experimental study, a masterbatch of CNC - ENR was prepared that entails covalent grafts of CNC with epoxidized natural rubber in a base-catalyzed reactive extrusion process, which was studied at varying temperatures. The aim of this study was to prepare a masterbatch of ENR-CNC composites with enhanced physico-mechanical properties that can be employed as a filler for hydrophobic rubber systems. Results showed successful covalent grafts

starting at 180 ºC, and progressive increase in tensile strength and minimal Payne effects for all composites. For the studied reaction, the employment of temperatures beyond 180 ºC deteriorated the rubber physical properties due to thermal degradation revealing that the optimal processing temperature for this reaction was 180 ºC. Finally, unvulcanized rubber composites were used to achieve these properties demonstrating that the ENR-CNC can be reprocessed and employed as a masterbatch filler to improve the dispersion of CNC in other hydrophobic polymer systems.

In the final experimental chapter of this thesis, CNC was modified with silane, compounded with natural rubber at different filler loadings, vulcanized, and characterized. It was revealed that hydrophobic modification of the CNC improves the dispersion of the CNC resulting in CNC percolation at 10% filler loading. The outcome of this was a 71% increase in tensile strength compared to unfilled natural rubber. Furthermore, at the 10% filler loading, the Payne effect is unnoticeable, and the composites remained processible at high filler loadings evidenced by the results from rheological studies. Based on these results, it can be concluded that this hydrophobic modification improves the dispersion of CNC and physical properties of the composite, and 10% filler loading is the optimal filler for the CNCs.

This work has demonstrated that the dispersion and interfacial adhesion of CNC in natural rubber and, hence, the properties of rubber composite can be improved by optimizing the fabrication method and surface modification of the CNCs. As a result, CNCs can be employed as a green filler for green composite development which provides an avenue to utilize the abundantly available CNC for sustainable material applications.

6.2 Recommendations for Future Work

Potential opportunities for future research can be categorized into short- and long-term projects as follows:

Short term:

- Optimization of the processing technique from Chapter 3. For this, an extruder with a side feeder should be employed to feed the natural rubber and CNC simultaneously. Employing the side feeder to feed the filler at a set feed rate will achieve better dispersion and ensure uniform and equal distribution of the CNC in the rubber matrix. The effects of screw speed, temperature, and feed rate should be studied to obtain the optimal extrusion properties for mixing. The physico-mechanical properties should be investigated and compared with the composite prepared by co-coagulation to obtain the optimum processing technique and this impacts the dispersion of the CNC in the rubber.
- Utilization of the ENR-CNC masterbatch from Chapter 4 as a filler reinforcment in natural rubber and investigation of the properties. It is proposed that this will enhance the dispersion of CNC in the natural rubber because the ENR carrying the CNC (ENR-g-CNC) is comparable with the natural rubber.
- Investigate the impact of the activator ZnO complex formed with CNCs and other curing agents on the vulcanization process and the processing efficiency and the resulting properties of the rubber. One way to do this could be to blend the CNC and all the curatives together and making a composite with this blend, then comparing the properties to making a composite with the CNCs before adding the curatives. This will provide insights into why the vulcanization time is shorter when CNC is employed as a filler.

- Explore simultaneous feeding (two feeders) for the silane modified CNCs in Chapter 5 to save time, energy, and cost of multiple step processes. This will also mitigate the possible scission of the rubber chains from the multiple steps of mixing. Furthermore, this will improve the mixing, dispersion and ensure that the CNC is evenly distributed in the composite.

Long term:

- Although CNC is desirable because of its properties, the cost of CNC limits its application in commodity products. Furthermore, the nanocomposite prepared using CNC as a sole filler may lack all the attributes desired for applications. Therefore, combining CNC with other fillers can provide a synergistic effect and provide nanocomposite with synergistic superior properties, which a composite material with an individual filler system may lack. Hybridization of CNC and carbon black to study the synergistic properties of CNC/CB-filled rubber composites by incorporating CNC as a secondary filler could interrupt undesirable CB networks that lead to Payne effects. The filler loadings can be optimized, and the properties investigated, and compared to the properties of NR containing CNC and CB alone. It is proposed that this will help to reduce the rolling resistance, improve driving fuel efficiency, and reduce vehicular carbon emissions associated with using only CB fillers alone.

References

1. Zhou Y, Fan M, Chen L, Zhuang J. Lignocellulosic fibre mediated rubber composites: An overview. *Compos B Eng*. 2015;76:180-191. doi:10.1016/J.COMPOSITESB.2015.02.028

2. Alam MN, Kumar V, Jung HS, Park SS. Fabrication of High-Performance Natural Rubber Composites with Enhanced Filler–Rubber Interactions by Stearic Acid-Modified Diatomaceous Earth and Carbon Nanotubes for Mechanical and Energy Harvesting Applications. *Polymers 2023, Vol 15, Page 3612*. 2023;15(17):3612. doi:10.3390/POLYM15173612

3. Mostafa A, Abouel-Kasem A, Bayoumi MR, El-Sebaie MG. Rubber-filler interactions and its effect in rheological and mechanical properties of filled compounds. *J Test Eval*. 2010;38(3). doi:10.1520/JTE101942

4. Bokobza L. Elastomer Nanocomposites: Effect of Filler–Matrix and Filler–Filler Interactions. *Polymers 2023, Vol 15, Page 2900*. 2023;15(13):2900. doi:10.3390/POLYM15132900

5. Tareen MHK, Hussain F, Zubair Z, et al.. Effects of carbon black on epoxidized natural rubber composites: Rheological, abrasion, and mechanical study. *J Compos Mater*. 2022;56(29):4473-4485. doi:10.1177/00219983221134512/

6. Mermet-Guyennet MRB, Gianfelice De Castro J, Varol HS, et al.. Size-dependent reinforcement of composite rubbers. *Polymer (Guildf)*. 2015;73:170-173. doi:10.1016/J.POLYMER.2015.07.041

7. Rashid AA, Rohana Yahya S. Mechanical Properties of Natural Rubber Composites Filled with Macro- and Nanofillers. Published online December 5, 2013:550-573. doi:10.1039/9781849737654-00550

8. Spahr ME, Rothon R. Carbon Black as a Polymer Filler. In: Springer, Cham; 2017:261-291. doi:10.1007/978-3-319-28117-9_36

9. Spahr ME, Rothon R. Carbon Black as a Polymer Filler. In: Springer, Cham; 2017:261-291. doi:10.1007/978-3-319-28117-9_36

10. Caldwell J, Al. E. *Identification of Research Needs to Resolve the Carcinogenicity of High-Priority IARC Carcinogens*.; 2009.

11. Ramanakumar A V., Parent MÉ, Latreille B, Siemiatycki J. Risk of lung cancer following exposure to carbon black, titanium dioxide and talc: Results from two case–control studies in Montreal. *Int J Cancer*. 2008;122(1):183-189. doi:10.1002/ijc.23021

12. Han Y, Guo Y, Gu J. Thermally conductive fillers. *Thermally Conductive Polymer Composites*. Published online January 1, 2023:111-147. doi:10.1016/B978-0-323-95231-6.00002-7

13. Shojaeiarani J, Bajwa D, Shirzadifar A. A review on cellulose nanocrystals as promising biocompounds for the synthesis of nanocomposite hydrogels. *Carbohydr Polym*. 2019;216:247-259. doi:10.1016/J.CARBPOL.2019.04.033

14. Panchal P, Ogunsona E, Mekonnen T. Trends in Advanced Functional Material Applications of Nanocellulose. *Processes*. 2018;7(1):10. doi:10.3390/pr7010010

15. Jantachum P, Phinyocheep P. Compatibilization of Cellulose Nanocrystal-Reinforced Natural Rubber Nanocomposite by Modified Natural Rubber. *Polymers (Basel)*. 2024;16(3). doi:10.3390/POLYM16030363

16. Singh S, Dhakar GL, Kapgate BP, et al.. Synthesis and chemical modification of crystalline nanocellulose to reinforce natural rubber composites. *Polym Adv Technol*. 2020;31(12):3059-3069. doi:10.1002/PAT.5030

17. Ojogbo E, Tzoganakis C, Mekonnen TH. Batch Mixing for the in Situ Grafting of Epoxidized Rubber onto Cellulose Nanocrystals. *ACS Sustain Chem Eng*. 2022;10(27):8743-8753. doi:10.1021/ACSSUSCHEMENG.2C01054

18. Eyley S, Thielemans W. Surface modification of cellulose nanocrystals. *Nanoscale*. 2014;6(14):7764-7779. doi:10.1039/C4NR01756K

19. Dhali K, Daver F, Cass P, Adhikari B. Surface modification of the cellulose nanocrystals through vinyl silane grafting. *Int J Biol Macromol*. 2022;200:397-408. doi:10.1016/J.IJBIOMAC.2022.01.079

20. Jiang W, Shen P, Yi J, Li L, Wu C, Gu J. Surface modification of nanocrystalline cellulose and its application in natural rubber composites. *J Appl Polym Sci*. 2020;137(39):49163. doi:10.1002/APP.49163

21. Shchipunov Y. Bionanocomposites: Green sustainable materials for the near future*. *Pure Appl Chem*. 2012;84(12):2579-2607. doi:10.1351/PAC-CON-12-05-04

22. Darder M, Aranda P, Ruiz-Hitzky E. Bionanocomposites: A new concept of ecological, bioinspired, and functional hybrid materials. *Advanced Materials*. 2007;19(10):1309-1319. doi:10.1002/adma.200602328

23. Abdul Khalil HPS, Chong EWN, Owolabi FAT, et al.. Enhancement of basic properties of polysaccharide-based composites with organic and inorganic fillers: A review. *J Appl Polym Sci*. 2019;136(12):47251. doi:10.1002/app.47251

24. Low DYS, Supramaniam J, Soottitantawat A, et al.. Recent developments in nanocellulose-reinforced rubber matrix composites: A review. *Polymers (Basel)*. 2021;13(4):1-35. doi:10.3390/polym13040550

25. Robertson CG, Hardman NJ. Nature of carbon black reinforcement of rubber: Perspective on the original polymer nanocomposite. *Polymers (Basel)*. 2021;13(4):1-28. doi:10.3390/polym13040538

26. Low DYS, Supramaniam J, Soottitantawat A, et al.. Recent developments in nanocellulose-reinforced rubber matrix composites: A review. *Polymers (Basel)*. 2021;13(4):1-35. doi:10.3390/polym13040550

27. Fan Y, Fowler GD, Zhao M. The past, present and future of carbon black as a rubber reinforcing filler – A review. *J Clean Prod*. 2020;247:119115. doi:10.1016/j.jclepro.2019.119115

28. Nagornaya MN, Razdyakonova GI, Khodakova SY. The Effect of Functional Groups of Carbon Black on Rubber Properties. In: *Procedia Engineering*. Vol 152. Elsevier Ltd; 2016:563-569. doi:10.1016/j.proeng.2016.07.656

29. Hassan HH, Ateia E, Darwish NA, Halim SF, Abd El-Aziz AK. Effect of filler concentration on the physico-mechanical properties of super abrasion furnace black and silica loaded styrene butadiene rubber. *Mater Des*. 2012;34:533-540. doi:10.1016/J.MATDES.2011.05.005

30. Payne AR. The dynamic properties of carbon black-loaded natural rubber vulcanizates. Part I. *J Appl Polym Sci*. 1962;6(19):57-63. doi:10.1002/app.1962.070061906

31. Leblanc JL. Simplified modeling calculations to enlighten the mechanical properties (modulus) of carbon black filled diene rubber compounds. *J Appl Polym Sci*. 2011;122(1):599-607. doi:10.1002/app.34174

32. Rharbi Y, Cabane B, Vacher A, Joanicot M, Boué F. Modes of deformation in a soft/hard nanocomposite: A SANS study. *Europhys Lett*. 1999;46(4):472-478. doi:10.1209/epl/i1999-00287-1

33. Drozdov AD, Dorfmann A. The Payne effect for particle-reinforced elastomers. *Polym Eng Sci*. 2002;42(3):591-604. doi:10.1002/pen.10974

34. PG M, D G. Molecular interpretation of the Payne effect. *Kautschuk Gummi Kunststoffe*. 1996;49(1):18-21.

35. Sternstein SS, Zhu AJ. Reinforcement mechanism of nanofilled polymer melts as elucidated by nonlinear viscoelastic behavior. *Macromolecules*. 2002;35(19):7262-7273. doi:10.1021/ma020482u

36. Montes H, Lequeux F, Berriot J. Influence of the Glass Transition Temperature Gradient on the Nonlinear Viscoelastic Behavior in Reinforced Elastomers. *Macromolecules*. 2003;36(21):8107-8118. doi:10.1021/ma0344590

37. Wypych G. FILLERS IN DIFFERENT PRODUCTS. In: *Handbook of Fillers*. Elsevier; 2016:823-872. doi:10.1016/b978-1-895198-91-1.50021-x

38. Prasertsri S, Rattanasom N. Mechanical and damping properties of silica/natural rubber composites prepared from latex system. *Polym Test*. 2011;30(5):515-526. doi:10.1016/J.POLYMERTESTING.2011.04.001

39. Neethirajan J, Parathodika AR, Hu GH, Naskar K. Functional rubber composites based on silica-silane reinforcement for green tire application: the state of the art. *Functional Composite Materials 2022 3:1*. 2022;3(1):1-15. doi:10.1186/S42252-022-00035-7

40. Kaewsakul W, Sahakaro K, Dierkes WK, Noordermeer JWM. Mechanistic aspects of silane coupling agents with different functionalities on reinforcement of silica-filled natural rubber compounds. *Polym Eng Sci*. 2015;55(4):836-842. doi:10.1002/PEN.23949

41. Wang X, Luo Z, Xu Y, Zhong J, Zhang H, Liang J. Preparation and performance of natural rubber latex treatment for silica filled natural rubber composites. *J Appl Polym Sci*. 2023;140(25):e53966. doi:10.1002/APP.53966

42. Jarnthong M, Peng Z, Nakason C, Lopattananon N. Surface Modification of Silica Nanoparticles for Reinforcement of Epoxidized Natural Rubber. *Adv Mat Res*. 2010;93-94:370-376. doi:10.4028/WWW.SCIENTIFIC.NET/AMR.93-94.370

43. Dileep P, Jacob S, Chandra CSJ, et al.. Functionalized Nanosilica for Vulcanization Efficiency and Mechanical Properties of Natural Rubber Composites. *Silicon*. 2022;14(8):4411-4422. doi:10.1007/S12633-021-01281-3

44. Xiao Y, Zou H, Zhang L, Ye X, Han D. Surface modification of silica nanoparticles by a polyoxyethylene sorbitan and silane coupling agent to prepare high-performance rubber composites. *Polym Test*. 2020;81:106195. doi:10.1016/J.POLYMERTESTING.2019.106195

45. Roy K, Debnath SC, Potiyaraj P. A critical review on the utilization of various reinforcement modifiers in filled rubber composites. *Journal of Elastomers and Plastics*. 2020;52(2):167-193. doi:10.1177/0095244319835869/

46. Sengloyluan K, Sahakaro K, Dierkes WK, Noordermeer JWM. Silica-reinforced tire tread compounds compatibilized by using epoxidized natural rubber. *Eur Polym J*. 2014;51(1):69-79. doi:10.1016/j.eurpolymj.2013.12.010

47. Chen L, Jia Z, Tang Y, Wu L, Luo Y, Jia D. Novel functional silica nanoparticles for rubber vulcanization and reinforcement. *Compos Sci Technol*. 2017;144:11-17. doi:10.1016/j.compscitech.2016.11.005

48. Qian Z, Peng Z. Reinforcing styrene-butadiene rubber composites by constructing multiple interaction between rubber and silica. *Polym Compos*. 2019;40(5):1740-1747. doi:10.1002/pc.24928

49. Spahr ME, Rothon R. Carbon Black as a Polymer Filler. In: Springer, Cham; 2017:261-291. doi:10.1007/978-3-319-28117-9_36

50. Flanigan CM, Beyer L, Klekamp D, Rohweder D, Stuck B, Terrill ER. Comparative study of silica, carbon black and novel fillers in tread compounds. *Rubber World*. 2012;245(5):18.

51. Kato A, Ikeda Y, Kohjiya S. Carbon Black-Filled Natural Rubber Composites: Physical Chemistry and Reinforcing Mechanism. In: *Polymer Composites*. Vol 1. Wiley-VCH Verlag GmbH & Co. KGaA; 2012:515-543. doi:10.1002/9783527645213.ch17

52. Pittayavinai P, Thanawan S, Amornsakchai T. Comparative study of natural rubber and acrylonitrile rubber reinforced with aligned short aramid fiber. *Polym Test*. 2017;64:109-116. doi:10.1016/j.polymertesting.2017.09.033

53. Kanny K, Mohan TP. Rubber nanocomposites with nanoclay as the filler. In: *Progress in Rubber Nanocomposites*. Elsevier Inc.; 2017:153-177. doi:10.1016/B978-0-08-100409-8.00005-X

54. Verge P, Peeterbroeck S, Bonnaud L, Dubois P. Investigation on the dispersion of carbon nanotubes in nitrile butadiene rubber: Role of polymer-to-filler grafting reaction. *Compos Sci Technol*. 2010;70(10):1453-1459. doi:10.1016/j.compscitech.2010.04.022

55. Li S, Li Z, Burnett TL, Slater TJA, Hashimoto T, Young RJ. Nanocomposites of graphene nanoplatelets in natural rubber: microstructure and mechanisms of reinforcement. *J Mater Sci*. 2017;52(16):9558-9572. doi:10.1007/s10853-017-1144-0

56. Phuhiangpa N, Phongphanphanee S, MS&E WS, 2020 undefined. Study of rubber/calcium carbonate composites. *iopscience.iop.org*.

57. Misman MA, Rashid AA, Yahya SR. Modification and application of starch in natural rubber latex composites. *Rubber Chemistry and Technology*. 2018;91(1):184-204. doi:10.5254/rct-18-82604

58. Raju G, Mas Haris MRH. Preparation and characterization of acidified chitosan immobilized in epoxidized natural rubber. *Polym Test*. 2016;53:1-6. doi:10.1016/j.polymertesting.2016.05.005

59. Jiang C, Bo J, Xiao X, et al.. Converting waste lignin into nano-biochar as a renewable substitute of carbon black for reinforcing styrene-butadiene rubber. *Waste Management*. 2020;102:732-742. doi:10.1016/j.wasman.2019.11.019

60. Jong L. Reinforcement effect of soy protein nanoparticles in amine-modified natural rubber latex. *Ind Crops Prod*. 2017;105:53-62. doi:10.1016/j.indcrop.2017.05.007

61. Arayapranee W, Na-Ranong N, Rempel GL. Application of rice husk ash as fillers in the natural rubber industry. *J Appl Polym Sci*. 2005;98(1):34-41. doi:10.1002/app.21004

62. Intharapat P, Kongnoo A, Kateungngan K. The Potential of Chicken Eggshell Waste as a Bio-filler Filled Epoxidized Natural Rubber (ENR) Composite and its Properties. Published online 2012. doi:10.1007/s10924-012-0475-9

63. Ishak ZAM, Bakar AA. An investigation on the potential of rice husk ash as fillers for epoxidized natural rubber (ENR). *Eur Polym J*. 1995;31(3):259-269. doi:10.1016/0014-3057(94)00156-1

64. Panchal P, Ogunsona E, Mekonnen T. Trends in Advanced Functional Material Applications of Nanocellulose. *Processes*. 2018;7(1):10. doi:10.3390/pr7010010

65. Thakur MK, Thakur VK, Prasanth R. Nanocellulose-Based Polymer Nanocomposites: An Introduction. In: *Nanocellulose Polymer Nanocomposites: Fundamentals and Applications*. Vol 9781118871904. Wiley Blackwell; 2014:1-15. doi:10.1002/9781118872246.ch1

66. Barja F. Bacterial nanocellulose production and biomedical applications. *J Biomed Res*. 2021;35(4):310. doi:10.7555/JBR.35.20210036

67. Carter N, Grant I, Dewey M, Bourque M, Neivandt DJ. Production and Characterization of Cellulose Nanofiber Slurries and Sheets for Biomedical Applications. *Frontiers in Nanotechnology*. 2021;3:729743. doi:10.3389/FNANO.2021.729743/BIBTEX

68. Kurniawan TW, Sulistyarti H, Rumhayati B, Sabarudin A. Cellulose Nanocrystals (CNCs) and Cellulose Nanofibers (CNFs) as Adsorbents of Heavy Metal Ions. *J Chem*. 2023;2023. doi:10.1155/2023/5037027

69. Hamad WY, Miao C, Beck S. Growing the Bioeconomy: Advances in the Development of Applications for Cellulose Filaments and Nanocrystals. *Industrial Biotechnology*. 2019;15(3):133-137. doi:10.1089/ind.2019.29172.qyh

70. Stone DA, Korley LSTJ. Bioinspired polymeric nanocomposites. *Macromolecules*. 2010;43(22):9217-9226. doi:10.1021/ma101661p

71. Dufresne A. Nanocellulose: A new ageless bionanomaterial. *Materials Today*. 2013;16(6):220-227. doi:10.1016/j.mattod.2013.06.004

72. Flauzino Neto WP, Mariano M, da Silva ISV, et al.. Mechanical properties of natural rubber nanocomposites reinforced with high aspect ratio cellulose nanocrystals isolated from soy hulls. *Carbohydr Polym*. 2016;153:143-152. doi:10.1016/J.CARBPOL.2016.07.073

73. Hubbe Martin GW. From Nanocellulose to Wood Particles: A Review of Particle Size vs. the Properties of Plastic Composites Reinforced with Cellulose-based Entities . *Bioresources*. 2020;15(1).

74. Pires JRA, Souza VGL, Fernando AL. Valorization of energy crops as a source for nanocellulose production – Current knowledge and future prospects. *Ind Crops Prod*. 2019;140:111642. doi:10.1016/j.indcrop.2019.111642

75. Roy K, Debnath SC, Potiyaraj P. A critical review on the utilization of various reinforcement modifiers in filled rubber composites. *https://doi.org/101177/0095244319835869*. 2019;52(2):167-193. doi:10.1177/0095244319835869

76. Zhao F, Bi W, Zhao S. Influence of crosslink density on mechanical properties of natural rubber vulcanizates. *Journal of Macromolecular Science, Part B: Physics*. 2011;50(7):1460-1469. doi:10.1080/00222348.2010.507453

77. Edwards DC. Polymer-filler interactions in rubber reinforcement. *J Mater Sci*. 1990;25(10):4175-4185. doi:10.1007/BF00581070

78. Kaushik M, Fraschini C, Chauve G, Putaux JL, Moores A. Transmission Electron Microscopy for the Characterization of Cellulose Nanocrystals. In: *The Transmission Electron Microscope - Theory and Applications*. InTech; 2015. doi:10.5772/60985

79. Trache D, Tarchoun AF, Derradji M, et al.. Nanocellulose: From Fundamentals to Advanced Applications. *Front Chem*. 2020;8:392. doi:10.3389/fchem.2020.00392

80. Ojogbo E, Jardin J, Mekonnen TH. Robust and sustainable starch ester nanocomposite films for packaging applications. *Ind Crops Prod*. 2021;160:113153. doi:10.1016/j.indcrop.2020.113153

81. Kaushik M, Fraschini C, Chauve G, Putaux JL, Moores A. Transmission Electron Microscopy for the Characterization of Cellulose Nanocrystals. In: *The Transmission Electron Microscope - Theory and Applications*. InTech; 2015. doi:10.5772/60985

82. Jardin JM, Zhang Z, Hu G, Tam KC, Mekonnen TH. Reinforcement of rubber nanocomposite thin sheets by percolation of pristine cellulose nanocrystals. *Int J Biol Macromol*. 2020;152:428-436. doi:10.1016/j.ijbiomac.2020.02.303

83. Li Y, Han B, Liu L, et al.. Surface modification of silica by two-step method and properties of solution styrene butadiene rubber (SSBR) nanocomposites filled with modified silica. *Compos Sci Technol*. 2013;88:69-75. doi:10.1016/j.compscitech.2013.08.029

84. Li Y, Han B, Wen S, et al.. Effect of the temperature on surface modification of silica and properties of modified silica filled rubber composites. *Compos Part A Appl Sci Manuf*. 2014;62:52-59. doi:10.1016/j.compositesa.2014.03.007

85. Castellano M, Conzatti L, Costa G, et al.. Surface modification of silica: 1. Thermodynamic aspects and effect on elastomer reinforcement. *Polymer (Guildf)*. 2005;46(3):695-703. doi:10.1016/j.polymer.2004.11.010

86. Kargarzadeh H, Sheltami RM, Ahmad I, Abdullah I, Dufresne A. Cellulose nanocrystal reinforced liquid natural rubber toughened unsaturated polyester: Effects of filler content and surface treatment on its morphological, thermal, mechanical, and viscoelastic properties. *Polymer (Guildf)*. 2015;71:51-59. doi:10.1016/j.polymer.2015.06.045

87. Yu HY, Chen R, Chen GY, Liu L, Yang XG, Yao JM. Silylation of cellulose nanocrystals and their reinforcement of commercial silicone rubber. *Journal of Nanoparticle Research*. 2015;17(9):1-13. doi:10.1007/s11051-015-3165-4

88. Xie Y, Hill CAS, Xiao Z, Militz H, Mai C. Silane coupling agents used for natural fiber/polymer composites: A review. *Compos Part A Appl Sci Manuf*. 2010;41(7):806-819. doi:10.1016/J.COMPOSITESA.2010.03.005

89. Shafik ES. Natural rubber biocomposites based on nanocrystalline and modified nanocrystalline cellulose: curing, mechanical, thermal and electrical properties. *Journal of Polymer Research*. 2021;28(10):1-9. doi:10.1007/S10965-021-02750-4/FIGURES/11

90. Imiete IE, Giannini L, Tadiello L, Orlandi M, Zoia L. The effect of sulfate half-ester groups on the mechanical performance of cellulose nanocrystal-natural rubber composites. *Cellulose*. 2023;30(14):8929-8940. doi:10.1007/S10570-023-05432-0/TABLES/6

91. Jardin JM, Zhang Z, Hu G, Tam KC, Mekonnen TH. Reinforcement of rubber nanocomposite thin sheets by percolation of pristine cellulose nanocrystals. *Int J Biol Macromol*. 2020;152:428-436. doi:10.1016/j.ijbiomac.2020.02.303

92. Flauzino Neto WP, Mariano M, da Silva ISV, et al.. Mechanical properties of natural rubber nanocomposites reinforced with high aspect ratio cellulose nanocrystals isolated from soy hulls. *Carbohydr Polym*. 2016;153:143-152. doi:10.1016/j.carbpol.2016.07.073

93. Mekonnen TH, Ah-Leung T, Hojabr S, Berry R. Investigation of the co-coagulation of natural rubber latex and cellulose nanocrystals aqueous dispersion. *Colloids Surf A Physicochem Eng Asp*. 2019;583:123949. doi:10.1016/j.colsurfa.2019.123949

94. Alex R, Sasidharan KK, Kurian T, Chandra AK. Carbon black master batch from fresh natural rubber latex. *Plastics, Rubber and Composites*. 2011;40(8):420-424. doi:10.1179/1743289810Y.0000000038

95. Ojogbo E, Tzoganakis C, Mekonnen TH. Effect of extrusion, batch-mixing, and co-coagulation on the dispersion of CNCs in natural rubber - CNC nanocomposites. *Compos Part A Appl Sci Manuf*. 2021;149:106580. doi:10.1016/J.COMPOSITESA.2021.106580

96. Mekonnen TH, Ah-Leung T, Hojabr S, Berry R. Investigation of the co-coagulation of natural rubber latex and cellulose nanocrystals aqueous dispersion. *Colloids Surf A Physicochem Eng Asp*. 2019;583:123949. doi:10.1016/J.COLSURFA.2019.123949

97. Yu S, Adams M, Gururajan B, Reynolds G, Roberts R, Wu CY. The effects of lubrication on roll compaction, ribbon milling and tabletting. *Chem Eng Sci*. 2013;86:9-18. doi:10.1016/j.ces.2012.02.026

98. Thakore SI. Chitin based rubber nanocomposites. In: *Advanced Structured Materials*. Vol 56. Springer Verlag; 2017:35-50. doi:10.1007/978-3-319-48806-6_3

99. Visakh PM, Thomas S, Oksman K, Mathew AP. Crosslinked natural rubber nanocomposites reinforced with cellulose whiskers isolated from bamboo waste: Processing and mechanical/thermal properties. *Compos Part A Appl Sci Manuf*. 2012;43(4):735-741. doi:10.1016/j.compositesa.2011.12.015

100. Sui G, Wong SC, Yue CY. Effect of extrusion compounding on the mechanical properties of rubber-toughened polymers containing short glass fibers. In: *Journal of Materials Processing Technology*. Vol 113. Elsevier; 2001:167-171. doi:10.1016/S0924-0136(01)00627-6

101. Ghosh P, Katare S, Patkar P, Caruthers JM, Venkatasubramanian V, Walker KA. Sulfur vulcanization of natural rubber for benzothiazole accelerated formulations: From reaction mechanisms to a rational kinetic model. *Rubber Chemistry and Technology*. 2003;76(3):592-693. doi:10.5254/1.3547762

102. Coran AY. Vulcanization. In: *The Science and Technology of Rubber*. Elsevier Inc.; 2013:337-381. doi:10.1016/B978-0-12-394584-6.00007-8

103. Coran AY. Vulcanization. In: *The Science and Technology of Rubber*. Elsevier Inc.; 2013:337-381. doi:10.1016/B978-0-12-394584-6.00007-8

104. Noordermeer JWM. Vulcanization. In: *Encyclopedia of Polymeric Nanomaterials*. Springer Berlin Heidelberg; 2014:1-16. doi:10.1007/978-3-642-36199-9_311-1

105. Chigondo F, Shoko P, Nyamunda BC, UpenyuGuyo, Moyo M. Maize Stalk As Reinforcement In Natural Rubber Composites. Published online 2013.

106. Lopattananon N, Panawarangkul K, Sahakaro K, Ellis B. Performance of pineapple leaf fiber–natural rubber composites: The effect of fiber surface treatments. *J Appl Polym Sci*. 2006;102(2):1974-1984. doi:10.1002/app.24584

107. Bendahou A, Habibi Y, Kaddami H, Dufresne A. Physico-chemical characterization of palm from Phoenix Dactylifera-L, preparation of cellulose whiskers and natural rubber-based nanocomposites. *J Biobased Mater Bioenergy*. 2009;3(1):81-90. doi:10.1166/jbmb.2009.1011

108. Da Costa HM, Nunes RCR, Visconte LLY, Furtado CRG. *Physical Properties and Swelling of Natural Rubber Compounds Containing Rice Husk Ash*.

109. Payne AR. The dynamic properties of carbon black loaded natural rubber vulcanizates. Part II. *J Appl Polym Sci*. 1962;6(21):368-372. doi:10.1002/app.1962.070062115

110. Highly Dispersible Silica | PPG Silica Products. Accessed February 19, 2024. https://www.ppgsilica.com/Applications/Rubber/Tires.aspx

111. Dominic M, Joseph R, Sabura Begum PM, Kanoth BP, Chandra J, Thomas S. Green tire technology: Effect of rice husk derived nanocellulose (RHNC) in replacing carbon black (CB) in natural rubber (NR) compounding. *Carbohydr Polym*. 2020;230:115620. doi:10.1016/J.CARBPOL.2019.115620

112. Chang B, Gupta A, Muthuraj R, Mekonnen T. Bioresourced fillers for rubber composites sustainability: Current development and future opportunities. *Green Chemistry*. Published online 2021. doi:10.1039/D1GC01115D

113. Sharma A, Thakur M, Bhattacharya M, Mandal T, Goswami S. Commercial application of cellulose nano-composites – A review. *Biotechnology Reports*. 2019;21:e00316. doi:10.1016/j.btre.2019.e00316

114. Gacitua W, Ballerini A, Zhang J. POLYMER NANOCOMPOSITES: SYNTHETIC AND NATURAL FILLERS A REVIEW. *Maderas Ciencia y tecnología*. 2005;7(3):159-178. doi:10.4067/s0718-221x2005000300002

115. Zhang C, Dan Y, Peng J, Turng LS, Sabo R, Clemons C. Thermal and Mechanical Properties of Natural Rubber Composites Reinforced with Cellulose Nanocrystals from Southern Pine. *Advances in Polymer Technology*. 2014;33(S1):n/a-n/a. doi:10.1002/adv.21448

116. Blanchard R, Ogunsona E, Hojabr S, et al.. Synergistic Crosslinking and Reinforcing Enhancement of Rubber Latex with Cellulose Nanocrystals for Glove Applications. *ACS Appl Polym Mater*. 2020;2(2):887-898. doi:10.1021/acsapm.9b01117

117. Eslami H, Tzoganakis C, Mekonnen TH. Surface graft polymerization of lactic acid from the surface of cellulose nanocrystals and applications in chloroprene rubber film composites. *Cellulose*. Published online 2020. doi:10.1007/s10570-020-03167-w

118. Eslami H, Tzoganakis C, Mekonnen TH. Constructing pristine and modified cellulose nanocrystals based cured polychloroprene nanocomposite films for dipped goods application. *Composites Part C: Open Access*. Published online 2020. doi:10.1016/j.jcomc.2020.100009

119. Singh S, Dhakar GL, Kapgate BP, et al.. Synthesis and chemical modification of crystalline nanocellulose to reinforce natural rubber composites. *Polym Adv Technol*. 2020;31(12):3059-3069. doi:10.1002/pat.5030

120. Correia CA, Valera TS. Cellulose Nanocrystals and Jute Fiber-reinforced Natural Rubber Composites: Cure characteristics and mechanical properties. *Materials Research*. 2019;22. doi:10.1590/1980-5373-MR-2019-0192

121. Grossman R. *The Mixing of Rubber*. 1st ed. Springer Netherlands; 1997. doi:10.1007/978-94-011-5824-4

122. Mok KL, Eng AH. Characterisation of Crosslinks in Vulcanised Rubbers: From Simple to Advanced Techniques†. Published online 2018.

123. El-Sabbagh SH, Yehia AA. *Detection of Crosslink Density by Different Methods for Natural Rubber Blended with SBR and NBR*.; 2007.

124. Farid AS. Determination of Crosslink Densities of Filled Rubbers by Cyclic Pre-straining. Published online 2005.

125. Li C, Liu Y, Cao P, et al.. Quaternary phosphonium modified epoxidized natural rubber: Effect of reaction time, reaction mechanism, thermal property and antimicrobial activity. *Polymer Bulletin*. 2014;71(10):2543-2557. doi:10.1007/s00289-014-1206-2

126. Bai W, Li K. Partial replacement of silica with microcrystalline cellulose in rubber composites. *Compos Part A Appl Sci Manuf*. 2009;40(10):1597-1605. doi:10.1016/j.compositesa.2009.07.006

127. Kraus G. Swelling of filler-reinforced vulcanizates. *J Appl Polym Sci*. 1963;7(3):861-871. doi:10.1002/app.1963.070070306

128. Chattopadhyay PK, Chattopadhyay S. Prediction of extent of swelling in ternery particulate rubber-nanocomposites: Development of modified kraus EQUATION. *Rubber Chemistry and Technology*. 2011;84(1):1-23. doi:10.5254/1.3518517

129. Da Costa HM, Nunes RCR, Visconte LLY, Furtado CRG. *Physical Properties and Swelling of Natural Rubber Compounds Containing Rice Husk Ash*.

130. Kraus G. Swelling of filler-reinforced vulcanizates. *J Appl Polym Sci*. 1963;7(3):861-871. doi:10.1002/app.1963.070070306

131. Boonstra BB. Role of particulate fillers in elastomer reinforcement: a review. *Polymer (Guildf)*. 1979;20(6):691-704. doi:10.1016/0032-3861(79)90243-X

132. Ismail H, Jaffri RM, Rozman HD. Oil Palm Wood Flour Filled Natural Rubber Composites: The Effects of Various Bonding Agents. *Int J Polym Mater*. 2001;49(3):311-322. doi:10.1080/00914030108039782

133. Brown RP, Soulagnet G. Microhardness profiles on aged rubber compounds. *Polym Test*. 2001;20(3):295-303. doi:10.1016/S0142-9418(00)00035-0

134. Larson K. Can You Estimate Modulus From Durometer Hardness for Silicones? Accessed July 19, 2020. https://www.dow.com/content/dam/dcc/documents/en-us/tech-art/11/11-37/11-3716-01-durometer-hardness-for-silicones.pdf?iframe=true

135. Ching YC, Ershad Ali M, Abdullah LC, et al.. Rheological properties of cellulose nanocrystal-embedded polymer composites: a review. *Cellulose*. 2016;23(2):1011-1030. doi:10.1007/s10570-016-0868-3

136. Fröhlich J, Niedermeier W, Luginsland HD. The effect of filler-filler and filler-elastomer interaction on rubber reinforcement. *Compos Part A Appl Sci Manuf*. 2005;36(4):449-460. doi:10.1016/j.compositesa.2004.10.004

137. Fröhlich J, Niedermeier W, Luginsland HD. The effect of filler-filler and filler-elastomer interaction on rubber reinforcement. *Compos Part A Appl Sci Manuf*. 2005;36(4):449-460. doi:10.1016/j.compositesa.2004.10.004

138. Mani JWG, Luther S, Schuster R, Hannover, Gorl U, Frankfurt. *Continuous Mixing Process- Properties of E-SBR/Silica/Silane Based Rubber Filler Composite*.; 2007.

139. De SK, White JR. *Rubber Technologist's Handbook - ASM International*. Vol 1. Rapra Technology Limited; 2001.

140. Jiang C, He H, Jiang H, Ma L, Jia DM. Nano-lignin filled natural rubber composites: Preparation and characterization. *undefined*. 2013;7(5):480-493. doi:10.3144/EXPRESSPOLYMLETT.2013.44

141. Yu P, He H, Jia Y, et al.. A comprehensive study on lignin as a green alternative of silica in natural rubber composites. *Polym Test*. 2016;54:176-185. doi:10.1016/J.POLYMERTESTING.2016.07.014

142. Hadi A, Mohammed MR. EFFECT OF EGG SHELLS POWDER ON SOME MECHANICAL AND PHYSICAL PROPERTIES OF NATURAL RUBBER (NR). *undefined*. Published online 2012.

143. Ooi ZX, Ismail H, Abu Bakar A. Synergistic effect of oil palm ash filled natural rubber compound at low filler loading. *Polym Test*. 2013;32(1):38-44. doi:10.1016/J.POLYMERTESTING.2012.09.007

144. Arayapranee W, Naranong N, Rempel GL. Application of rice husk ash as fillers in the natural rubber industry. *J Appl Polym Sci*. 2005;98(1):34-41. doi:10.1002/APP.21004

145. Dominic MCD, Joseph R, Begum PMS, et al.. Cellulose Nanofibers Isolated from the Cuscuta Reflexa Plant as a Green Reinforcement of Natural Rubber. *Polymers 2020, Vol 12, Page 814*. 2020;12(4):814. doi:10.3390/POLYM12040814

146. Misman MA, Rashid AA, Yahya SR. Modification and application of starch in natural rubber latex composites. *Rubber Chemistry and Technology*. 2018;91(1):184-204. doi:10.5254/RCT-18-82604

147. Jong L. Dynamic Mechanical Properties of Soy Protein Filled Elastomers. *undefined*. 2005;13(4):329-338. doi:10.1007/S10924-005-5526-Z

148. Blanchard R, Ogunsona EO, Hojabr S, Berry R, Mekonnen TH. Synergistic Cross-linking and Reinforcing Enhancement of Rubber Latex with Cellulose Nanocrystals for Glove Applications. *ACS Appl Polym Mater*. 2020;2(2):887-898. doi:10.1021/ACSAPM.9B01117/SUPPL_FILE/AP9B01117_SI_001.PDF

149. Xu X, Liu F, Jiang L, Zhu JY, Haagenson D, Wiesenborn DP. Cellulose nanocrystals vs. Cellulose nanofibrils: A comparative study on their microstructures and effects as polymer reinforcing agents. *ACS Appl Mater Interfaces*. 2013;5(8):2999-3009. doi:10.1021/am302624t

150. Ogunsona EO, Muthuraj R, Ojogbo E, Valero O, Mekonnen TH. Engineered nanomaterials for antimicrobial applications: A review. *Appl Mater Today*. Published online 2019. doi:10.1016/j.apmt.2019.100473

151. Trinh BM, Mekonnen T. Hydrophobic esterification of cellulose nanocrystals for epoxy reinforcement. *Polymer (Guildf)*. 2018;155:64-74. doi:10.1016/j.polymer.2018.08.076

152. Miao C, Hamad WY. Alkenylation of cellulose nanocrystals (CNC) and their applications. *Polymer (Guildf)*. 2016;101:338-346. doi:10.1016/J.POLYMER.2016.08.099

153. Liu Y, Wei Y, Liu R, et al.. Preparation of Epoxidized Natural Rubbers with Improved Aging Resistance by Covalently Bridging Graphene and Antioxidants. *J Inorg Organomet Polym Mater*. 2020;30(5):1553-1565. doi:10.1007/S10904-019-01300-2

154. Al-Samarrai MN, Hamzah R, Sam ST, et al.. Slow Release Material from Epoxidized Natural Rubber and Rice Husk Composites for Agriculture Applications. *J Phys Conf Ser*. 2018;1019(1):012063. doi:10.1088/1742-6596/1019/1/012063

155. Ishak ZAM, Bakar AA. An investigation on the potential of rice husk ash as fillers for epoxidized natural rubber (ENR). *Eur Polym J*. 1995;31(3):259-269. doi:10.1016/0014-3057(94)00156-1

156. Ismail H, Rozman HD, Jaffri RM, Mohd Ishak ZA. Oil palm wood flour reinforced epoxidized natural rubber composites: The effect of filler content and size. *Eur Polym J*. 1997;33(10-12):1627-1632. doi:10.1016/S0014-3057(97)00020-7

157. Jiang C, He H, Yao X, Yu P, Zhou L, Jia D. Self-crosslinkable lignin/epoxidized natural rubber composites. *J Appl Polym Sci*. 2014;131(23):n/a-n/a. doi:10.1002/APP.41166

158. Jiang C, He H, Yao X, Yu P, Zhou L, Jia D. In situ dispersion and compatibilization of lignin/epoxidized natural rubber composites: reactivity, morphology and property. *J Appl Polym Sci*. 2015;132(23):42044. doi:10.1002/APP.42044

159. Xu T, Jia Z, Luo Y, Jia D, Peng Z. Interfacial interaction between the epoxidized natural rubber and silica in natural rubber/silica composites. *Appl Surf Sci*. 2015;328:306-313. doi:10.1016/J.APSUSC.2014.12.029

160. Matchawet S, Kaesaman A, Bomlai P, Nakason C. Electrical, dielectric, and dynamic mechanical properties of conductive carbon black/epoxidized natural rubber composites: *http://dx.doi.org/101177/0021998315602941*. 2015;50(16):2191-2202. doi:10.1177/0021998315602941

161. Nie J, Mou W, Ding J, Chen Y. Bio-based epoxidized natural rubber/chitin nanocrystals composites: Self-healing and enhanced mechanical properties. *Compos B Eng*. 2019;172:152-160. doi:10.1016/J.COMPOSITESB.2019.04.035

162. Arroyo M, López-Manchado MA, Valentín JL, Carretero J. Morphology/behaviour relationship of nanocomposites based on natural rubber/epoxidized natural rubber blends. *Compos Sci Technol*. 2007;67(7-8):1330-1339. doi:10.1016/J.COMPSCITECH.2006.09.019

163. Tian M, Zhen X, Wang Z, Zou H, Zhang L, Ning N. Bioderived Rubber-Cellulose Nanocrystal Composites with Tunable Water-Responsive Adaptive Mechanical Behavior. *ACS Appl Mater Interfaces*. 2017;9(7):6482-6487. doi:10.1021/ACSAMI.6B16308

164. Cao L, Fu X, Xu C, Yin S, Chen Y. High-performance natural rubber nanocomposites with marine biomass (tunicate cellulose). *Cellulose*. 2017;24(7):2849-2860. doi:10.1007/S10570-017-1293-Y

165. Cao L, Huang J, Chen Y. Dual Cross-linked Epoxidized Natural Rubber Reinforced by Tunicate Cellulose Nanocrystals with Improved Strength and Extensibility. *ACS Sustain Chem Eng*. 2018;6(11):14802-14811. doi:10.1021/ACSSUSCHEMENG.8B03331

166. Fernandes RMB, Visconte LLY, Nunes RCR. Curing Characteristics and Aging Properties of Natural Rubber/Epoxidized Natural Rubber and Cellulose II. *http://dx.doi.org/101080/009140372010531806*. 2011;60(5):351-364. doi:10.1080/00914037.2010.531806

167. Mayr H, Koschinsky R, Will E, Bäuml E. Acid- and base-catalyzed ring-opening reactions or a sterically hindered epoxide. *Journal of Organic Chemistry*. 2002;52(7):1342-1344. doi:10.1021/JO00383A033

168. Ly M, Mekonnen TH. Cationic surfactant modified cellulose nanocrystals for corrosion protective nanocomposite surface coatings. *Journal of Industrial and Engineering Chemistry*. 2020;83:409-420. doi:10.1016/J.JIEC.2019.12.014

169. Ogunsona EO, Misra M, Mohanty AK. Influence of epoxidized natural rubber on the phase structure and toughening behavior of biocarbon reinforced nylon 6 biocomposites. *RSC Adv*. 2017;7(15):8727-8739. doi:10.1039/C6RA27177D

170. Nie J, Mou W, Ding J, Chen Y. Bio-based epoxidized natural rubber/chitin nanocrystals composites: Self-healing and enhanced mechanical properties. *Compos B Eng*. 2019;172:152-160. doi:10.1016/J.COMPOSITESB.2019.04.035

171. Gengenbach TR, Major GH, Linford MR, Easton CD. Practical guides for x-ray photoelectron spectroscopy (XPS): Interpreting the carbon 1s spectrum. *Journal of Vacuum Science & Technology A*. 2021;39(1):013204. doi:10.1116/6.0000682

172. Li L, Chan CM, Weng LT. The effects of specific interactions on the surface structure and composition of miscible blends of poly(vinyl alcohol) and poly(N-vinyl-2-pyrrolidone). *Polymer (Guildf)*. 1998;39(11):2355-2360. doi:10.1016/S0032-3861(97)00534-X

173. Ojogbo E, Tzoganakis C, Mekonnen TH. Effect of extrusion, batch-mixing, and co-coagulation on the dispersion of CNCs in natural rubber - CNC nanocomposites. *Compos Part A Appl Sci Manuf*. 2021;149:106580. doi:10.1016/J.COMPOSITESA.2021.106580

174. Ogunsona EO, Misra M, Mohanty AK. Influence of epoxidized natural rubber on the phase structure and toughening behavior of biocarbon reinforced nylon 6 biocomposites. *RSC Adv*. 2017;7(15):8727-8739. doi:10.1039/C6RA27177D

175. Tang Z, Liu Y, Guo B, Zhang L. Malleable, Mechanically Strong, and Adaptive Elastomers Enabled by Interfacial Exchangeable Bonds. *Macromolecules*. 2017;50(19):7584-7592. doi:10.1021/ACS.MACROMOL.7B01261/SUPPL_FILE/MA7B01261_SI_004.AVI

176. Li H, Yang L, Weng G, Xing W, Wu J, Huang G. Toughening rubbers with a hybrid filler network of graphene and carbon nanotubes. *J Mater Chem A Mater*. 2015;3(44):22385-22392. doi:10.1039/C5TA05836H

177. Ogunsona EO, Misra M, Mohanty AK. Influence of epoxidized natural rubber on the phase structure and toughening behavior of biocarbon reinforced nylon 6 biocomposites. *RSC Adv*. 2017;7(15):8727-8739. doi:10.1039/C6RA27177D

178. Du Z, Du Y, Gong Y, et al.. Effects of mixing temperature on the extrusion rheological behaviors of rubber-based compounds. *RSC Adv*. 2021;11(56):35703-35710. doi:10.1039/D1RA05929G

179. Peng Y, Xia C, Via B. Characterization of Cellulose Nanocrystal Suspension Rheological Properties Using a Rotational Viscometer. *For Prod J*. 2021;71(3):290-297. doi:10.13073/FPJ-D-21-00026

180. Belyadi H, Fathi E, Belyadi F. Hydraulic Fracturing Chemical Selection and Design. *Hydraulic Fracturing in Unconventional Reservoirs*. Published online 2017:107-120. doi:10.1016/B978-0-12-849871-2.00008-3

181. Arrigo R, Mascia L, Clarke J, Malucelli G. Structure Evolution of Epoxidized Natural Rubber (ENR) in the Melt State by Time-Resolved Mechanical Spectroscopy. *Materials (Basel)*. 2020;13(4). doi:10.3390/MA13040946

182. Setz LFG, Silva AC, Santos SC, Mello-Castanho SRH, Morelli MR. A viscoelastic approach from α-Al2O3 suspensions with high solids content. *J Eur Ceram Soc*. 2013;33(15-16):3211-3219. doi:10.1016/J.JEURCERAMSOC.2013.06.002

183. Singh S, Dhakar GL, Kapgate BP, et al.. Synthesis and chemical modification of crystalline nanocellulose to reinforce natural rubber composites. *Polym Adv Technol*. 2020;31(12):3059-3069. doi:10.1002/PAT.5030

184. Caldwell J, Al. E. *Identification of Research Needs to Resolve the Carcinogenicity of High-Priority IARC Carcinogens*.; 2009. Accessed October 3, 2019. https://monographs.iarc.fr/wp-content/uploads/2018/06/TR42-Full.pdf

185. Blanchard R, Ogunsona EO, Hojabr S, Berry R, Mekonnen TH. Synergistic Cross-linking and Reinforcing Enhancement of Rubber Latex with Cellulose Nanocrystals for Glove Applications. *ACS Appl Polym Mater*. 2020;2(2):887-898. doi:10.1021/ACSAPM.9B01117/SUPPL_FILE/AP9B01117_SI_001.PDF

186. Singh S, Dhakar GL, Kapgate BP, et al.. Synthesis and chemical modification of crystalline nanocellulose to reinforce natural rubber composites. *Polym Adv Technol*. 2020;31(12):3059-3069. doi:10.1002/PAT.5030

187. Roy K, Pongwisuthiruchte A, Chandra Debnath S, Potiyaraj P. Application of cellulose as green filler for the development of sustainable rubber technology. *Current Research in Green and Sustainable Chemistry*. 2021;4:100140. doi:10.1016/J.CRGSC.2021.100140

188. Sahlin K, Forsgren L, Moberg T, Bernin D, Rigdahl M, Westman G. Surface treatment of cellulose nanocrystals (CNC): effects on dispersion rheology. *Cellulose*. 2018;25(1):331-345. doi:10.1007/S10570-017-1582-5/FIGURES/7

189. Yu F, Fei X, He Y, Li H. Poly(lactic acid)-based composite film reinforced with acetylated cellulose nanocrystals and ZnO nanoparticles for active food packaging. *Int J Biol Macromol*. 2021;186:770-779. doi:10.1016/J.IJBIOMAC.2021.07.097

190. Gan L, Liao J, Lin N, Hu C, Wang H, Huang J. Focus on Gradientwise Control of the Surface Acetylation of Cellulose Nanocrystals to Optimize Mechanical Reinforcement for Hydrophobic Polyester-Based Nanocomposites. *ACS Omega*. 2017;2(8):4725-4736. doi:10.1021/ACSOMEGA.7B00532/ASSET/IMAGES/AO-2017-00532C_M004.GIF

191. Xu J, Wu Z, Wu Q, Kuang Y. Acetylated cellulose nanocrystals with high-crystallinity obtained by one-step reaction from the traditional acetylation of cellulose. *Carbohydr Polym*. 2020;229:115553. doi:10.1016/J.CARBPOL.2019.115553

192. Yu HY, Chen R, Chen GY, Liu L, Yang XG, Yao JM. Silylation of cellulose nanocrystals and their reinforcement of commercial silicone rubber. *Journal of Nanoparticle Research*. 2015;17(9):1-13. doi:10.1007/S11051-015-3165-4/FIGURES/7

193. Danish Ali S. *Surface Functionalization of Cellulose Nanocrystals with Silanes and Their Compounds with Natural Rubber*.; 2018. Accessed July 19, 2020. https://boa.unimib.it/bitstream/10281/199113/2/phd_unimib_799145.pdf#page=112

194. Bauer F, Gläsel HJ, Decker U, et al.. Trialkoxysilane grafting onto nanoparticles for the preparation of clear coat polyacrylate systems with excellent scratch performance. *Prog Org Coat*. 2003;47(2):147-153. doi:10.1016/S0300-9440(03)00117-6

195. Pei A, Zhou Q, Berglund LA. Functionalized cellulose nanocrystals as biobased nucleation agents in poly(l-lactide) (PLLA) – Crystallization and mechanical property effects. *Compos Sci Technol*. 2010;70(5):815-821. doi:10.1016/J.COMPSCITECH.2010.01.018

196. Raquez JM, Murena Y, Goffin AL, et al.. Surface-modification of cellulose nanowhiskers and their use as nanoreinforcers into polylactide: A sustainably-integrated approach. *Compos Sci Technol*. 2012;72(5):544-549. doi:10.1016/J.COMPSCITECH.2011.11.017

197. de Oliveira Taipina M, Ferrarezi MMF, Yoshida IVP, Gonçalves M do C. Surface modification of cotton nanocrystals with a silane agent. *Cellulose*. 2013;20(1):217-226. doi:10.1007/S10570-012-9820-3/FIGURES/8

198. Viet D, Beck-Candanedo S, Gray DG. Dispersion of cellulose nanocrystals in polar organic solvents. *Cellulose*. 2007;14(2):109-113. doi:10.1007/S10570-006-9093-9

199. El-Sabbagh SH, Yehia AA. *Detection of Crosslink Density by Different Methods for Natural Rubber Blended with SBR and NBR*.; 2007.

200. Mok KL, Eng AH. Characterisation of Crosslinks in Vulcanised Rubbers: From Simple to Advanced Techniques†. Published online 2018.

201. Farid AS. Determination of Crosslink Densities of Filled Rubbers by Cyclic Pre-straining. Published online 2005.

202. Xie K, Yu Y, Shi Y. Synthesis and characterization of cellulose/silica hybrid materials with chemical crosslinking. *Carbohydr Polym*. 2009;78(4):799-805. doi:10.1016/J.CARBPOL.2009.06.019

203. Mekonnen TH, Haile T, Ly M. Hydrophobic functionalization of cellulose nanocrystals for enhanced corrosion resistance of polyurethane nanocomposite coatings. *Appl Surf Sci*. 2021;540:148299. doi:10.1016/J.APSUSC.2020.148299

204. Trinh BM, Smith M, Mekonnen TH. A nanomaterial-stabilized starch-beeswax Pickering emulsion coating to extend produce shelf-life. *Chemical Engineering Journal*. 2022;431:133905. doi:10.1016/J.CEJ.2021.133905

205. Ojogbo E, Blanchard R, Mekonnen T. Hydrophobic and Melt Processable Starch-Laurate Graft Polymers: Synthesis, Structure – Property Correlations. *Journal Of Polymer Science Part A-Polymer Chemistry*. Published online 2018.

206. Yuan Y, Lee TR. Contact angle and wetting properties. *Springer Series in Surface Sciences*. 2013;51(1):3-34. doi:10.1007/978-3-642-34243-1_1/FIGURES/16

207. Wooley K, Discher D, Vlassopoulos D, Shakesheff K. Some thoughts on superhydrophobic wetting. *Soft Matter*. 2008;5(1):51-61. doi:10.1039/B811945G

208. Blanchard R, Ogunsona E, Hojabr S, et al.. Synergistic Crosslinking and Reinforcing Enhancement of Rubber Latex with Cellulose Nanocrystals for Glove Applications. *ACS Appl Polym Mater*. 2020;2(2):887-898. doi:10.1021/acsapm.9b01117

209. Kim DY, Park JW, Lee DY, Seo KH. Correlation between the Crosslink Characteristics and Mechanical Properties of Natural Rubber Compound via Accelerators and Reinforcement. *Polymers 2020, Vol 12, Page 2020*. 2020;12(9):2020. doi:10.3390/POLYM12092020

210. Kraus G. Swelling of filler-reinforced vulcanizates. *J Appl Polym Sci*. 1963;7(3):861-871. doi:10.1002/app.1963.070070306

211. Liyana Mamauod SN, Fauzi B, Suhaimi NA, Fauzi R, Romli AZ. Preparation and charaterization of treated bis [3-(triethoxysi-lyl) propyl] tetrasulfide (Si-69) -hybrid CB/PCC fillers reinforced NR/ SBR composites: Cure characteristic, Mooney viscosity and cross-link density. *Advanced Composites Letters*. 2018;27(6):261-265. doi:10.1177/096369351802700602

212. Visakh PM, Thomas S, Oksman K, Mathew AP. Crosslinked natural rubber nanocomposites reinforced with cellulose whiskers isolated from bamboo waste: Processing and mechanical/thermal properties. *Compos Part A Appl Sci Manuf*. 2012;43(4):735-741. doi:10.1016/j.compositesa.2011.12.015

Appendix

Supporting Information from for Chapter 3

Solid content of ejected solution from NR/CNC co-coagulation

After co-coagulation, ejected solutions were stored in 20 mL scintillation vials. Aluminium pans were measured using an analytical balance (Mettler Toledo AG285) and tared and approximately 4 g of ejected solution were added to each corresponding weigh pan in triplicate. Weighed pans and samples were brought to a vacuum oven (Shel Lab) set to 55 °C and sealed until fully dry (overnight). After drying and cooling the pans containing the dry product were weighed, with the amount of dry solid determined by difference between the mass of loaded pan and mass of dry pan. The values for each of the CNC/NR latex mixtures were averaged and reported as percentages.

Table 6.1. Average weight of ejected solutions.

Sample	Average wt.%
2.5% CNC	0.6348
5% CNC	0.7582
7.5% CNC	0.8333
10% CNC	0.9685